UNIVERSITÀ DEGLI STUDI DI PAVIA

DOTTORATO IN SCIENZE CHIMICHE E FARMACEUTICHE E INNOVAZIONE INDUSTRIALE (XXXV Ciclo)

Coordinatore: Chiar.mo Prof. Giorgio Colombo

SENSING, CAPTURE AND DISPOSAL OF NANOPARTICULATE

Tesi di Dottorato di
Luca Preti

AA 2021/2022

Tutor
Chiar.mo Prof. Piersandro Pallavicini

Co-tutor
Chiar.ma Dr.ssa Maria Lucia Protopapa

SUMMARY

Abstract

The aim of this PhD project was the creation of a new material with the purpose of capture and detection of the widely used noble metal nanoparticles from an aqueous environment. It was used a new method based on the well-known concept of molecular imprinted polymers (MIPs) called Nanoparticles imprinted matrices (NAIM). This method is based on doping a polymer matrix with nanoparticles and, after their removal by chemical reaction, on forming in the matrix empty cavities of the proper size and shape for the capture of nanoparticulate. A method has been optimized for the preparation of silica gel matrices by sol-gel synthesis, with embedded silver (AgNPs) or gold (AuNPs) nanoparticles of different sizes and shapes. After fine tuning of the sol gel synthesis, by changing the reaction conditions such as the organosilane precursor (TEOS and TMOS), the catalyst (acidic or basic behavior) and the dynamic control chemical additive (CTAB or N,N-dimethylformamide), almost crack-free monoliths were obtained (with the color of the embedded NPs) and a method was studied for the complete oxidation of the templating NPs inside the monoliths. It was found that both AuNPs and AgNPs can be easily removed by strong acidic conditions, such as aqua regia or nitric acid solutions. ICP-OES analysis shows that after the acidic treatment almost all the metal ions are released in the supernatant leaving the monolith residue free. For AgNPs it was also studied methods of oxidation by smooth reagents such as cysteamine hydrochloride and iron nitrate solutions. Following the oxidation reaction by spectrophotometric kinetics it was found that the complete removal of AgNPs from the silica matrix occurs in few hours. A full morphological and compositional characterization of the monoliths was carried out before and after the removal of the template NPs. The monolith samples were analyzed by porosimetric analysis, FTIR spectroscopy, Raman spectroscopy, XRD analysis and SEM imaging. The results highlight the absence of the templating NPs after the removal process, the increase of internal surface of the monoliths and the removal of the organic components related to the coating of the NPs. The presence of cavities of size and shape complementary to the starting template NPs was also observed. The monoliths were ground, and the powder of silica gel monoliths was used to improve the contact surface during the reuptake process. The reuptake ability of the powders was investigated by adding them to 7 nm diameter AgNPs colloidal solution, with controlled stirring and contact time.

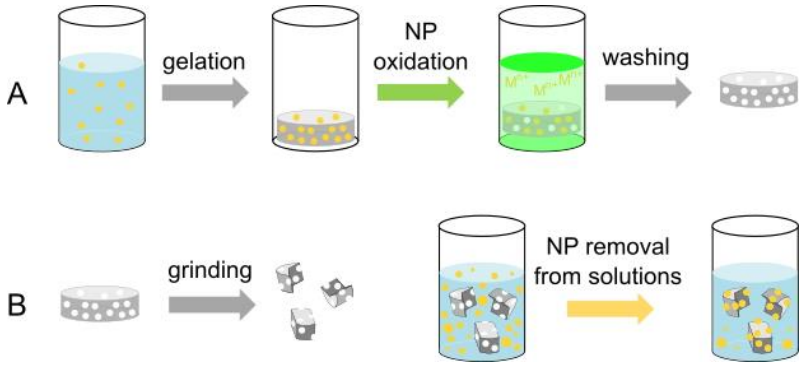

Figure 0 A) schematic illustration of the templated silica gel monolith synthesis; B) schematic illustration of the reuptake process made by ground monolith.

The reuptake processes were carried out on solutions with different NPs concentration, different time, and different size of the templated cavities. The results showed that the reuptake process is time dependent, and it is selective, depending on the best match of the NPs diameter/cavity size. The produced templated silica gel powders were also used as active site in the attempt of preparing sensing systems based on quartz crystal microbalances, with the purpose of selective sensing of AgNPs in aqueous solution.

NOTE: this PhD was granted by Regione Lombardia (and in part by Università degli Studi di Pavia), within a collaborative project with ENEA. The initial agreement included a period to be spent in the Laboratorio ENEA di Materiali e processi industriali sostenibili 4.0 - MaPlS4.O – KmRosso – Bergamo, that included as a goal the training of the PhD student in the use of up to date instrumentations and technology in the innovative materials field. Due to the pandemic emergency, the mentioned laboratory was not available during the PhD period. A collaborative plan was reprojected with the ENEA labs in Brindisi.

Regione Lombardia is gratefully acknowledged for the financial support. ENEA labs are gratefully acknowledged for the technical and scientific support.

PART 1: INTRODUCTION

1.1 Nanotechnology

Nanotechnology is the field of science that encompasses the understanding and control of matter at extremely minute sizes, ranging from approximately 1 to 100nm, where unique phenomena enable novel applications. At this size, matter can take chemical and physical properties different from the bulk material. Nanotechnology involves imaging, measuring, modelling and manipulating matter in the nanometer range. Research and development in nanotechnology is directed toward understanding and creating improved materials, devices, and systems that exploit these new properties. Nanotechnology-enabled products have found applications in many sectors. These include transportation, materials, energy, electronics, medicine, agriculture and environmental science, and consumer and household products.[1;2]

The large-scale opportunities of production application of nanotechnology and nanomaterials determine the prospects for their market growth. In the latest research Global Nanotechnology Market Outlook 2024, the RNCOS analysts expect the global nanotechnology market to grow at compound annual growth rate (CAGR) of nearly 17% during the forecasted period. While BCC analysts optimistically predict global market for nanotechnology growth at a CAGR of 19.4% by 2023. The global nanotechnology market is expected to reach more than USD 91.8 billion by 2028, growing at a CAGR of 15.80%, in terms of revenue, between 2020 and 2028. According to the optimistic estimates in the Research and Markets' Global Nanotechnology Market & Forecast to 2024 Report, the global nanotechnology market will exceed USD 125 billion as late as 2024.[3]

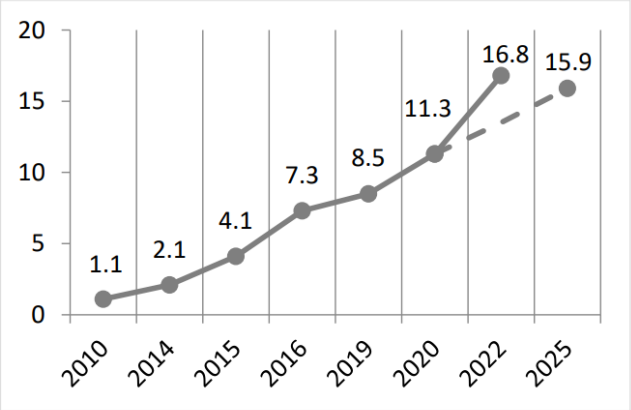

Figure 1 global value of nanotechnology on market [3].

1.2. Nanotoxicology

The novel properties of nanoengineered materials lead to the potential for different toxicity compared with the bulk material. The field of nanotoxicology studies the possible effects of the nanomaterials on the human health and the impact of these kind of materials in the environment.

Despite its clear definition the term "nano" is not uniformly used: we consider nanoparticles the objects with size below the limit inducing physical or chemical processes that may create unknown, unexpected properties in the materials involved. There is tacit agreement among biologists and toxicologists that particles that can take different, partly not yet defined paths in organisms are referred to as nanoparticles.

The specific uptake paths and special features of the nanosized materials lead to the assumption that there are special mechanisms that play a role in biological systems. Three principles have been identified that involve unique characteristics of nanoparticles or nanomaterials and justify, therefore, the use of the term "nanotoxicology":

1.2.1 The transport principle

Phagocytosis is not the only relevant process for the uptake of the nanoparticles inside the cells. Other mechanisms are responsible for the uptake of metals, metal oxides, or other particulate nanosized systems by the cells and for the different biological reactions. Although particles with diameters below 100 nm are capable of getting into the cell by almost any vesicle transport pathway, further options can be considered, for example transport of nanoparticles into cells bound to receptors or even diffusion through the plasma membranes, which is referred to as an adhesive interaction. The effects observed are influenced by the different uptake mechanisms: in the case of uptake by vesicular processes, particles are sheathed by membranes (for example, caveolae). Free transport through the membrane, however, would be assumed to be more critical, as it allows particles to achieve direct contact with the plasma proteins and with other molecules of the cell. The uptake of nanoparticles particles may have fatal consequences for the cell if the material consists of, for example, an incompatible metal and/ or is removed owing to physiological conditions: Zinc is an essential element that we need to take in with the food each day to ensure that our body cells and immune system have the power to control

important processes such as the regulation of the genes. This process may interfere with the control functions of the cell and cause it to commit a programmed cell death, which is known as apoptosis. Particles that do not dissolve but remain stable for a long time or accumulate in cells may become active in another way while obeying the second principle discussed below.

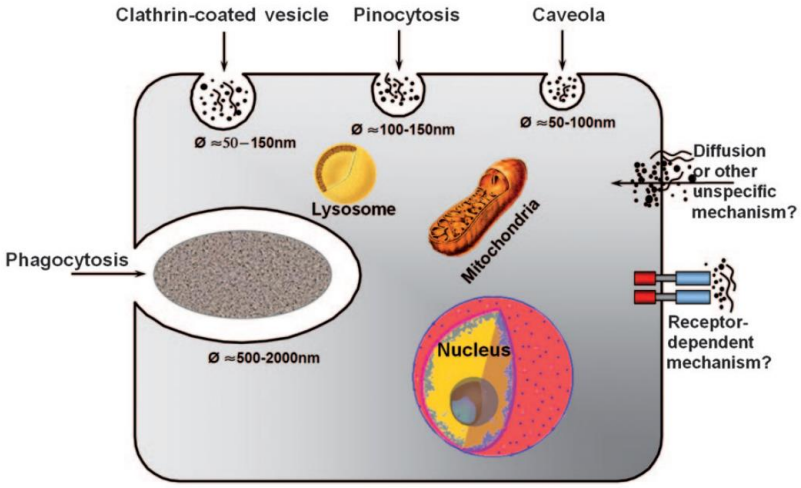

Figure 2 Proposed cellular uptake mechanism for nanoparticles [4].

1.2.2 The Surface principle

Particles that are not soluble but rather stable for extended periods, or biopersistent and able to accumulate in cells, can become active in another way, thus leading to the surface principle. Comparing particles of different sizes, it becomes evident that surfaces and volumes change in parallel with the diameters. A reduction in particle size can improve and accelerate reactions in the case of catalysis or other chemical processes, it increases the reactivity with cells or their components in the biological system. As there are considerably more atoms available on the particle surfaces for smaller particles, they can interact with the environment much more efficiently. Particles with sizes of 100 nm or less have a pronounced exponentially increasing number of atoms, or molecules lying on their surface to potentiate both positive (for example antioxidation or transport of therapeutic agents) and negative effects (such as oxidation or protein binding).

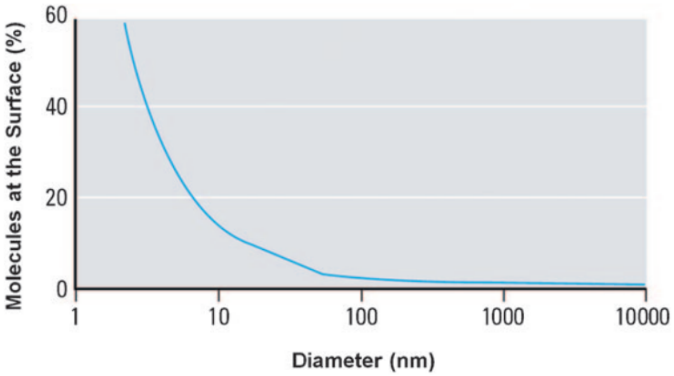

Figure 3 Surface Molecules as A Function Of Particle Size [4].

It is also demonstrated that not only physical but also chemical properties considerably influence the effects of nanoparticles on living systems. They found that the size-dependent toxicity of particles can manifest itself in different ways: Although smaller particles may be more toxic than the larger particles (CuO), larger particles can be more effective than smaller particles (TiO_2); other materials (iron oxides) show no size-dependent effects.

1.2.3 The Material Principle

Almost all materials (metals, metal oxides, polymers, carbon materials, etc.) can be manufactured as nanosized objects. Manufacturing changes the materials physical or chemical properties. These properties are often determined by the characteristics of the surfaces of the particles, fibers, or platelets, but they may also result from the low number of the corresponding molecules or atoms. For biological systems encountering such objects, the materials constituting the nanofractions are rather relevant despite uniform shapes and sizes. This reveals that, following the transport principle, small size is of relevance to health but is not the only factor that causes a harmful toxic impact. Furthermore, the respective particle must be reactive, meaning that reactions either take place on its surface or are catalyzed or that molecules or atoms come off the material to trigger the corresponding reactions in the cell.[4]

1.3. Possible uptake paths in Human body

There are numerous applications of nanomaterials with manifold ways for humans to use and be affected by them. The main toxicologically relevant portals of entry into the human organism are inhalation, uptake via olfactory nerve, dermal exposure, Uptake via the gastrointestinal tract.

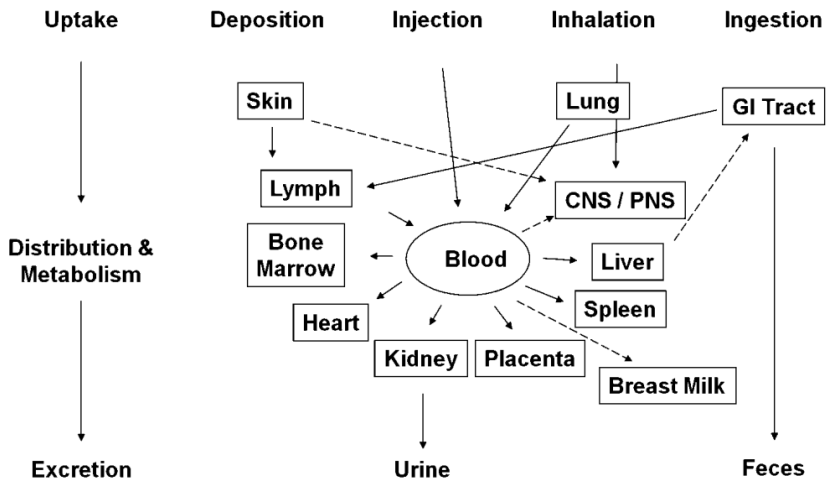

Figure 4 Routes Of Nanoparticles Within The Human Body [4]

The lung is the organ that transports the air via the respiratory tract to the alveoli, where oxygen and carbon dioxide are exchanged with the environment. There are 300 million alveoli to facilitate this gas exchange via diffusion, encompassing a surface area of approximately 140 m^2. The air in the lumen of the alveoli has a proximity of some hundred nanometers away from the flowing blood. The lumen and alveoli are separated by an epithelial and endothelial layer.[5] It was shown in animal tests that high doses of nanoscale particles can overcome the thin air– blood barrier to transmigrate into the blood and avoid the mucociliary clearance.

Nanoparticles of small sizes can be incorporated via the nerve fibers in the olfactory epithelium. Instillation/inhalation tests on rodents using different particles have demonstrated that nanoscale carbon particles, gold particles, oxide particles, and others are conveyed by transsynaptic transport. Nanoparticles can reach the brain directly by passing the olfactory epithelium and the nervus olfactorius located in the roof of the nose. It is also conceivable that systemic uptakes take place via the nervus trigeminus und the

sensoric nerve fibers in the tracheobronchial tract. The quantities reaching the brain via the olfactory nerve are very small, however, they can bypass the blood–brain barrier.[6]

The skin of humans is an organ that protects the organism from environmental stresses and pathogens while avoiding heat and fluid losses. It is composed of three main layers: The epidermis, dermis, and subcutis. The outer layer of the epidermis, the corneal layer (stratum corneum and stratum corneum disjunction), mostly consists of a 5–20 mm layer of dead squamous epithelial cells (keratinocytes), which is a first mechanical barrier against all nanoparticles. The uptake of nanoparticles, especially of the non-lipophilic type that are contained mainly in cosmetics and in sunscreen, is hampered by the very anatomic structure and the continuous regeneration of the human skin from within. Although it was found that the skin does not react acutely to the nanoparticles, it was shown by another group that very small particles (sizes below 10 nm) are capable of penetrating through to the epidermis or dermis. Particle surface coatings or functionalization, which are often used to prevent agglomeration, may strongly influence the penetration. As the corneal layer of stressed or diseased skin is not intact, it is as a rule more permeable to all kinds of particles and must be regarded independently.[7]

The gastrointestinal tract is a complex barrier tissue that fulfils different functions. In the stomach, food is digested at a pH value of approximately 2. The nutrients are taken up by the small and large intestines by the intestinal epithelium and are distributed in the body via the bloodstream. Since the blood vessels are however one or several cell layers below the intestinal epithelium, it is not easy for macromolecules or nanoparticles to migrate into the bloodstream.[7] While in some animal experiments it was found that 50 to 100 nm-sized polystyrene particles absorbed through the intestinal wall to get into the lymphoid system, other studies maintain that there is no uptake at all. It seems clear that there is a lack of information about this path of nanoparticle uptake.[8]

1.4. Biological Effect of Nanoparticles on Human body

To accurately predict the hazards of these new materials for humans, different biological models are used to determine their potential exposure and toxicity elucidates the in vitro in vivo relationship and its extrapolation to humans. In vitro studies are understood as being very simplified biological models that enable a rapid, low-cost estimation of the

effects of xenobiotic substances or nanomaterials. A comparison of different cell types isolated from different tissues or organisms enables evaluation of more than just the tissue-specific effects. Only animal experiments (in vivo) can provide sufficient answers to the complex issues of absorption, distribution, metabolism, and excretion (ADME). However, the constant improvement of in vitro models to simulate complex multicellular systems or entire organs allows an ever more differentiated investigation of possible mechanisms of action and will reduce the need for animal experiments in the long run.[9]

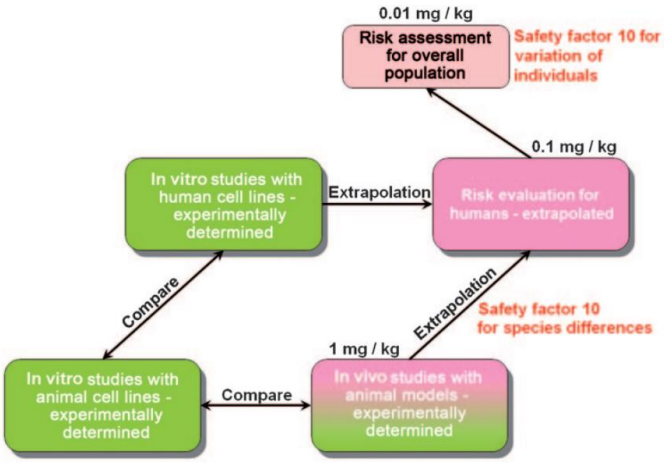

Figure 5 The evaluation process of toxicity of nanoparticles for humans [4].

Although the exact mechanisms of action of nanoparticles, nanofibers, or nanoplates are not yet completely understood, it seems plausible that the specific surfaces of the nanomaterials is key factors in the formation of free reactive oxygen species (ROS).[10] Large quantities of free radicals (for example, superoxide anions and hydroxyl radicals) in cells can cause cellular damage by interacting with their components (lipids, proteins, and DNA) in an uncontrolled way. ROS formation can have different causes: 1) ROS may form directly on the surfaces of nanoobjects; 2) transition metals may act as catalysts for formation of ROS; 3) nanoobjects cause damage to the mitochondria, thus disturbing the balance in the respiratory chain; 4) during activation of macrophages and neutrophils by nanoobjects, these cells themselves produce ROS or RNS (reactive nitrogen species).[11;12]

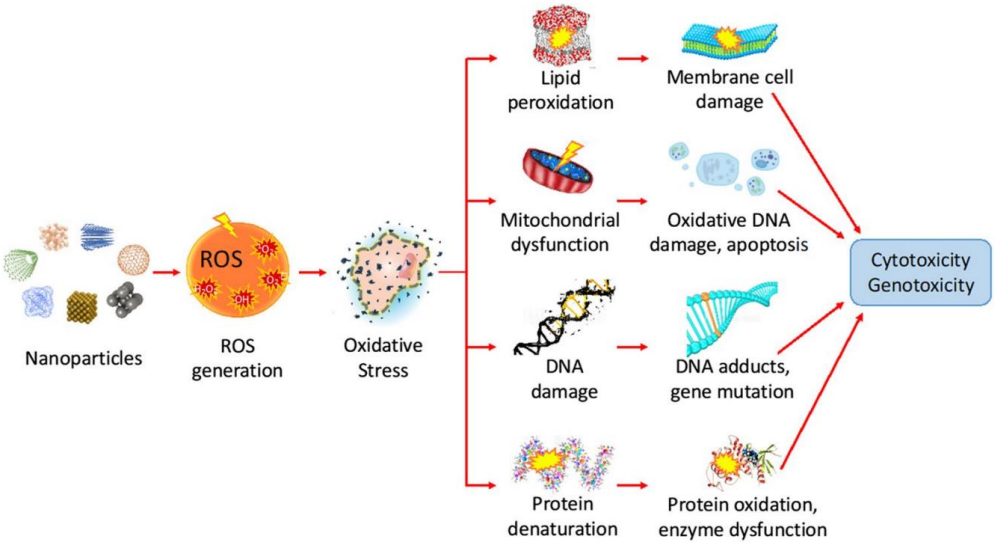

Figure 6 Toxicity mechanism of nanoparticles mediated by reactive oxygen species generation [13].

Not all nanoparticles produce adverse health effects, in fact, as described before, the toxicity of nanoparticles depends on various factors. In addition, the toxicity of any nanoparticle to an organism is determined by the individual's genetic complement, which provides the biochemical toolbox by which it can adapt to and fight toxic substances.[13]

The possible worst adverse health effects associated with nanoparticles are reported in the image below (Figure 7): diseases associated with inhaled nanoparticles are asthma, bronchitis, emphysema, lung cancer, and neurodegenerative diseases, such as Parkinson's and Alzheimer's diseases. Nanoparticles in the gastro-intestinal tract have been linked to Crohn's disease and colon cancer. Nanoparticles that enter the circulatory system are related to occurrence of arteriosclerosis, and blood clots, arrhythmia, heart diseases, and ultimately cardiac death. Translocation to other organs, such as liver, spleen, etc, may lead to diseases of these organs as well. Exposure to some nanoparticles is associated to the occurrence of autoimmune diseases, such as: systemic lupus erythematosus, scleroderma, and rheumatoid arthritis.[14]

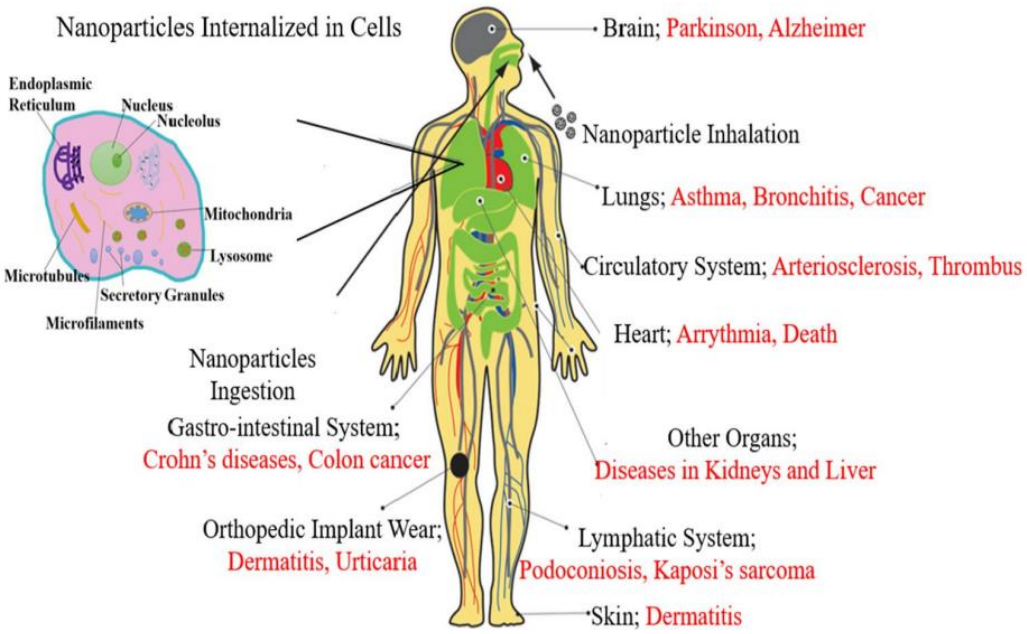

Figure 7 Diseases associated with long term contact with nanoparticles in the main areas of exposition [14].

1.5. Nanoparticles in the environment

The increasing use of nanoparticles and nanomaterials is a risk to our health, and it is also a big threat to the environment. At this regard, it has to be stressed that living in a given environment implies the contact with, and the adsorption/ingestion of, chemical species contained in it, NPs includes. NPs can enter the environment throughout their life cycle as spills or leaks: discharge during the synthesis processes of nanomaterials; discharge during use; after discharge during waste disposal. The nanoparticulate stream can end up directly in the environment or through specialized facilities such as wastewater treatment plants or landfills, it is likely that these nanoobjects will flow through discharges from wastewater treatment plants, the use of biosolids in the soil or through leachate from landfills. From a global assessment of the presence of nanoparticulate in the environment, it is observed that: landfills (about 65-93%) and soils (about 10-30%) are the major contributors, followed by emissions into water and air (respectively 6 and 2%).[15] The presence of nanoparticles in the environment is negatively reflected whether they are dispersed in the soil or in water:

1.5.1. Effects of nanoparticles on aquatic environment

The aquatic environment is more prone to be contaminated with the NPs mainly due to increase in the consumer products like sunscreens and cosmetics which contain NPs like TiO_2, ZnO_2, Ag. NPs are toxic for the aquatic animals such as fish or daphnia and for unicellular organisms as well. Susceptibility to toxicity for aquatic animals varies from species to species. The engineered NPs are highly toxic and selective pathway mechanism exists for the fish and rodents. The NPs may enter the aquatic animals through gills and ingestion. Along the particle size which provides a large surface area to volume ratio, the biocompatibility of the NPs with organism also depends on the surface charge and its chemical reactivity. The particle size and later on biodegradation of the particles may have hazardous biological effects on aquatic organisms together the generation of ROS species from the NPs.[16]

1.5.2. Effects of nanoparticles on soil environment

It is highly important to study interactions between nanoparticles and the soil environment to find the fate and effects. Enzyme activity in soil can be measured to predict anthropogenic effects on the soil environment. Soils are enriched with a variety of microbes. NPs showed toxic effects to enzyme activities at very low concentrations, and they also showed concentration-dependent effects on the growth rate and population of *Lumbricus rubellus* earthworms. In particular, exposure to high concentrations of AgNPs for a longer period of time may deplete their population growth to zero. These particles also affect immune cells of earthworms. The presence of nanoparticles can also lead to soil denitrification, affecting the health of earthworms, small crustaceans, and soil bacteria.[16]

1.5.3. Toxicity of nanoparticles on plants

A problem involving both the aquatic environment and the soil is the toxicity of nanoparticles in plants. Some of the recognized channels that have a role in the entry, and subsequent route of NPs in plants, include accidental release, direct application, contaminated soil/water, and atmospheric discharge/release. Ideally, NPs enter the plant by the roots and generally move from the xylem to pericycle, through cortex. Upon plant-cell entry, these metal-based NPs usually convert to reactive ions, which subsequently

alter the biochemical activity of proteins by reacting with proteins-associated reactive groups. As one of the unique characteristics which nanomaterials possess is large surface area because of which different molecules and inorganic ions can be easily absorbed from the nutrient medium or soil, resulting in chlorosis and wilting. The initial reaction between plants and NPs mainly decides their uptake from the soil/medium, their build-up in the plant system, and subsequent transfer through the different levels of the food web. This mechanistic plant-uptake of NPs is usually by energy-expended active-transport, including various processes like cell-signaling, cell damage repair, and plasma membrane regulation. These nanomaterials utilize the natural openings in plants for entry, with evolved mechanisms to evade the plant-surface barriers like:
-Cuticle, that is the first and foremost protective and oily covering on the plant surface;
-Suberin, that is composed of complex fatty acid and found on plants roots and tubers. It helps in developing an interactive middle layer with the soil;
-mucilage and exudates which are basically complex and long-chain plant carbohydrates;
-cell wall (composed of cellulose), which acts as a structural sieve and permits entry of only those NPs that are compatible with the pore-size of the cell;
-channels and transport proteins facilitate the entry into plant-cells of metal NPs;
-specific ion transporters are responsible for the most of the metal-based NPs Plants-uptake.

Movement of NPs across the cells is basically mediated through plasmodesmata connecting different plant cells. Both translocation and accumulation of NPs are well-regulated and linked processes. Nanoparticles are either channelized through the system to different parts or get collected at a constructive site. This movement and localization of NPs in plants, apart from being plant species specific, depend on the NP size, shape, concentration, and chemical composition; stage of plant growth; and the environment of NPs.

Nanomaterials interact with different species of plants via physical or chemical means. Such interactions cause different signaling that further lead to generation of reactive oxygen species. Like other living organism, plants also respond to all kinds of stress, whether natural or caused by the exposure to some toxic substances. Plants generate a variety of ROS species as a response to heavy-metal and NP-mediated stresses and detoxification. ROS can cause different consequences in plants such as damages by oxidation, cause lipid peroxidation and lead to ion transport alteration across cell

membrane. Moreover, it leads to destruction of mitochondrial DNA and certain protein to be encoded are stopped or malfunctioned. Similar situation arises in chloroplast of the plants. Once plants are induced to stress, significant production of ROS happens, which results in oxidative damage, and finally cell death.[15;16]

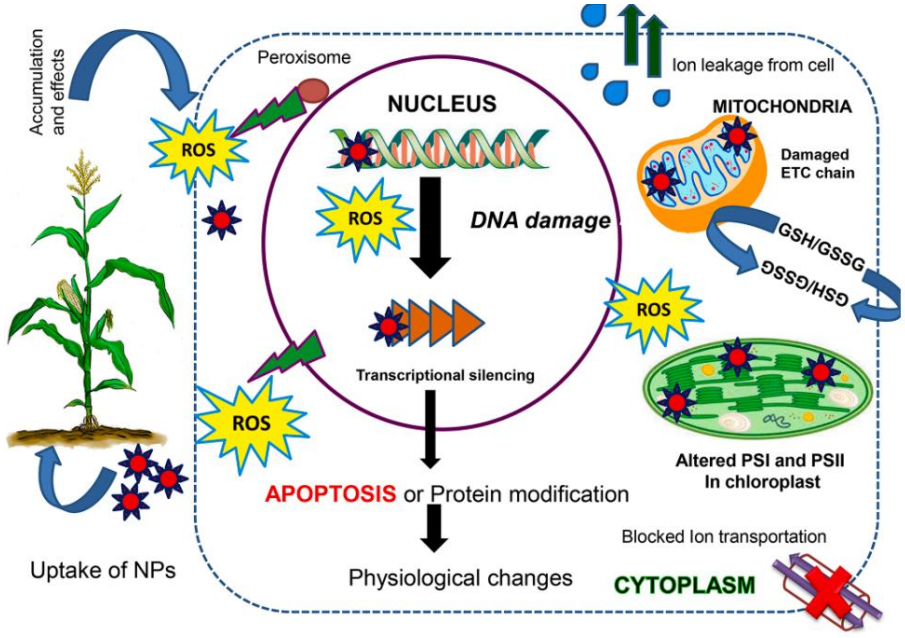

Figure 8 Overview of uptake of nanoparticles and ROS mediated consequences in plants and their organelle [15].

1.6. Silver Nanoparticles

Today, nanotechnology is used in a broad spectrum of scientific fields (biotechnology, medicine, pharmacy, ecology, electronics and others). The possibility of applying nanomaterials for use in agriculture, veterinary medicine, food industry and cosmetology is also being explored. The group of materials of particular interest includes nanoparticles of silver, gold, zinc, selenium, titanium dioxide and carbon nanotubes. In particular, silver nanoparticles, thanks to their unique properties, are seen as a leader in the fight against pathogenic microbial activity.[17]

1.6.1. Diffusion of Silver Nanoparticles

Silver has a strong effect as antiseptic agent. Compared to the bulk form of silver, the increased surface area of nanoparticles is the feature responsible for this increased ability. This results in better contact with microorganisms, and more effective biocidal activity, thanks to increased, sustained release of the Ag^+ antimicrobial ion. Silver nanoparticles are effective against a broad spectrum of Gram-negative and Gram-positive bacteria, including some antibiotic-resistant strains. The group of Gram-negative bacteria, against which the biocidal activity of silver nanoparticles has been confirmed, includes *Acinetobacter, Escherichia, Pseudomonas* and *Salmonella*. The effective action of silver nanoparticles is also reported against Gram positive bacteria: *Bacillus, Enterococcus, Listeria, Staphylococcus* and *Streptococcus*. Research has shown that silver nanoparticles can also be an effective weapon in the fight against viruses by inhibiting their replication. Their activity has been confirmed even against the HIV-1 and influenza virus. Silver nanoparticles are also effective and fast-acting agent that destroys different types of fungi such as *Aspergillus, Candida* and *Saccharomyces*.

Progress in the development of nanotechnology, particularly in the development of new methods of synthesis of silver nanoparticles, meant that the introduction of silver nanoparticles to a variety of consumer products has become very popular. The unique properties of silver nanoparticles attracted the attention of many industries, particularly those in which an antiseptic effect is particularly desirable. This applies to food, textile, construction, medicine, cosmetology, pharmacy and other branches of industry. Silver nanoparticles are also used in the power industry and in biomedicine, in which they act as receptors in labelling of biological materials.[17]

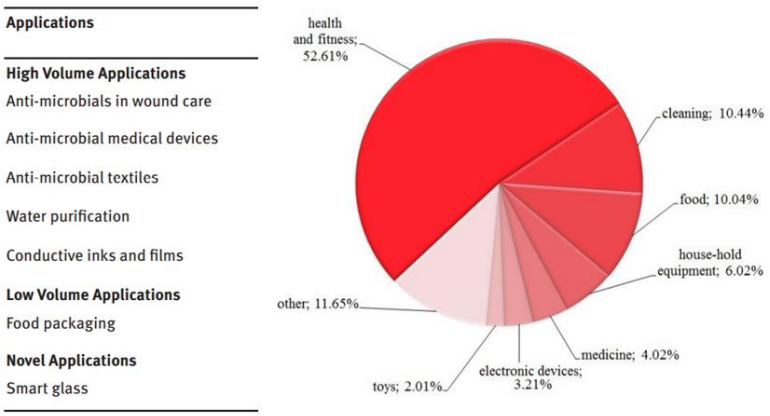

Figure 9 Categories of products containing silver nanoparticles [17].

The study and development of devices containing AgNPs is a very thriving area now and spans a wide range of sectors. Here are reported the main application areas: -medical devices and therapy synthetic materials functionalized by silver nanoparticles which may be used for production of catheters has been developed. Coating containing silver nanoparticles has antibacterial and disinfectant properties. A group of market products containing silver nanoparticles includes, among others, Acticoat Wound Care with nanocrystalline silver, and I-Flow SilverSoaker Nanosilver catheters.[17] A process for preparing granules coated with silver nanoparticles acting as an antibacterial and antifungal agent has been patented: this product inactivates a broad range of bacteria, such as *Staphylococcus aureus*, *Chlamydia trachomatis*, *Providencia stuarti*, *Vibrio vulnificus*, *Bacillus subtitilis* and *Streptococcus paratyphi*.[18] Silver nanoparticles are also used in the materials applied in wounds and burns dressings. Nanostructured silver particles are embedded in the hydrophilic coating as a part of a fiber composite. This layer is in direct contact with the surface of the skin and its main task is to disinfect wounds and absorb body fluids.[19] The use of silver nanoparticles to reduce the attachment of bacteria to the surface of dental implants (to prevent biofilm formation, which causes the risk of infection around the implant surface) is also known. The presence of silver nanoparticles in dental materials and prosthetic implants helps to avoid contamination and infection.[17]

-Cosmetics containing silver nanoparticles are used to prevent contamination with pathogenic microorganisms of products at contact with human body. In addition, the biological purity in the final products should be also ensured. A method of using AgNPs as an ingredient in cosmetics dyeing mixture has been patented. Since the color is dependent to NPs size, the product can be used in dyeing of cosmetic foundations, eye

shadows, powders, lipsticks, inks, varnishes, or eyebrow pencils.[20] A soap incorporating silver nanoparticles is also known and in 2013 the method for its preparation was patented.[21] Silver nanoparticles have also been used in the production of toothpaste and oral care gels.[22]

-building materials containing silver nanoparticles obtain biocidal effect. Another patent shows a method of their incorporation in the structure of the building materials, in particular polyurethane foam. These materials may be used as roofing, insulation, siding, upholstery, and other applications to avoid the formation of molds fungi and algae.[23] A paint using silver nanoparticles is also known, which, thanks to the presence of silver nanoparticles, has biocidal properties.[24]

-purification of air and water using filters doped with silver nanoparticles. A method of enriching polyurethane foam with silver nanoparticles by physical adsorption of the nanoparticles on the foam surface has been patented. The authors suggest that their resulting material can be used as a filter for drinking water, in which, the bacterial flora contamination poses a threat to human health. To avoid the risk of microbial growth, a method of impregnating the air filter with silver nanoparticles has been developed. Results of microbiological tests confirmed that the impregnation of baghouse with silver nanoparticles allows for almost total elimination of microbiological contamination of the air. Silver nanoparticles may be used also for rearing and farm animals breeding. Animal droppings and feed are a source of air pollution, especially with odors such as ammonia and hydrogen sulphide that are highly dangerous for the environment.[17;25] Application of silver nanoparticles in the rural area has been studied, particularly in activities that improve the plant growth.[26]

There is a large group of companies participating in the development and diffusion of silver nanoparticles: Blue Nano, Cambrios, Agfa, Blue Nano, Carestream Advanced Materials, Cima Nanotech, Dow Chemical, PolyIC, Ferro, Saint-Gobain, Sigma Technologies, Suzhou NanoGrid Technology and Sumitomo Metals and Mining, Nano Silver Manufacturing Sdn Bhd, NovaCentrix, Advanced Nano Products Co. Ltd., Ames Goldsmith Corporation, Creative Technology Solutions Co. Ltd., Applied Nanotech Holdings, Inc., NanoMas Technologies, Inc., ras materials, SILVIX Co., Ltd. and Bayer MaterialScience AG.[17]

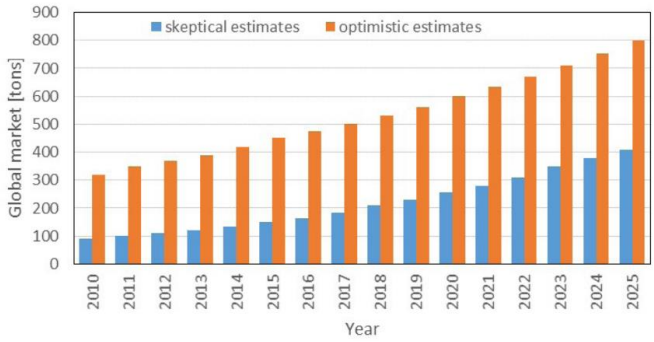

Figure 10 The global market for silver nanoparticles [17].

1.6.2. Silver Nanoparticles in the environment

Silver Nanoparticles can escape from the manufacturing factory during the production process, including drying the solution, mechanical grinding, mixing, and packaging, resulting in the release of AgNPs into the atmosphere. Also, the widespread use of AgNPs in disinfection sprays promotes the emission of AgNPs to the air. Surface disinfectants can cause AgNPs to deposit on surfaces and would probably transfer to a duster cloth after cleaning and then go down the drain during laundering. Added in anti-odor sprays and used in rooms, AgNPs could also end their way in the open air by transport. If they are stable enough, long distance mobility in the air would be expected. Additionally, their large surface area provides abundant reactive sites for dusts, microbes and pollution, making the AgNPs much more toxic than the original particles.

The airborne particles may also coalesce to large agglomerates during transport, and deposit on surfaces by gravitation, or be washed down to terrestrial or aquatic systems by rain. Processes such as direct disposal of AgNP product, waste incineration or landfill, AgNPs suspended in air depositing on the land, and sewage sludge recycling as a fertilizer to agricultural soils could cause AgNPs to enter soils. The fate and transport of AgNPs in soils is governed by a few variables, such as the particle size, surface charge and the soil environment. NPs may also adsorb organic contaminants and act as carriers for transport of contaminants. As AgNPs are always modified by the stabilizing agents and possess a surface charge, the electrostatic interaction with different soil types alters their mobility.

AgNPs may enter the aquatic system in several ways: silver leached out from nanosilver consumer products, and eventually end up in streams and rivers; suspended AgNPs in air

finally depositing on water; runoff scouring AgNP polluted soils or landfill sewage sludge could result in AgNPs migrating to surface water. The water environment could largely affect the mobility of AgNPs. Normal organic matter NOM could adsorb on nanoparticles, and act as stable agents to make AgNPs more mobile in aquatic systems, divalent cations (e.g. Ca^{2+} and Mg^{2+}), commonly present in natural waters, could easily induce the aggregation of AgNPs. Colloidal clusters would probably deposit in the sediment, reducing the bioavailability for aquatic organisms and plants. As previously explained AgNPs are not highly stable and can easily be oxidized to give a slow dissolution of Ag^{+} in aquatic environments. Ag^{+} binds with negatively charged ligands, such as S_2^{-}, SO_4^{2-} and CO_3^{2-}. In marine waters, as sodium chloride is the dominant salt, Ag^{+} associates with Cl^{-} to a great extent, and the main species observed are silver chloride salts, making silver more mobile in seawater. The main forms of Ag^{+} varied significantly at varied pH, the type and concentration of ligands, and the strength of silver binding with these ligands. As speciation greatly influences the fate and transport of AgNPs, they would behave quite differently in various water conditions.[27]

1.6.3. Toxicity of Silver Nanoparticles

While the use of AgNPs have increased manifold, their discharge in the environment becomes inevitable, which subsequently hampers the soil and aquatic life forms. There is no doubt that the antibacterial activity of AgNPs is a complex process, and several possible modes of action are proposed: generation of reactive oxygen species (ROS), direct attachment to cell membrane and disruption of membrane integrity, changes in membrane permeability, interaction with proteins and disruption of their regular function and interference with DNA replication and causing DNA damage.[27]

Since the oxidation of metallic silver is thermodynamically favored at room temperature, a layer of Ag^{+} is readily formed in the ambient environment. For AgNPs, the large surface area facilitates exposure to O_2 and they are much more reactive than bulk silver. A first model of reaction:

$$2Ag_{(s)} + 1/2O_{2(aq)} + 2H^{+}_{(aq)} \rightleftharpoons 2Ag^{+}_{(aq)} + H_2O_{(l)}$$

$\Delta G^0 = -91.3$ kJ/mol a 298 K

Since the exchange of 4 electrons is unlikely, a reaction mechanism has been proposed in which a first atom of silver reacts with oxygen to give Ag^{+} and a molecule of H_2O_2:

$$O_2 + H^+ \xrightarrow[Slow]{Ag^0} Ag^+ + H_2O_2 \xrightarrow[Fast]{Ag^0} Ag^+ + H_2O$$

The oxidation reaction of nanoparticles does not consist in an equilibrium of species present in solution, but the Ag^0 species is always destined to disappear (as can be seen from the negative value of the reaction previously reported) in more or less long times depending on the conditions in which it is find the nanoparticles. The oxidation speed depends on several factors such as: size of the nanoparticles, reaction speed increases with the decrease of the NPs size (higher surface energy); the concentration of oxygen in solution, it has been shown that the degradation of AgNPs is completely inhibited in an anaerobic environment; the reaction is also inhibited in a reducing environment; the pH increases the oxidative speed as the pH of the system is lowered; increasing the temperature also increases the speed of the reaction.[28]

It's known that silver ions have biocidal effect, but the toxicity of AgNPs could not be fully explained by the Ag^+ in AgNPs solutions, and the particles served as sources of Ag^+. it's been found both the nanoparticles and Ag^+ contributed to the toxicity of AgNPs to human hepatoma HepG2 cells. In another study evaluating the effect of AgNPs on a common grass *Lolium multiorum*, AgNPs exposed seedlings showed abnormal growth with highly vacuolated and collapsed cortical cells and broken epidermis and root cap, whereas no such abnormalities were found in seedlings exposed to the same concentration of $AgNO_3$, suggesting the toxicity of AgNPs was higher than of Ag^+.[29] To discern the toxicity of AgNPs and Ag^+ an experiment in anaerobic conditions that prevented the oxidation of AgNPs it's been performed. Results showed that Ag^+ was 20 times more toxic to E. coli than AgNPs, while the presence of common ligands could largely decrease the Ag^+ toxicity, which might explain the higher toxicity of AgNPs than Ag^+. Further studies revealed that AgNPs did not inhibit the growth of E. coli under strictly anaerobic conditions, whereas the AgNP toxicity greatly increased after exposure to air. In conclusion, adverse effects can be caused by AgNPs, involving developmental abnormality, DNA damage, gene expression variation and metabolic disturbance, which is dependent on concentration. Levels of AgNP toxicity vary significantly, depending on the size, shape and capping agents, as well as the exposure pathway. Dissolved Ag^+ plays a vital role in the AgNP toxicity, while AgNPs acted as the source of Ag^+ and the carrier to deliver NPs to organisms.[30]

To verify the toxicity of nanoparticles on living systems, in vivo and in vitro experiments were carried out on both mammals and non-mammals. The results of these experiments are reported in the following tables where are reported the organism species, the AgNPs doses, the exposure method, and the measured effects.[27]

Ag NP size/ nm	Organism	Dose concentration	Exposure method	Effect measured
14.6 ± 1.0	Female Fischer 344 rats	3×10^6 particles cm^{-3} (133 μg m^{-3})	Inhalation exposure: 6 h per day, 0,1, 4, 7 days	AgNPs detected in lung, blood, liver, kidney, spleen, brain, and heart; rapid clearance of AgNPs from lung
13–15	Sprague–Dawley rats	Low-dose (1.73×10^4 particles cm^{-3}, 0.5 μg m^{-3}); medium-dose (1.27×10^5 particles cm^{-3}, 3.5 μg m^{-3}); high-dose (1.32×10^6 particles cm^{-3}, 61 μg m^{-3})	Inhalation exposure: 6 h per day, 5 times per week, 4 weeks	No remarkable changes in nasal cavity and lungs; size and number of goblet cells containing neutral mucins increased
22.18 ± 1.72	C57BL/6 mice	1.91×10^7 particles cm^{-3}	Inhalation exposure: 6 h per day, 5 times per week, 2 weeks	Expression of several genes associated with motor neuron disorders, neurodegenerative disease, and immune cell function
18	Sprague–Dawley rats	Low-dose (0.7×10^6 particles cm^{-3}); medium-dose (1.4×10^6 particles cm^{-3}); high-dose (2.9×10^6 particles cm^{-3})	Inhalation exposure: 6 h per day, 5 times per week, 13 weeks	Decreased tidal volume and minute volume, lung inflammation
12–16	Sprague–Dawley rats	Low-dose (1.73×10^4 particles cm^{-3}); medium-dose (1.27×10^5 particles cm^{-3}); high-dose (1.32×10^6 particles cm^{-3})	Inhalation exposure: 6 h per day, 5 times per week, 4 weeks	No significant changes in body weight, hematology and blood biochemical values for both male and female rats
25	Adult-male C57BL/ 6N mice	100, 500, 1000 mg kg^{-1}	Intraperitoneal injection for 24 h	Free radical induced oxidative stress, gene expression alteration and neurotoxicity
20, 80, 110	Male Wistar rats	23.8, 26.4, 27.6 μg mL^{-1}	Intravenous injection: once per day, 5 consecutive days	Size dependent tissue distribution
Colloidal silver	Weaned piglets	25, 50 and 100 μg per g diet	Ingestion exposure: mixed with diet for 5 weeks	No lactobacilli proportion observed, no AgNPs accumulation in skeletal muscles or kidneys, and only small contents found in liver
60	Fischer 344 rats	10 mL kg^{-1}	Ingestion exposure: 90 days	Gender-related differences in accumulation of AgNPs in kidneys
60	Sprague–Dawley rats	Low-dose group (30 mg kg^{-1}); medium-dose group (300 mg kg^{-1}); high-dose group (1000 mg kg^{-1})	Ingestion exposure: mixed with diet for 28 weeks	Significant dose-dependent changes in the alkaline phosphatase, cholesterol values; dose-dependent accumulation of silver content in all the tissues examined; gender-related differences in accumulation of AgNPs in kidneys

Figure 11 Toxicity of AgNPs on mammals. In the image are reported the main investigated living models for mammals living forms, the size, the dose concentration, the exposure method, and the measured effects [27].

Ag NP size/nm	Organism	Dose concentration	Exposure time	Effect measured
11.6 ± 3.5	Zebrafish embryos	0.04–0.71 nM	120 h	Dose-dependent mortality and developmental abnormality
3, 10, 50, 100	Zebrafish embryos	0.25, 2.5, 25, 100, 250 μM	24–120 h	Almost 100% mortality at 120 h post-fertilization, generation of a variety of embryonic morphological malformations
41.6 ± 9.1	Zebrafish embryos	0.02–0.7 nM	120 h	Dose-dependent mortality and developmental abnormality
49.6	Japanese medaka (*Oryzias latipes*)	1, 25 μg mL^{-1}	1, 2, 4 days	Cellular and DNA damage, carcinogenic and oxidative stresses, induction of genes related metal detoxification/metabolism regulation and radical scavenging action
25	Japanese medaka (*Oryzias latipes*)	100–1000 μg mL^{-1}	70 days	Retarded development, reduced pigmentation and morphological malformations in embryos
3–40	Rainbow trout (*Oncorhynchus mykiss*)	Cells grown: 10–20 mg L^{-1}. cytotoxicity: 0.1–10 mg L^{-1}	48 h	Cytotoxicity: membrane integrity showing reduction in viability, higher levels of oxidative stress
35 nm for PVP-AgNPs 40 nm for Citrate-AgNPs	*Daphnia magna*	PVP-AgNPs: 3.1–50 μg L^{-1}; citrate-AgNPs: 0.625–5.0 μg L^{-1}; $AgNO_3$: 0.16–2.5 μg L^{-1}	24 h	AgNPs disrupt protein metabolism and signal transduction, induce metal responsive and DNA damage repair genes $AgNO_3$ caused a downregulation of developmental processes, particularly in sensory development
30 ± 5	Estuarine polychaete (*Nereis diversicolor*)	Expected final concentrations: 250 ng Ag per g sediment	Ingestion exposure: sediment mixed with AgNPs as diet, 10 days	Direct internalization of AgNPs into gut epithelium
20	Soil nematode (*Caenorhabditis elegans*)	0.05, 0.1, 0.5 mg L^{-1} AgNPs and $AgNO_3$	Ingestion exposure, 24–72 h	Increased expression of the superoxide dismutases-3 (sod-3) and abnormal dauer formation protein (daf-12) genes, concurrently with significant decreases in reproduction ability
10, 80	Earthworm (*Eisenia fetida*)	20, 100, 500 mg kg^{-1}	14 days	Dose-dependent inhibition of the activities of AP and Na^+, K^+-ATPase
Solid dispersion, 3 μm	Fruit fly (*Drosophila melanogaster*)	Acute toxicity: 10–100 mg L^{-1} Ag; chronic toxicity: 5 mg L^{-1} Ag	Ingestion exposure: AgNPs prepared in solid dispersion were added into culture medium, 10 days	Acute toxicity: 50% of the tested flies unable to leave the pupae, did not finish developmental cycle Chronic toxicity: influence the fertility of Drosophila during the first three filial generations
10	Fruit fly (*Drosophila melanogaster*)	50, 100 μg mL	Ingestion exposure: 24, 48 h	Upregulation of the expression of heat shock protein 70 and induction of oxidative stress

Figure 12 Toxicity of AgNPs on non-mammals. In the image are reported the main investigated living models for non-mammals living forms, the size, the dose concentration, the exposure method, and the measured effects [27].

1.7 Capture of nanoparticles in environment

Although NPs are not yet regulated, they are already included in lists of emerging pollutants. Despite that, there are very few reports on the presence and the behavior of NPs in the environment, because of the general lack of analytical methods able to detect and to quantify the rather wide range of NPs. In general, the analysis of metal nanoparticles can be separated in five major areas: bulk concentration (ppm of NPs in the matrix); bulk composition (elemental analysis of the NPs after segregation by size); size or size distributions of individual nano-objects; elemental composition of individual nano-objects; chemical speciation (e.g., AgNPs). In general, these techniques consist of the separation of the nanoparticles from the matrix by filtration or size exclusion methods and further compositional or imaging analysis.[31]

Filtration	Size fractionation	Down to 1 kDa	
Micro-filtration	Size-exclusion membrane	100 nm–1 µm	SEM
Nano-filtration	Size-exclusion membrane	0.5–1 nm	TEM, AFM
Cross-flow ultrafiltration (CFUC)	Size-exclusion membrane	1 nm–1 µm	TEM, ICP-MS
Dialysis	Size-exclusion membrane	0.5–100 nm	TEM, SEM
Size-exclusion chromatography (SEC)	Packed porous beads as stationary phase	0.5 –10 nm	ICP-MS ICP-OES
Ulltracentrifugation (UC)	Acceleration up to 10^6 g	100 Da–10 GDa	SET, TEM, EDS, XRF, ICP-MS, ICP-OES
Field-flow fractionation (FFF)	Physical separation on an open tube based on applied field	1 nm–1 µm	ICP-MS ICP-OES
Electrophoretic mobility (EM)	Charge-size distribution along a gradient	3 nm–1 µm	ICP-MS ICP-OES

Figure 13 in the table are reported the main ways for the separation of nanoparticulate from liquid media and their characterization techniques [31].

In literature there is a lack of methods for the removal of nanoparticles from the environment. Specially in aqueous media, there are only few works based on filter systems for nanoparticles. They are mainly based on nanofibers membrane and activated carbon that interact with non-specific electrostatic interactions and size exclusion ways with nanoparticles.[32;33] As studies have found a higher incidence of chronic pulmonary diseases in workers exposed to certain types of nanoscale particles, filter systems for airborne nanoparticles are more studied. These devices are mainly based on electrostatic interactions of membranes with the atmospheric nanoparticles.[34]

1.8 Perspectives and scope

In this work strategies are proposed for the development and full characterization of new kind of 3-dimensional materials useful for the capture of noble metal nanoparticles. These materials are based on the new concept for the selective recognition and capture of NPs named NPs imprinted matrices (NAIM). It is analogous to the well-known concept of molecularly imprinted polymers (MIP) in which the molecular analyte is imprinted in a polymer by polymerization of proper monomers with which it chemically associates. The removal of the template forms complementary cavities capable of selective recognition of the analyte. Instead of molecular species, here, NPs are imprinted in various matrices. Chemical methods for the (fast) disposal of nanoparticulate with smooth reagents (i.e. adhering to the principles of green chemistry) are also proposed in this work, to assure the removal of the NP from the silica materials, and the reusability of the void, imprinted materials and the recovery of silver after a reuptake cycle.

PART 2: TEMPLATED SILICA GEL MONOLITHS

2.1 BACKGROUND

2.1.1 Nanoimprinted matrices

Nanoparticle imprinted matrices (NAIMs) are used for the selective recognition of NPs based on their size and shape. NAIM follows the well-known approach of molecularly imprinted polymers (MIPs), however, here the imprinting templates are NPs instead of molecular species. It should be noted that imprinting of larger and more chemically complex objects such as bacteria and bio-conjugates has already been demonstrated using the MIP approach.[34;35] Though very few NAIM systems have been developed, two principal approaches can be distinguished. The Langmuir–Blodgett technique is used to co-deposit mono layers of polymers with NPs. Voids formed after removal of the NPs showed size selectivity. Metallic NPs bearing different chain-length stabilizing shells were selectively recognized by the NAIMs after removal of the NPs. In the second approach, the initial adsorption of the NPs is followed by filling the non-occupied areas with self-assembled monolayers. NPs having similar diameter were recognized independently on the metallic core. In both methodologies, nanoparticle speciation, where NPs with similar core composition are differentiated according to a physical or chemical parameter, e.g., size or shape was demonstrated.[36]

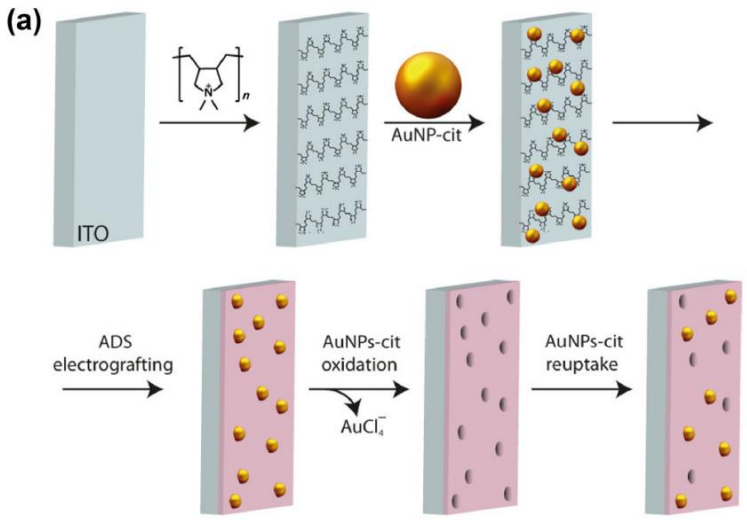

Figure 14 schematic approach of NAIM formation by SAM formation [34].

It is important to note that the described matrices are bidimensional structure used for speciation of nanoparticles. In this work is proposed the synthesis of three-dimensional silica gel matrix realized by sol gel method in which, the interaction between the NPs and complementary size cavities has been studied.

2.1.2 Sol gel method to produce silica monoliths

Silica sol-gel technology was first discovered in the late 19th century. It that allows the formation of large (cm range) monolithic inorganic structures at low temperature. The sol-gel reaction can be divided into the following steps: (1) the hydrolysis of an alkoxysilane; (2) the condensation of hydrated silica to form siloxane bonding (Si-O-Si); and (3) the polycondensation of the linkage of an additional silanol group to form larger, 3D oligomers.

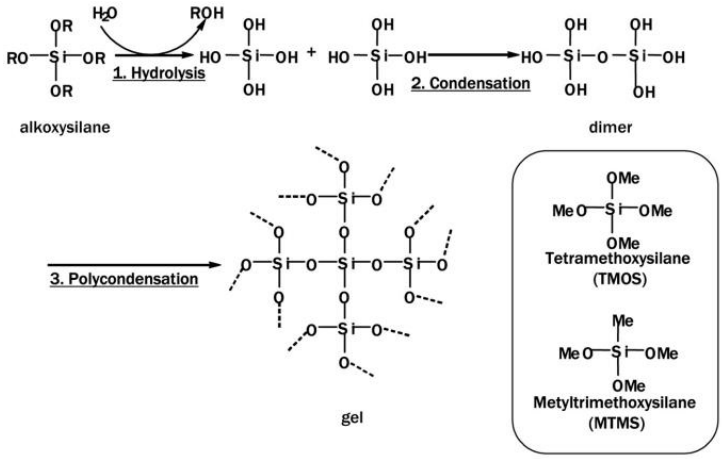

Figure 15 typica sol gel reaction and monomer compounds [35].

The most common starting reagents are tetramethoxysilane (TMOS) or tetraethoxysilane (TEOS), mostly because they are relatively cheap, commercially available and can be readily hydrolyzed and condensed under mild conditions. The properties of each individual sol-gel matrix can be altered by several factors. These include the nature of the catalyst, temperature, the reagent concentrations, the reaction time and the rate of hydrolysis and condensation. In turn, the rate of hydrolysis depends on several parameters:

- the molar ratio H_2O/alkoxide, in which the hydrophobic or hydrophilic character of the precursors should also be considered. Due to the partially hydrophobic nature of the ethoxy groups, TEOS and water are immiscible in all proportions, and it is necessary to add a co-solvent to achieve miscibility and allow hydrolysis.

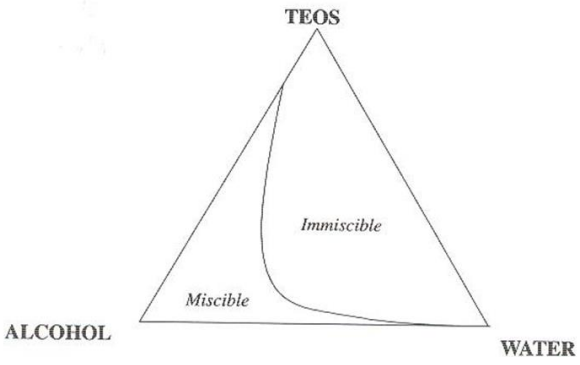

Figure 16 The phase diagram of TEOS/Ethanol/water. The diagram defines the minimum amount of ethanol required to obtain miscibility in any given mixture of water and TEOS. Since ethanol is a product of hydrolysis, the precursor and water can also be mechanically mixed and made to react to start to the production of ethanol and then to miscibility.

Different co-solvents can be used, including alcohols, formamide, dimethylformamide, dioxane and THF. The choice of co-solvents is important since the use of an alcohol different from the one generated by the hydrolysis of the alkoxide can lead to transesterifications and influence the entire hydrolysis-condensation sequence. The co-solvent can also influence the drying process. When the co-solvent is chosen primarily for the latter parameter, it is usually called a drying control chemical additive (DCCA).

- Nature of the R groups (bulky substituents hinder hydrolysis), influencing the process by the inductive effect (that is important in stabilizing transition states involving the formation of negative or positive charges). It should also be remembered that large alkoxy groups lead to crowding of the transition state, which raises activation energy, and this causes a lowering of the rate of hydrolysis. Accordingly, tetramethoxysilane (TMOS) hydrolyzes faster than tetraethoxysilane (TEOS).

The kinetics of hydrolysis in a neutral environment is very slow, for this reason the reaction is carried out in acid or base catalysis.

$$Si(OR)_n + H_2O \rightarrow Si(OR)_{n-1}(OH) + ROH$$

Hydrolysis in acid solution implies to the protonation of the oxygen of the alkoxide group, the silicon becomes more electrophilic and therefore more susceptible to nucleophilic

attack by water. The mechanism is of the SN2 type and involves the formation of an intermediate with 5 terms.

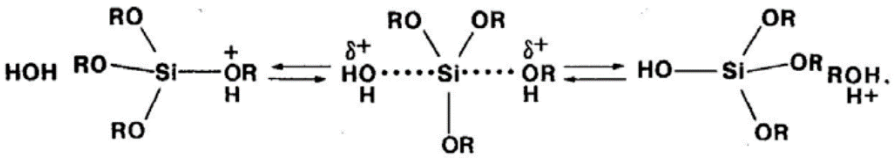

On the other hand, the hydrolysis of silicon alkoxides in a basic environment proceeds also with SN2 mechanism, but with hydroxyl attack on silicon. The substitution of the alkoxy groups is always faster as the number of substituted groups increases (inductive effect). Under conditions of basic catalysis, therefore, the tendency is to have completely hydrolyzed monomers.

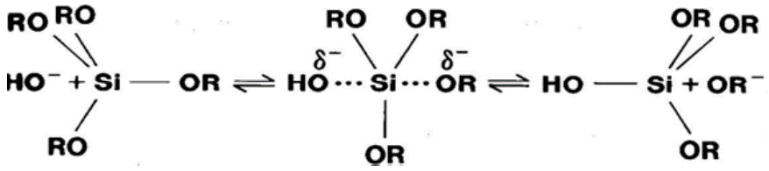

Hydrolysis with basic catalysis has an initially slow course whose speed increases as the alkoxy groups are replaced by OH groups, and it is complete and irreversible. Conversely, the condensation with basic catalysis is faster and proceeds by addition of completely hydrolyzed monomer to the Si–O- groups of the growing cluster, leading to the formation of spherical particles and a strongly crosslinked network. As a consequence, highly porous gels are formed. With acid catalysis, on the other hand, the hydrolysis reaction is faster initially, but the reverse re-esterification reaction is also favored. Condensation slows down as the degree of substitution increases and proceeds mainly by reaction of neutral species with protonated Si-OH groups, leading to the formation of poorly branched chains.[37]

2.1.3 AgNPs doped silica gel matrix

Literature presents some articles describing the preparation of silica gel doped with silver nanoparticles. The aim of these articles is mainly focused on the preparation of antifouling and anti-mold devices or coatings, that exploit the combination of the porous structure of silica gel matrix and the release of silver ion as antiseptic agent. AgNPs can be introduced inside the monolith before the formation of the monolith by direct introduction of NPs in

the gelling solution or after the formation of the monolith by chemical or photoinduced reduction of silver ions inside the structure. Green synthesis of AgNPs is usually employed for these preparations, because this allows the as-produced NPs to not react/aggregate inside the gelling solution thanks to their thick coating of organic matter. However, this kind of syntheses has the big drawback of lack of reproducibility and heterogeneous distribution of the size and shape of the nanoparticles.[38;39]

2.2 EXPERIMENTAL DETAILS

2.2.1 Material and instrumentation

2.2.1.1 Reagents

Silver nitrate ACS reagent, 99.0%; Gold(III) Chloride solution 99.9%; (30 wt % in dilute HCl); Sodium borohydride ≥98.0%; L-ascorbic acid ≥99.0%; poly(ethylene glycol) methyl ether thiol (HS-PEG-Ome, MW 2000 and MW 750); Triton^{TM} x-100 (laboratory grade); Tetrahydrofuran, ≥99.9%, Merck life and Sciences (Milano Italy); SYLGARD^{TM} 184 Silicone elastomer Kit was supplied by Dow Chemical (Midland, MI, USA); potassium hexacyanoferrate(II), ≥98.5%, Merck life and Sciences (Milano Italy); Iron(III) Chloride, 97%, Merck life and Sciences (Milano Italy); Iron(III) nitrate nonahydrate, Merck life and Sciences (Milano Italy); Hydroquinone, 99.0%, Merck life and Sciences (Milano Italy); N,N-Dimethylformamide, >99.0% Sigma Aldrich; tetramethyl orthosilicate (TMOS), 98%, Merck life and Sciences (Milano Italy); tetraethyl orthosilicate, ≥99.0%, Merck life and Sciences (Milano Italy); sodium chloride, >99.5%, Merck life and Sciences (Milano Italy); cetrimonium bromide (CTAB) , Merck life and Sciences (Milano Italy); methanol, HPLC gradient grade, >99.9%, Merck life and Sciences (Milano Italy); Cysteamine hydrochloride, 97%, Sigma Aldrich; Sodium Hydroxide ≥98%, pellets; nitric acid ≥65%; Hydrochloric acid ≥37% have all been bought by Merck Life Sciences, Milano, Italy, and used without further purification.

2.2.1.2 Glassware pre-treatment

All the glassware used in the synthesis was pre-treated with aqua regia (acid solution 3:1 HCl(37%):HNO_3(65%)) for 15 minutes and then washed three times with bidistilled water in an ultrasound bath for 5 minutes.

2.2.1.3 Instrumental procedures

Ultracentrifugation

Ultracentrifugation was carried out using the ultracentrifuge Hermle Z366 with polypropylene 10 mL tubes or 1.5 mL Eppendorf.

Ultrafiltration (Falcon and peristaltic pump)

Ultrafiltration was carried out using the ultracentrifuge Hermle Z366 with the falcon rotor and centrifugal filters Ultracel^{R}-10K. It was also used a molecular weight cut off filter

(MWCO 5000) with peristaltic pump to concentrate and purification of nanoparticle solutions.

pH measurement

Measurement of pH was carried out with a XS Instruments pH-meter (pH 50 model) with a Thermo Scientific Orion 91022 BNWP combined glass electrode. Electrode calibration was carried out before measurements, with buffer solutions at pH=4, pH=7 and pH=10.

UV-Vis-NIR Spectroscopy

Absorption spectra were collected on a Varian Cary 60 Spectrophotometer, either in 1 mm or 1 cm optical glass cuvettes.

FT-IR Spectroscopy

Vibrational Analysis was performed through FTIR Nicolet™ iS™ 50 by Thermo Fisher Scientific, employing the ATR accessory equipped with a diamond crystal as internal reflection element (IRE). Spectra were recorded in absorbance ranging from 4000 to 400 cm^{-1} with 4 cm^{-1} in resolution.

Transmission Electron Microscopy (TEM)

Colloidal solutions were diluted 10-100 times with bidistilled water and 10 µL were dropped on nickel grids (300 mesh) covered with a Parlodion membrane and dried in a desiccator. Images were acquired by using a JEOL JEM-1200 EX II 140 microscope with a 100kV acceleration voltage.

Scanning Electron Microscopy

Samples were sputtered with gold and observed with a ZEISS EVO MA10 microscope (Carl Zeiss, Oberkochen Germany). Images were collected in high vacuum, at room temperature at different magnifications. It was also used a field-scanning electron microscope, provided with a Schottky ZEISS Meriln ® source and column GEMINI II, was used for the analysis of the samples structure and morphology at the ENEA Lab in Brindisi.

Determination of Ag by ICP-OES spectroscopy

The total silver removed from a monolith is analyzed by ICP directly on the washing solution. The removal of silver is made by one of the following methods; i) treatment with nitric acid 63% (U.P.); ii) treatment with a solution 0.1 M of Cysteamine Hydrochloride (and Ag oxidation by O_2); treatment with a solution of iron(III) nitrate 0.1 M. The washing process is made by dipping the monolith inside the solution and left to

react till the monolith becomes colorless. The monolith was kept dipped in the solution for further 48 h. The same operation is made also on the powder of ground monoliths. The receiving aqueous solutions were separated from the solid (decantation in the case of monoliths, centrifugation in the case of powders). The aqueous samples were analyzed for the metal content by Inductively Coupled Plasma Optical Emission Spectroscopy (ICP-OES) on Perkin Elmer Optima 3300 DV instrument.

Raman spectroscopy

Raman spectra were carried out by means of the Raman spectrometer LabRam HR Evolution by Horiba Scientific, equipped with a continuous laser source of wavelength 633 nm. The beam focused onto the sample by the 100X objective had a diameter of about 2 μm and a maximum power of 17 mW.

Porosimetric analysis

BET surface area analysis was performed by means of the nitrogen surface absorption technique (at the cryogenic temperature of 77 °K) using the AUTOSORB IQ system of the Quantachrome. To eliminate any traces of contaminants absorbed during the exposure to the atmosphere, the samples were initially pre-treated in an oven at a temperature of 60 °C for 24 hours. Subsequently, the various samples were inserted inside the measuring cell for a degassing treatment in vacuum (about 0.1 Torr) at a temperature of 120 °C for 180 minutes with a heating ramp of 10 °C/min. The choice of degassing parameters was carried out to obtain an effective removal of moisture (or any volatile substances) from the surface of the sample without inducing any irreversible change.

XRD Analysis

X-Ray Diffraction analysis of the powders was carried out by means of Multipurpose Empyrean (Malvern-Analytical); diffractometer equipped with Cu anode (Kα = 1.540 Å). The equatorial divergence of the incident X-ray beam was controlled by using a Programmable Divergence Slit (Fixed 0.5°) with antiscatter slit (1°) and with Soller slit (0.04 rad.), while a Soller slit (0.04 rad.) with antiscatter slit (7.5 mm) were placed in front of the detector. The samples were placed on a sample stage for powders in spinning active mode (rotation time 16 s). A 2D solid-state hybrid pixel (PIXcel^{3D}) was used as detector.

2.2.2 Nanoparticles preparation

2.2.2.1 Citrate silver nanoparticles of 7 nm diameter

Silver nanoparticles capped with citrate with a diameter between 7 and 10 nm were prepared using a synthesis optimized by our laboratory.[40] Prepare: 10 ml of 1% w/v $AgNO_3$ solution; 10 ml of 1% w/v sodium citrate solution; 5 ml of a 0.075% solution in $NaBH_4$ and 1% w in sodium citrate. 100 mL of bidistilled water and the reducing solution are separately cooled in an ice bath for at least 20 minutes. Subsequently, the following additions are made to the volume of water under vigorous stirring: 1 mL of $AgNO_3$, 1 mL of citrate and after a minute 0.5 mL of ice-cold reducing solution. The stirring is suspended to avoid aggregation phenomena and the solution is allowed to return to room temperature.

2.2.2.2 Citrate silver nanoparticles of 100 nm diameter

AgNPs with average size of 100 nm were synthesized by a seed growth method inspired by the work of Xing Et al. "Size Control Synthesis of Monodisperse, Quasi-Spherical Silver Nanoparticles to Realize Surface-Enhanced Raman Scattering Uniformity and Reproducibility".[41] SEED preparation: Typically, 1 mL of an aqueous solution of sodium citrate (1 wt %), 0.25 mL of an aqueous $AgNO_3$ solution (1 wt %), and 0.2 mL of an aqueous NaCl solution (20 mM) were successively added to 1.05 mL of water under stirring at room temperature. After 5 min of premixing, the citrate-silver-NaCl premixture was quickly added into 47.5 mL of the boiling water. 1 minute before the addition of the citrate silver-NaCl premixture, 80 µL of the aqueous AA (ascorbic acid) solution (0.1 M) are added. After heating and stirring for 1 h, the resulting solution was allowed to cool to room temperature, and a dispersion containing AgNPs with a bright yellow color was finally obtained. GROWTH: The solution of silver−ammonia complex was first prepared for the synthesis of Ag NPs. Typically, 2 mL of the aqueous $AgNO_3$ solution (1 wt %) was mixed with 800 µL of ammonia water (25− 28%). For the synthesis of 100 nm Ag NPs, typically, 2 mL of the original solution of AgNP seeds was added into water (47.5 mL) under stirring in a 250 mL flask at room temperature. Subsequently, the aqueous solution of the silver−ammonia complex (700 µL, 43 mM) and aqueous AA solution (20 mL, 2.5 mM) were added into the flask in succession. After vigorous stirring for 1 h, the resulting Ag NPs were concentrated by the centrifugation (10K rpm, 10 minutes) and redispersed in the aqueous solution (40 mL) and PEGylated (PEG_{2K}-SH) for 1 night.

2.2.2.3 Citrate Gold nanoparticles of 20 nm diameter

The gold nanoparticles were synthesized according to the Turkevich method. A solution obtained by placing 87 µl of a stock solution is brought to the boil of tetrachloroauric acid (1.44 M) in 500 ml of bidistilled water. The heating is then turned off and, under magnetic stirring, are added 25 ml of a 1.7×10^{-2} M solution of sodium citrate dihydrate. The solution's color turns to gray, to purple and finally to red; it is left under stirring for two and a half hours.

2.2.2.4 Citrate Gold nanoparticles of 100 nm diameter

AuNPs with average size of 100 nm were synthesized by seed growth method inspired by the article of Li Et al. "*Controllable synthesis of stable urchin-like gold nanoparticles using hydroquinone to tune the reactivity of gold chloride*".[42] GOLD SEED: The spherical gold seeds were synthesized using citrate as reductant and stabilized. 183 µL HAuCl4 solution (0.041 M) was put into a flask with 30 mL of deionized water and heated to boil with magnetic stirring. When the solution was boiling, 900 µL of 1 w/v% sodium citrate aqueous solution was added. The reaction mixture was kept at its boiling point until the solution became red-burgundy in color. The solution was then cooled under magnetic stirring to allow the full formation of the spherical gold seeds. The seeds solution was used within 1 day after preparation.

GROWTH: A 30 mM hydroquinone aqueous solution was prepared by dissolving 33 mg of solid hydroquinone in 10 mL of bidistilled water. This solution was used within 1 day. For a typical synthesis , to obtain AuNPs with an approximate diameter of 100 nm, 610 µL of aqueous HAuCl4 (0.041 M) was put into 96 mL of deionized water under vigorous stirring, and, subsequently, 500 µL of gold seeds, 220 µL of 1% sodium citrate, and 1 mL of 30 mM hydroquinone were added in sequence. The solution was kept under stirring at room temperature for 30 min.

2.2.2.5 Citrate Prussian blue nanocubes 40 nm diameter

The fallowing solution are prepared:

- 100 mL of a solution of 1 mM $FeCl_3$ and 5 mM citric acid;
- 100 mL of a 1 mM solution of $K_4[Fe(CN)_6]$ and 5 mM citric acid.

The two solutions are thermostated at 60°C, once the temperature is reached, they are combined under stirring and left to thermostat for another 5 minutes. Subsequently the solution is allowed to return at room temperature. The product is ultracentrifuged at 13000 rpm for 25 minutes and the collected pellet is redispersed in 10 mL to obtain a more concentrated product with a more homogeneous dimensional distribution.

2.2.2.6 Triton-X 100 Gold nanostars

The preparation of Au Nanostars was carried out according to a seed growth method developed by our group.[43] A seed solution was obtained by mixing 5.0 mL of 0.2 M Triton X-100 with 5.0 mL of 0.5 mM $HauCl_4$ and quickly adding 600 µL of ice cooled 0.01 M $NaBH_4$.The resulting light orange solution (containing spheroidal AuNP with d < 5nm) was kept in an ice bath and used within 1 hour. For the growth process, 50 mL of 0.2 M Triton X-100 were put in a 250 mL flask under magnetic stirring at room temperature and then the following addictions were made in fast and sequential fashion: 2.5 mL $AgNO_3$ 4 mM, 50 mL $HauCl_4$ 1 M, 1.7 mL ascorbic acid 78.8 mM and finally 120 µL of a freshly prepared seed solution. The solution quickly turned from pale yellow to colorless and, after the last addition, to violet and eventually blue-black color, after that stirring was stopped.

2.2.2.7 Pegylation of Metal nanoparticles with PEG Thiols

7 nm AgNPs were functionalized with PEG_{750}-SH, 100 nm AgNPs, 18 nm AuNPs, 100 nm AuNPs and GNS were functionalized with PEG_{2000}-SH. The capping citrate anion is replaced with PEG-SH by adding a quantity of PEG-SH (of the chosen mw) as a solid in 100 mL of NPs solution to have a small excess of ligand (typical PEG-SH concentration = 10^{-5} M was used for all kind of nanoparticles). It is left to react by keeping the container closed for 24 hours under stirring. The pegilated NP are subsequently purified by ultracentrifugation. For the smaller nanoparticles (AgNPs 7nm) ultrafiltration is used: a filter with MWCO=5000 connected to a peristaltic pump allows concentrations processes followed by additions of fresh solvent to eliminate excess reaction products and coater. In a typical ultrafiltration process, a volume of 100 mL of pegylated AgNP is concentrated to 25 mL.

2.2.3 Silica Gel Monoliths preparation

2.2.3.1 TEOS Silica gel monoliths

Silica gel was prepared by poly-condensation and hydrolysis of precursor TEOS (Tetraethyl orthosilicate) under acidic conditions.[44] Ethanol (9.5 ml) was added to precursor TEOS (7.8 ml), followed by gradual addition of triflic acid (3 ml of 0.04 M) and aqueous solution of 1:4 concentrated PEG_{750}-S@AgNPs 7 nm (0.5 mL). The solution was divided in 4 vials: 2 were left at room temperature and 2 were put at 40°C for a week. The as prepared monoliths were not used for the reuptake experiments.

2.2.3.2 TMOS Silica Gel monoliths with CTAB

TMOS was used as precursor to improve the reaction speed and CTAB was used as Dynamic control chemical additive (DDCA) additive inspired by the article Rottman Et al. "*Surfactant-induced modification of dopants reactivity in sol-gel matrixes"*.[45;46] Silica gel was prepared by poly-condensation and hydrolysis of precursor TMOS under basic conditions. In a beaker are added in sequence: 2.5 mL of PEG_{750}-SH@AgNPs 7 nm solution; 2.5 mL TMOS (Tetramethyl orthosilicate); 2.5 mL of methanol; add 0.5 mL of CTAB solution (0.9 g in 10 mL of methanol). To catalyze the gelation process 100 µL of $5*10^{-2}$ M NaOH are added. After stirring for 5 minutes, the wells of a 24 multiwell are filled with 0.5 mL of the solution, covered with parafilm, and left to gel at room temperature for 3 days. Then, pinholes are made on parafilm, and another three days are spent for the aging process. Finally, multiwell is put in oven at 70 ° C for 24 hours to eliminate the solvent residues.

2.2.3.3 TMOS Silica Gel monoliths with DMF

DMF was used as DDCA additive in the preparation of TMOS in basic catalysis inspired by the article of Adachi Et al. *"The role of N,N-dimethyformamide, a DCCA, in the formation of sol gel silica monoliths by sol gel method"*.[47] In a beaker are added in sequence: 2.5 mL of PEG_{750}-SH@AgNPs 7 nm solution; 2.5 mL TMOS (Tetramethyl orthosilicate); 2.5 mL of methanol; 1 mL of DMF (N,N-Dimethylformamide as dynamic control chemical additive). To catalyze the gelation process 100 µL of $5*10^{-2}$ M NaOH are added. After stirring for 5 minutes, the wells of a 24 multiwell are filled with 0.5 mL of the solution, covered with parafilm, and left to gel at room temperature for 3 days. Then, pinholes are made on parafilm, and another three days are spent for the aging

process. Finally, multiwell is put in oven at 70 ° C for 24 hours to eliminate the solvent residues.

2.2.3.4 Preparation of monoliths at different AgNPs 7 nm concentrations

A starting solution of AgNPs $5.78*10^{-4}$ M (in Ag) is concentrated 4 and 10 times by ultrafiltration. Starting from 100 mL of a stock solution, the volume is reduced to 25 mL by ultrafiltration with MWCO (mwco=5K) filter and peristaltic pump. To further concentrate the solution up to 10 times, an ultrafiltration step with falcon tubes (10K filters) is used on the 4 times concentrated AgNPs (10 minutes at 4500 rcf). The concentration steps lead to silver losses; therefore, the final concentration was measured by ICP analysis.

2.2.3.5 Preparation of monoliths at different AuNPs 20 nm concentrations

A starting solution of PEG_{2000}-S@AuNPs $2.38*10^{-4}$ M (in Au) can be concentrated by ultracentrifugation (25 minutes, 13K rpm) for a maximum of 100 times. Monoliths were prepared using the starting PEG_{2000}-S@AuNPs solution, 20x and 100x concentrated PEG_{2000}-S@AuNPs solutions. In a beaker are added in sequence: 2.5 mL of PEG_{2000}-S@AuNPs solution; 2.5 mL TMOS (Tetramethyl orthosilicate); 2.5 mL of methanol; 1 mL of DMF (N,N-Dimethylformamide as dynamic control chemical additive).To catalyze the gelation process 100 µL of $5*10^{-2}$ M NaOH are added. After stirring for 5 minutes, the wells of a 24 multiwell are filled with 0.5 mL of the solution, covered with parafilm, and left to gel at room temperature for 3 days. Then, pinholes are made on parafilm, and another three days are spent for the aging process. Finally, multiwell is put in oven at 70 ° C for 24 hours to eliminate the solvent residues.

2.2.3.6 Preparation of monoliths doped with Gold Nanostars

A starting solution of PEG_{2000}-S@GNS is concentrated by ultracentrifugation (25 minutes, 13K rpm) 100 times. In a beaker are added in sequence: 1 mL of GNS solution; 1 mL TMOS (Tetramethyl orthosilicate); 1 mL of methanol; 0.33 mL of DMF (N,N-Dimethylformamide as dynamic control chemical additive). To catalyze the gelation process 33 µL of $5*10^{-2}$ M NaOH are added. After stirring for 5 minutes, the wells of a 24 multiwell are filled with 0.5 mL of the solution, covered with parafilm, and left to gel at room temperature for 3 days. Then, pinholes are made on parafilm, and another three days are spent for the aging process. Finally, multiwell is put in oven at 70 ° C for 24 hours to eliminate the solvent residues.

2.2.3.6 Preparation of AuNPs 100 nm doped Silica Gel Monolith

The colloidal solution of PEGylated PEG_{2000}-S@AuNPs was concentrated using centrifugation (13K rpm, 5 minutes), removal of the supernatant and redissolution in a small volume of bidistillated water. In particular 100 mL were concentrated to 2.5 mL. The solution was then poured into a beaker and magnetically stirred. To the aqueous suspension 1 mL TMOS, 1 mL Methanol, 0.4 mL of DMF and 40 µL of NaOH 0.05M were added in sequence. After stirring for 5 minutes, the wells of a 24 multiwell were filled with 0.5 mL of the solution, covered with parafilm, and left on a slowly moving reciprocating shaker for 1 night. The monoliths were allowed to form a gel at room temperature for 3 days. Then, pinholes were made on parafilm, and another three days were allowed for the aging process. Finally, multiwell were put in oven at 70 ° C for 24 hours to eliminate the solvent residues.

2.2.3.7 Preparation of AgNPs 100 nm doped Silica Gel Monolith

The suspension of PEGylated PEG_{2000}-S@AgNPs was concentrated by centrifugation (13K rpm, 5 minutes) from 100 mL to 2.5 mL, as described above. The solution was then transferred into a Beaker and magnetically stirred. Then, to the aqueous suspension were added in sequence: 1 mL TMOS, 1 mL Methanol, 0.4 mL of DMF and 40 µL of NaOH 0.05M. After stirring for 5 minutes, the wells of a 24 multiwell were filled with 0.5 mL of the solution, covered with parafilm, and left on a reciprocating shaker for 1 night. The monoliths were allowed to complete gelification at room temperature for 3 days. Then, pinholes were made on parafilm, and three more days were allowed for the ageing. Finally, the multiwell plate was put in an oven at 70 ° C for 24 hours to eliminate the solvent residues.

2.2.3.8 TMOS Silica Gel monoliths with Prussian Blue Nanoparticles

In a beaker were added in sequence: 2.5 mL of citrate-coated PBNPs solution; 2.5 mL TMOS (Tetramethyl orthosilicate); 2.5 mL of methanol; 1 mL of DMF (N,N-Dimethylformamide as dynamic control chemical additive). To catalyze the gelation process 100 µL of $5*10^{-2}$ M HNO_3 are added (basic conditions lead to a fast decomposition of PB). After stirring for 1 hour, the wells of a 24 multiwell were filled with 0.5 mL each of the solution, covered with parafilm, and allowed to gel at room temperature for 10 days. Then, pinholes were made on parafilm, and further three days

were allowed to complete the process. Finally, the multiwell plate was heated in oven at 70 ° C for 24 hours to eliminate the solvent residues.

2.2.3.9 Preparation of Blank monoliths starting from TMOS precursor

Blank monoliths are samples without template nanoparticles used to see the behavior of only silica matrix in different experiments. The synthesis was the same of the other gels but using the same volume of bidistilled water instead of aqueous NPs solution. The obtained monoliths were colorless, transparent, and crack free.

2.2.4 Oxidation of template Nanoparticles inside monoliths

2.2.4.1 Removal of AgNP templates from monoliths

The removal of templating AgNPs is carried out by slow immersion of the monolith in the washing (i.e. oxidizing) solution. The used washing solutions were: i) cysteamine hydrochloride 0.1 M; ii) 0.1 M ferric nitrate; iii) HNO_3 63%. Using nitric acid, a complete discoloration of the monoliths was observed within 5 minutes. The washing processes with cysteamine hydrochloride and ferric nitrate were slower and it took from 1 to 3 days to observe the complete monolith decoloration, depending on the concentration of NPs in the monolith.

2.2.4.2 Removal of AuNP templates from monoliths

The removal of template AuNPs was carried out by slow immersion of the monolith in a solution of aqua regia. The gold oxidation reaction took place in about 1 minute, with the monolith becoming colorless.

2.2.4.3 Oxidative kinetic of AgNPs by cysteamine hydrochloride and ferric nitrate

The Uv-Vis spectra were made on the monoliths prepared with “standard concentration” NP (i.e. NP obtained from standard syntheses, without additional concentrations steps). Such monoliths have a sufficiently low absorbance to avoid saturation when examined in a spectrophotometer. For recording a UV-Vis spectrum of a monolith as such, a 1 cm plastic cuvette (Blank against air) is used as a support and container. The spectrophotometric kinetics were carried out in a 1 cm plastic cuvette (Blank against

water) filled by the washing solution (cys HCl 0.1 M or $Fe(NO_3)_3$) in which the monolith was then gently placed, being careful not to cause cracks. The kinetics lasted 2 hours. Noticeably, it was impossible to record kinetics using HNO_3 as washing solution, due to the too fast process.

2.2.5 Reuptake process of AgNPs 7 nm diameter

2.2.5.1 Grinding monoliths

The monoliths were ground both by ball milling (300 rpm 10 minutes) and by mortar and pestle to increase the exposed surface of the solid, i.e. to allow NPs to reach also the internal cavities of the material (not reachable in the monoliths).

2.2.5.2 Removal of template NPs in ground monoliths

The NPs removal on the powders of ground monoliths was carried out by washing with HNO_3 63% (AgNPs case) or acqua regia (AuNPs and nanostars). The ground powder was subsequently separated from the acid solution by ultracentrifugation. This was followed by 4 rinsing cycles with bidistilled water. The acidic pH favors the oxidation of AgNPs, while basic pH deteriorates the silica matrix. For this reason, the solid was redispersed in water and microaddition of 0.1 M NaOH were used to brought it to neutrality. The solid was centrifuged 3 times and dried in an oven at 70°C for one night.

2.2.5.3 Reuptake process of AgNPs 7 nm by monolith powder in suspension

The process was carried out by stirring an amount of ground powder (equivalent to the weight of a monolith = 0.16g) in a vial, in the presence of the starting AgNPs solution with controlled stirring time (500 rpm, 1 hour). The solid powder was then removed by centrifugation (2 cycles: first 5min at 13K rpm; second: 5 min 15K rpm). Under these conditions, only the ground silica particles and the reuptaken AgNPs adhering to the silica particles fall down in the pellet, while free AgNPs remain in the supernatant. Moreover, the centrifugation process was also made on the starting AgNPs solution only (i.e. with no added silica powder) in order to measure the absorbance in the supernatant, to be used as the reference. By measuring the relative loss of absorbance

$$\Delta abs = (Abs_{AgNPs} - Abs_{reacted}) / Abs_{AgNPs}$$

on the LSPR band of AgNPs allows us to determine the fraction of AgNPs captured by the templated gel particles.

It has to be noted that this kind of procedure was not successful when larger NPs were used. As a matter of fact, under the same ultracentrifugation conditions, most of the AuNPs (18nm), AgNPs (100 nm), AuNPs (100 nm) and AuNS fell down to form a pellet at the bottom of the tube. This did not allow to discriminate between free and reuptaken NPs. The reuptake processes have always been performed using monolith powder ground with mortar and pestle as the ball milling technique does not allow the complete grinding of the solid.

2.2.6 Preparation of functionalized Quartz crystal microbalances sensing system

The functionalization of quartz crystal microbalances (QCMs) was tried on different devices:

- QCMs with silver electrodes, Resonance frequency 10 MHz purchased from RS Components;
- QCMs with silver electrodes, Resonance frequency 20 MHz purchased from RS Components;
- QCMs with Gold electrodes, Resonance frequency 10 MHz purchased from BIOAGE.

The oscillation frequency was measured with a frequency counter AGILENT 53181A 1.5 GHz. The QCM functionalization procedure: application of Kapton mask to avoid the functionalization of the quartz disk; Polydimethylsiloxane (PDMS) solution was prepared mixing elastomer and crosslinker precursors in proportion 1:10 and then dilute in THF to obtain a solution 1%. A layer of PDMS was applied by spin coating (1000 rpm for 5 minutes); 0.01g powder of silica gel was forced through a grid and dropped on the QCM during the spinning (3000 rpm for 1 minute); the Kapton mask was removed and the QCM was put at 70°C overnight.

2.3 RESULTS AND DISCUSSION

2.3.1 Nanoparticles synthesis and characterization

2.3.1.1 Silver nanoparticles of 7 nm diameter

Colloidal solutions of AgNPs with 7 nm diameter were prepared following the procedure described in paragraph 2.2.2.1. The obtained colloid is dark yellow transparent color, presents a sharp LSPR band centered at 394 nm, typical of small, spherical silver nanoparticles. The absorbance value has high values and reaches saturation in a spectrophotometric measurement. Spectra were collected by diluting 1 mL of colloid with 2 mL of bidistilled water. The nanoparticles diameter has been measured by DLS analysis and TEM imaging and it was found an average size of 7.2±4 nm. The colloid shows a negative Z potential of -18 mV due to the citrate coating. The starting solution has a concentration of $5.8*10^{-4}$ M of total silver.

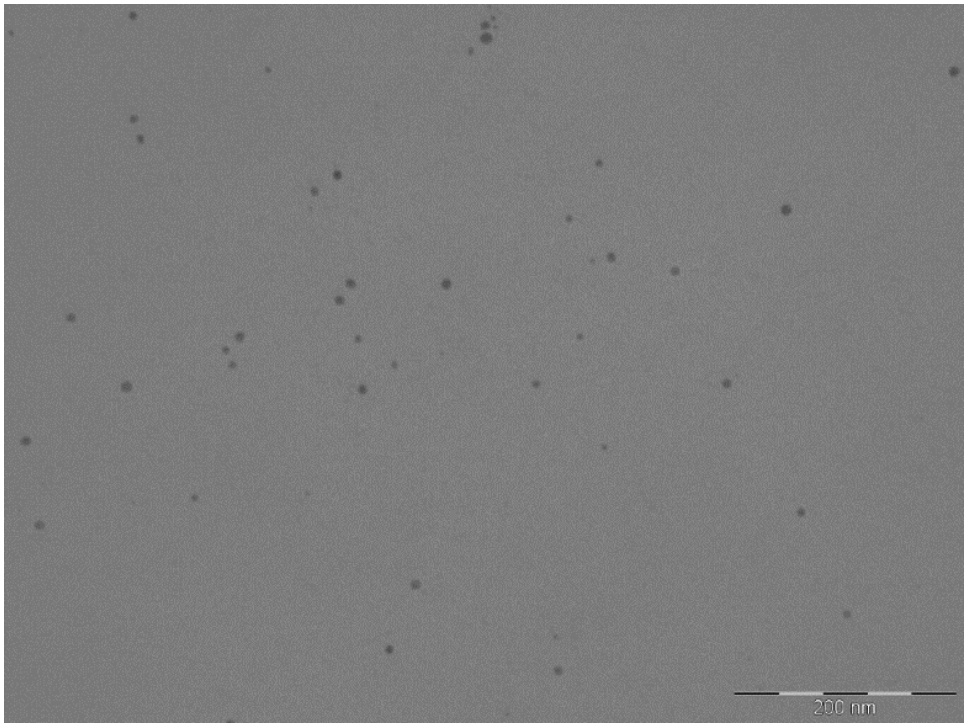

Figure 17 TEM image of citrate@AgNPs.

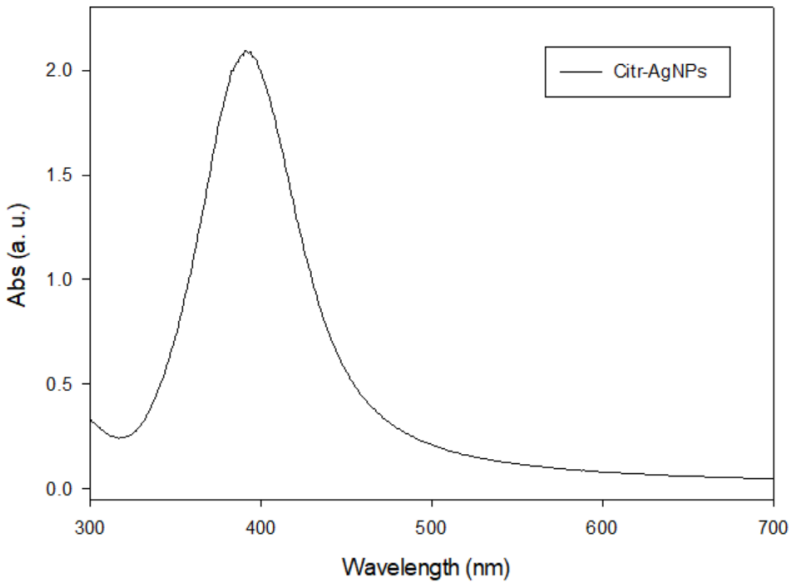

Figure 18 Extinction spectrum of typical citrate@AgNPs solution diluted 1:3.

To improve the NPs stability during the process of inclusion in silica gels, and to allow a further workup for concentrating the particles, a surface coating with PEG thiols (PEGylation step) was carried out with MeO-PEG_{750}-SH. As can be seen by the red shift at 400 nm in the following spectra, the functionalization took place. It was also calculated by TGA analysis that the number of PEG molecules per nanoparticle is ~1570.

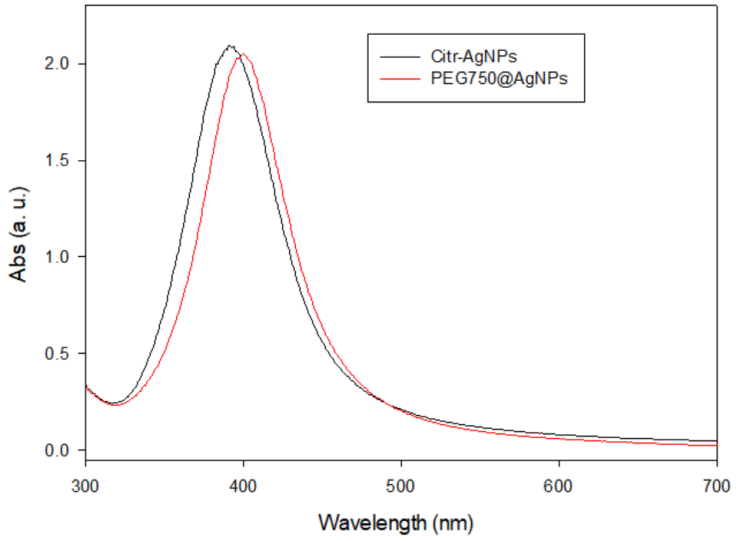

Figure 19 Extinction spectra of PEG_{750}@AgNPs and Citrate@AgNPs, it can be observed the red shift due to the change of coating.

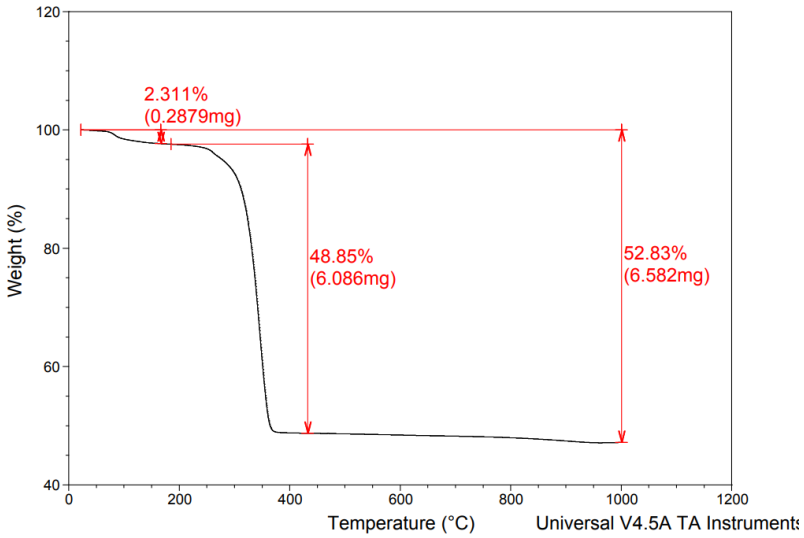

Figure 20 TGA analysis on PEG750@AgNPs. First step (2.311%) is associated to humidity, second step (48.85%) is associated to the $PEG_{750}SH$. The total silver mass is 100-52.83%. From the silver mass, the dimensions of AgNPs (as determined by TEM) and Ag density, the mass of a single AgNP can be calculated. This allows to calculate the total number of AgNPs in the sample, and the moles of AuNPs in the sample. The mol PEG/molAgNPs quotient gives the number of PEG-SH per particle

Nanoparticles were concentrated 4 times and purified by ultrafiltration as described in paragraph 2.2.1.3. The silver concentration of the resulting solution was measured by ICP analysis and resulted $4.66*10^{-4}$ M. The obtained solution was further concentrated by ultracentrifugation to obtain 1 mL of solution (starting colloid 100 times concentrated) with a final concentration of silver $1.12*10^{-2}$ M.

2.3.1.2 Silver nanoparticles 100 nm diameter

The preparation of larger AgNPs is described in paragraph 2.2.2.2. The Seed AgNPs looks like a yellow, slightly turbid solution. The UV-Vis spectrum shows the characteristic LSPR sharp band at 404 nm. From the TEM images it can be said that the NPs have a spheroidal shape, with an average diameter of 40 nm. After the growth process, a green-brown apparently turbid colloidal solution is obtained. The new spectra show 2 large bands with max at 421 and 549 nm, Figure 21C, that is consistent with the absorption spectrum of a colloidal solution of quasi-spherical AgNPs with 100 nm diameter, reported in ref. 39 (the paper that inspired our synthesis). A size of121 nm and a irregular spherical shape are disclosed by TEM images of the colloid, Figure 21B. The apparent turbidity of their solution is a scattering phenomenon, due to the larger dimensions of the particles.

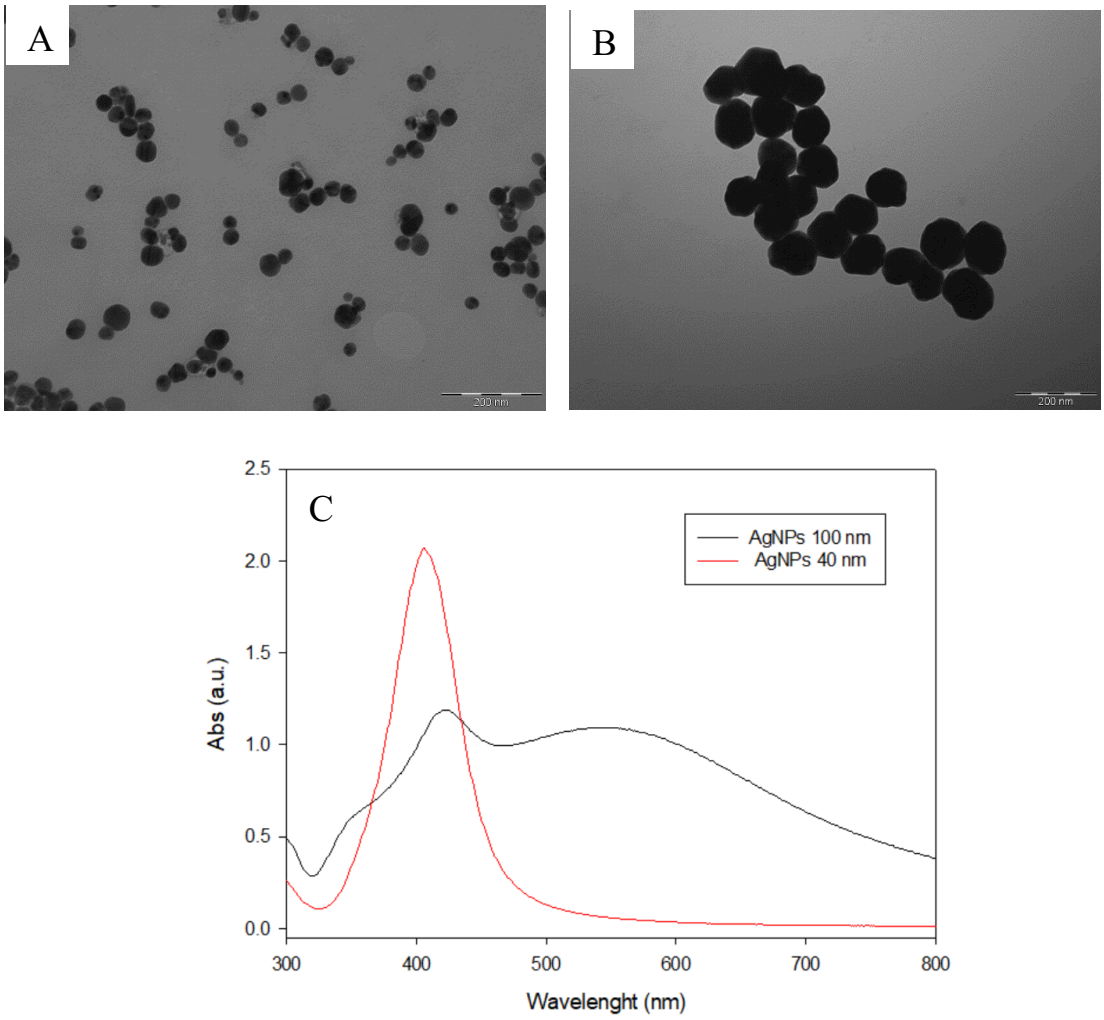

Figure 21 A) TEM image of SEED AgNPs with average size of 40 nm; B) TEM image of Growth AgNPs with average size of 100 nm; C) Extinction spectra of SEED and Growth nanoparticles.

2.3.1.3 Gold nanoparticles of 20 nm diameter

Citrate gold nanoparticles are synthesized following the standard procedure described in paragraph 2.2.2.3 yielding monodisperse spherical nanoparticles with average size of 18nm. UV-Vis spectrum shows the typical LSPR band centered at 519 nm. Full characterization of nanoparticles is performed by TEM images, Z potential and Hydrodynamic diameter measured by DLS. Coherently with the average size calculated from TEM images it is found a Hydrodynamic diameter of 21 nm and a Z potential of -32 mV due to the negative citrate coating.

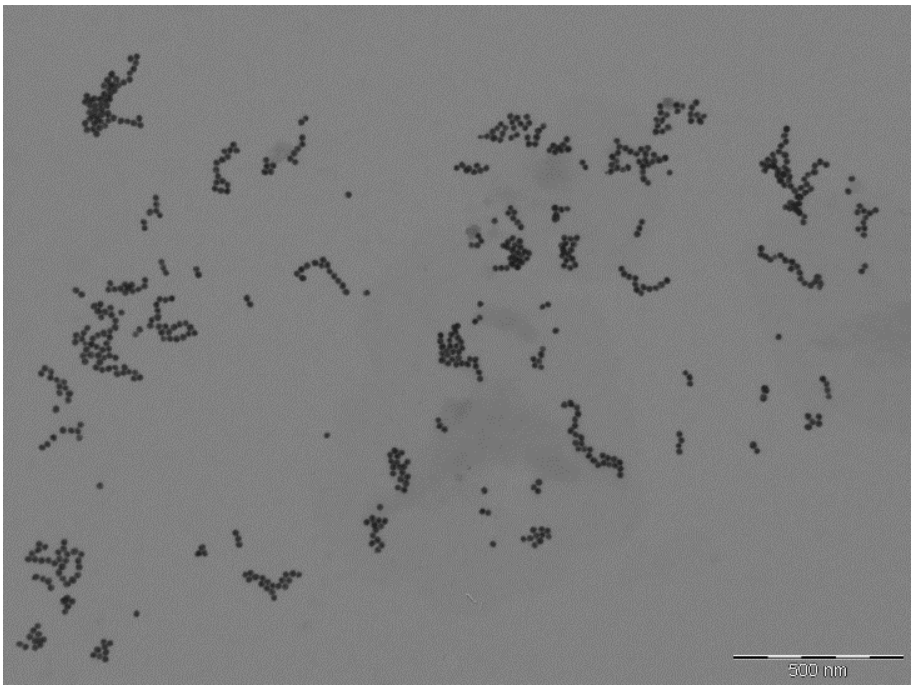

Figure 22 TEM image of citrate@AuNPs of 20 nm diameter

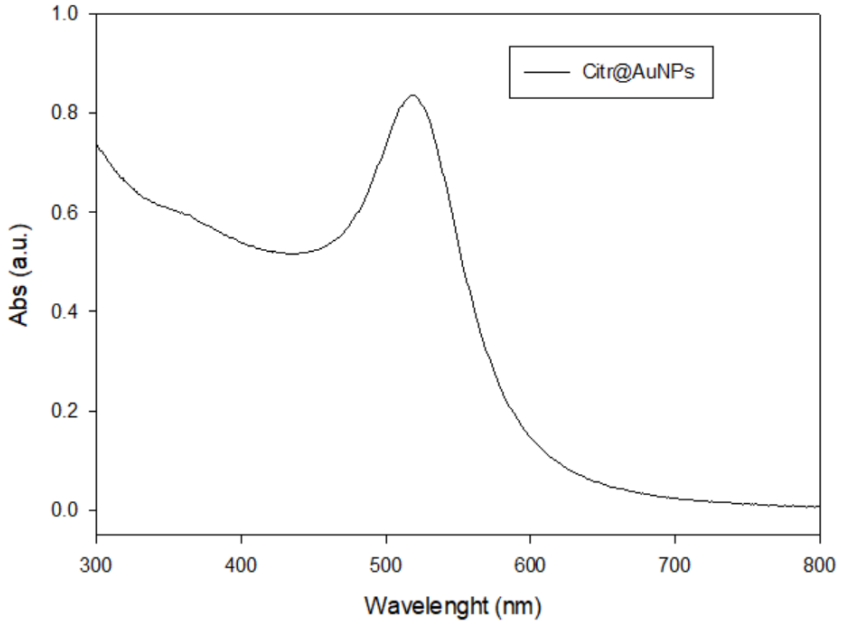

Figure 23 Typical spectrum of Citrate@AuNPs.

Nanoparticles are functionalized with MeO-PEG_{2000}-SH to obtain more stable colloid. The red shift of the LSPR band to 524 nm shows the coating process took place.

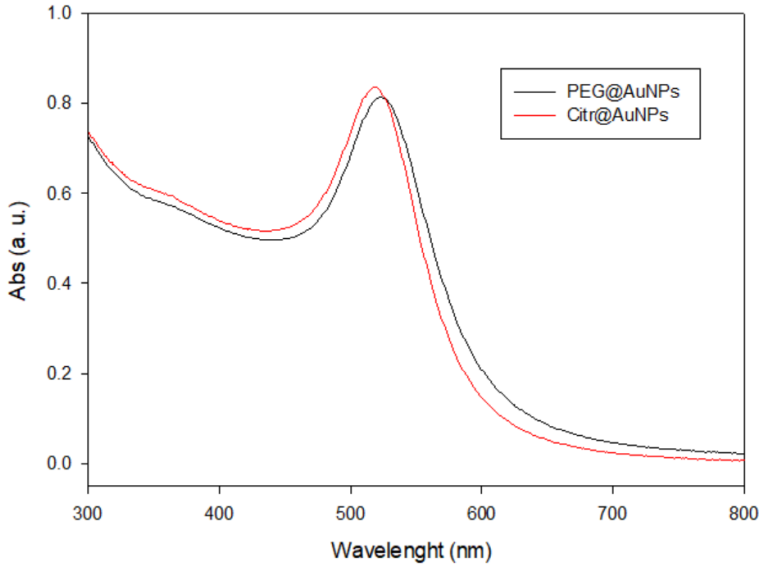

Figure 24 Extinction spectra of PEG_{2000}@AuNPs and Citrate

2.3.1.4 Gold nanoparticles of ~ 100 nm diameter

Citrate-coated AuNPs with ~ 100 nm diameter are synthesized by a seed growth process that use Hydroquinone as reducing agent described in paragraph2.2.2.4. The obtained seed solution has the typical red color and UV-Vis spectrum of the spherical AuNPs of ~20 nm diameter. After the growth process the solution is of turbid blue with purple reflexes color. The UV-Vis spectrum shows a large LSPR band centered at 612 nm. Both seed and growth solutions have been characterized by TEM images and DLS analysis to check the size and shape of the growth product: it consists of spheroidal AuNPs with average diameter of 115 nm.

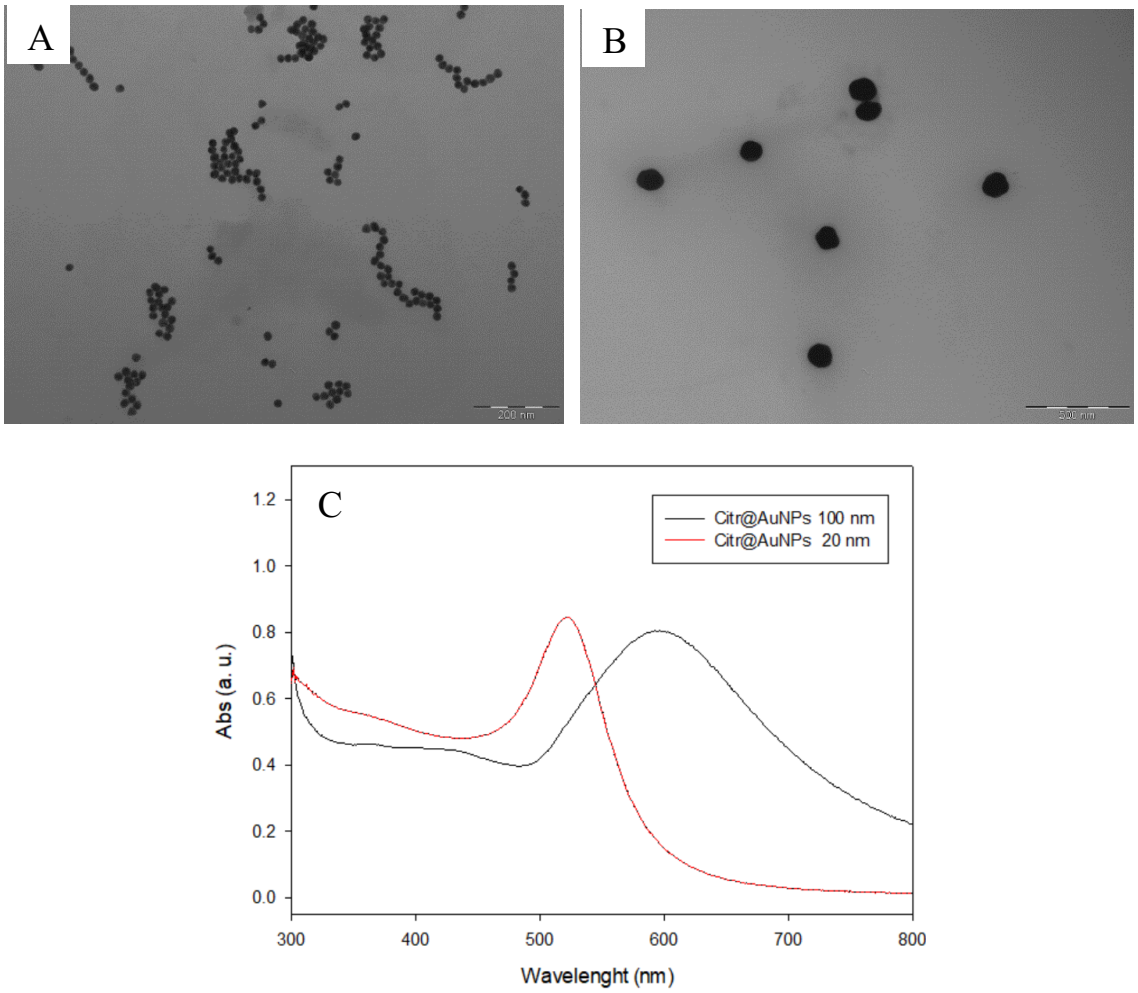

Figure 25 A) TEM image of SEED AuNPs with average size of 20 nm; B) TEM image of growth AuNPs with average size of 115 nm; C) Extinction spectra of SEED and Growth AuNPs.

Nanoparticles are functionalized with MeO-PEG$_{2000}$-SH to obtain a more stable colloid both in the concentration procedures and during the formation of silica gel.

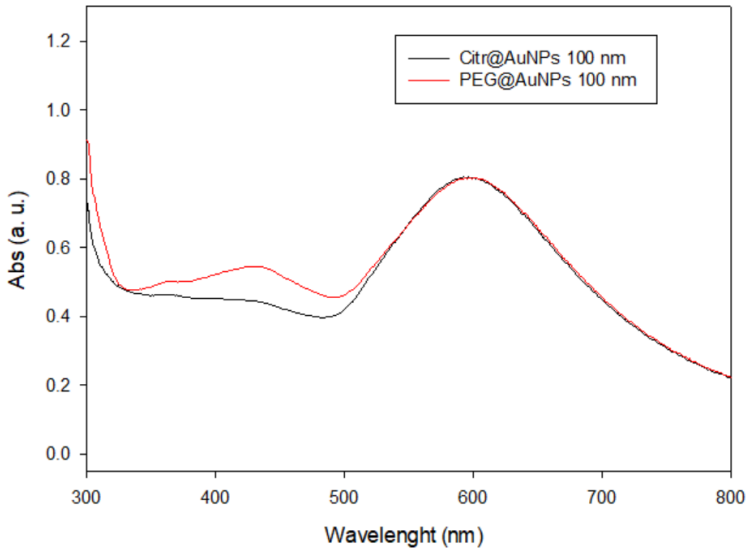

Figure 26 Extinction spectra of Citrate@AuNPs and PEG$_{2000}$@AuNPs.

2.3.1.5 Gold nanostars

Gold nanostars were prepared according to the method developed in our laboratory and described in paragraph 2.2.2.6. The seed-growth synthesis exploits the non-ionic surfactant triton X-100 to direct the anisotropic growth of small, spherical Au seed. The product is a blue-gray solution with multiple LSPR bands. GNS are characterized by TEM images, the solution is mainly made by 5- and 6-branched stars with average size of ~100 nm (tip to tip distance).

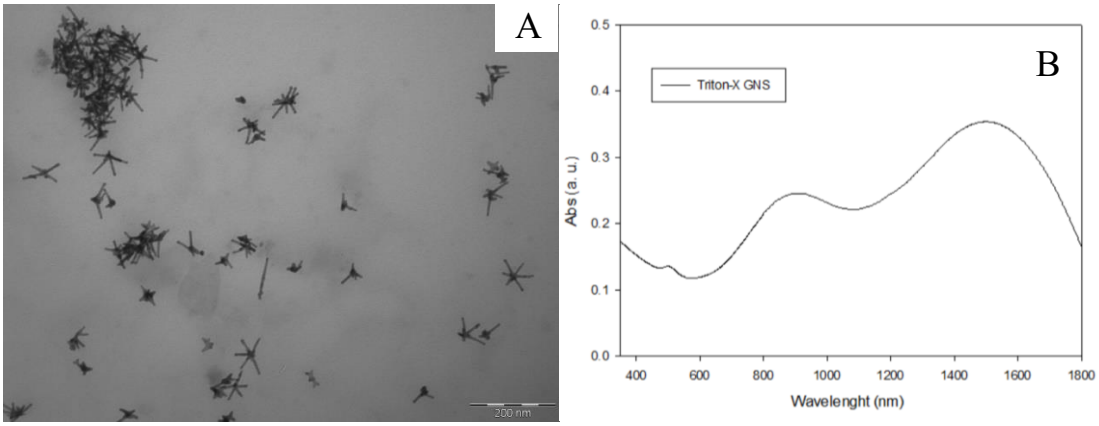

Figure 27 A) TEM image of Golden nanostars; B) Extinction spectrum of golden nanostars.

2.3.1.6 Citrate Prussian blue nanocubes

Prussian blue nanoparticles are synthetized following the method described in paragraph 2.2.2.5 From the UV-Vis spectrum of the solution diluted 100 times it's been observed the classic band centered at 740 nm associated to the electron transfer process between the Iron III and iron II centers. TEM images shows that the product is made up of nanocubes with an average side length of 40 nm.

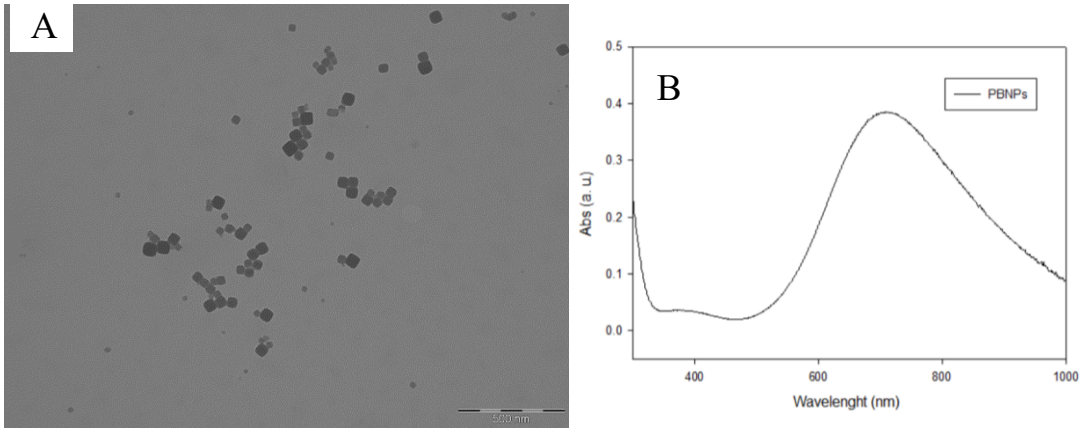

Figure 28 A) TEM image of Prussian blue nanocubes; B) Extinction spectrum of Prussian blue nanoparticles.

2.3.2 Silica Gel monoliths synthesis and characterization

2.3.2.1 TEOS Silica Gel Monoliths doped with metal nanoparticles

The preparation reported in paragraph 2.2.3.1 using TEOS as organosilane precursor and acidic conditions can't be used for the synthesis of silica gel doped with metal nanoparticles. It was performed the synthesis of:

- Silica gel monolith doped with PEG@AgNPs 7 nm diameter: the acidic conditions together the long gelation time of the precursor solution led to the complete oxidation of the nanoparticles. The resulting monolith was colorless. As we used a non oxidating acid (triflic acid), we can conclude that oxidation took place thanks to the $O_2 + 4e^- + 4H^+ \rightleftharpoons 2H_2O$ half reaction ($E° = 1.23$ V), that is favored by acidic conditions.
- Silica gel monolith doped with PEG@AuNPs 20 nm diameter: nanoparticles are inert in the solution environment, but the long gelation time led to an exclusion process of the nanoparticles on the external surface of the monolith. The result monolith was colorless with a gray film or large gray spots on the external surface.

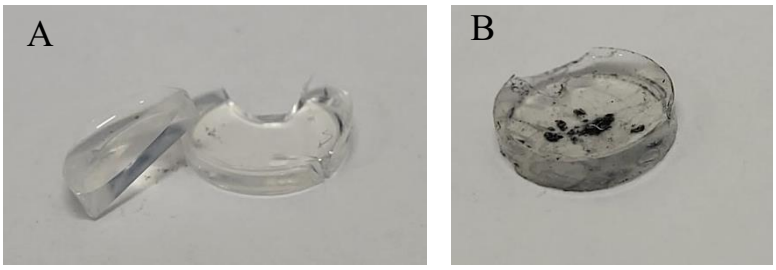

Figure 29 A) TEOS silica gel monolith doped with PEG@AgNPs; B) TEOS silica gel monolith doped with PEG@AuNPs.

2.3.2.2 TMOS Silica Gel monoliths with CTAB doped with AgNPs 7 nm

The use of TMOS as organosilane precursor allows the use of the proportion 1:1:1 methanol:water:TMOS useful for a better regulation of the added AgNPs (the water part of the mixture). The use of basic catalyst NaOH depresses the oxidating ability of atmospheric oxygen and avoid the AgNPs oxidation in the sol. Moreover, the gelation time is reduced. To improve the porosity and avoid the cracks of the material CTAB was used as DCCA (Dynamic Control Chemical Additive). Yellow transparent monoliths almost crack free were produced. Ahe UV-Vis absorption spectrum carried out on the monolith displays the characteristic LSPR band centered at 405 nm, due to the embedded AgNPs. It was also observed that the monoliths slowly loose color and become colorless

with time (the complete discoloration occurs in about 6 months). This process may be due to the presence of Br^- (from CTAB) that together with residual absorbed humidity and air contact promote the AgNPs oxidation, with the formation of the poorly soluble AgBr. From SEM images (Figure 31) it is possible to observe a microporous structure with average size of 5 nm. However, the nanoparticles are too small and diluted in the solid to be observed.

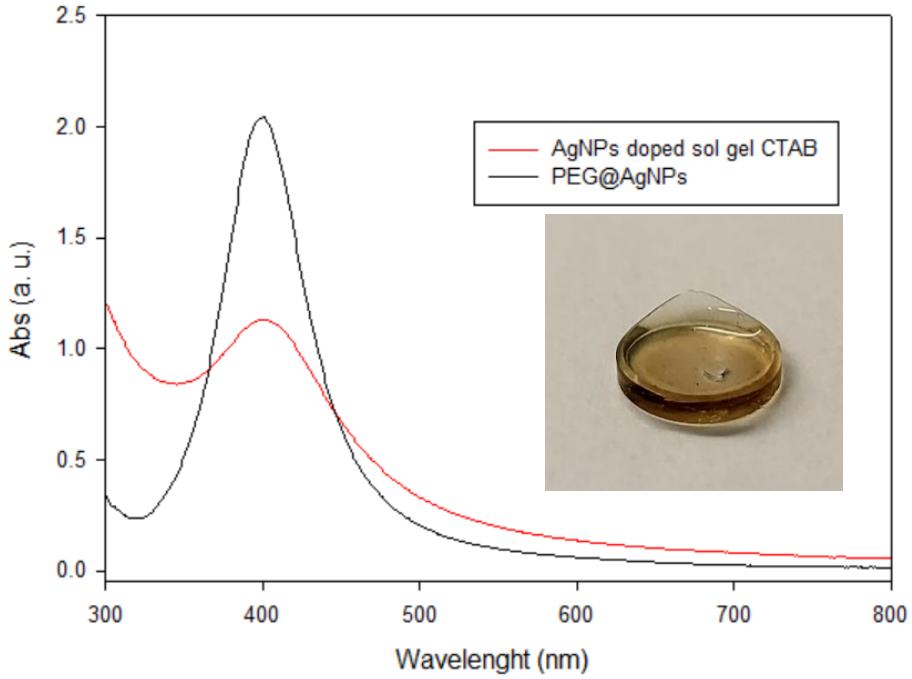

Figure 30 TMOS/CTAB silica gel doped with PEG@AgNPs monolith image and extinction spectrum.

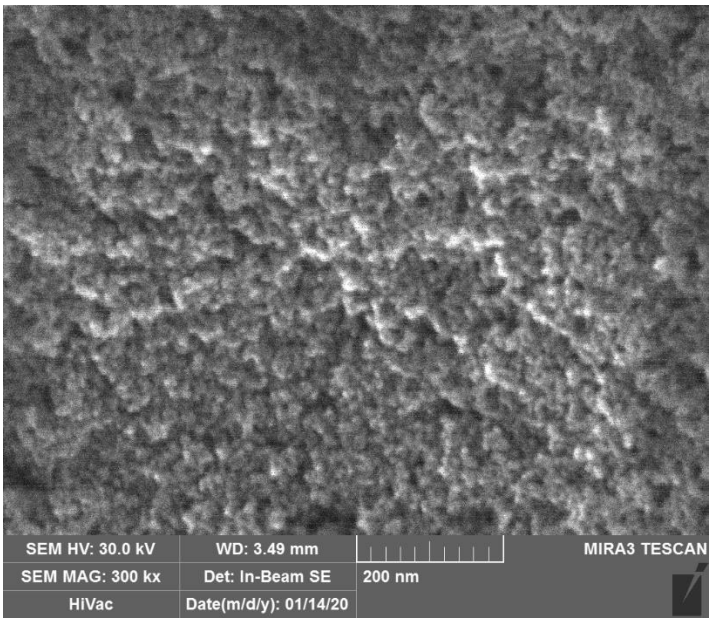

Figure 31 SEM image of TMOS/CTAB silica gel doped with PEG@AgNPs at 300k magnification.

2.3.2.3 TMOS Silica Gel monoliths with DMF doped with AgNPs 7 nm

To avoid the oxidation of the AgNPs inside the monolith over time CTAB was replaced with N,N-Dimethylformamide (DMF) as DCCA. The obtained monoliths were bright yellow and almost crack free, and their UV-Vis spectrum showed the expected LSPR band of AgNPs embedded inside the material. The monolith has diameter of 7 mm and it is 2 mm high, with a mass of 0.076 g. The use of DMF allows the production of monoliths with AgNPs stable inside the structure over time. This preparation was used as standard for the synthesis of nanoparticles doped silica gel monoliths.

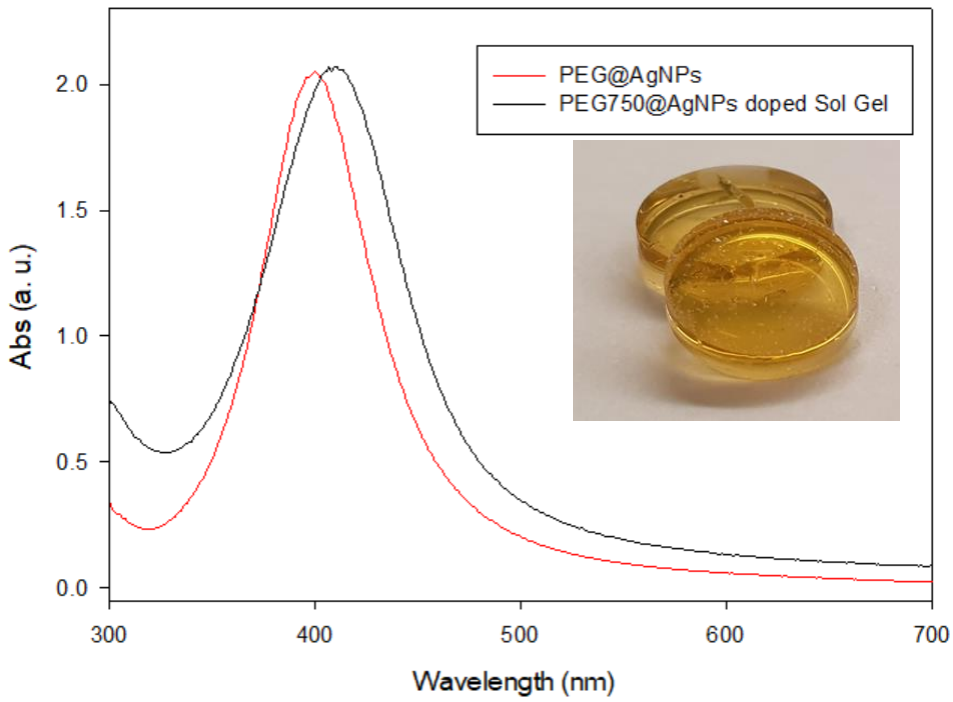

Figure 32 TMOS/DMF silica gel doped with PEG@AgNPs monolith image and extinction spectrum.

SEM imaging was also carried out on the samples, and it was possible to see the microporous structure of the silica gel matrix, but AgNPs were too small and diluted to be observed (Figure 33). To see small AgNPs inside the material and for a better understanding of the impact of their removal from the solid, monoliths were prepared with a higher AgNPs concentration.

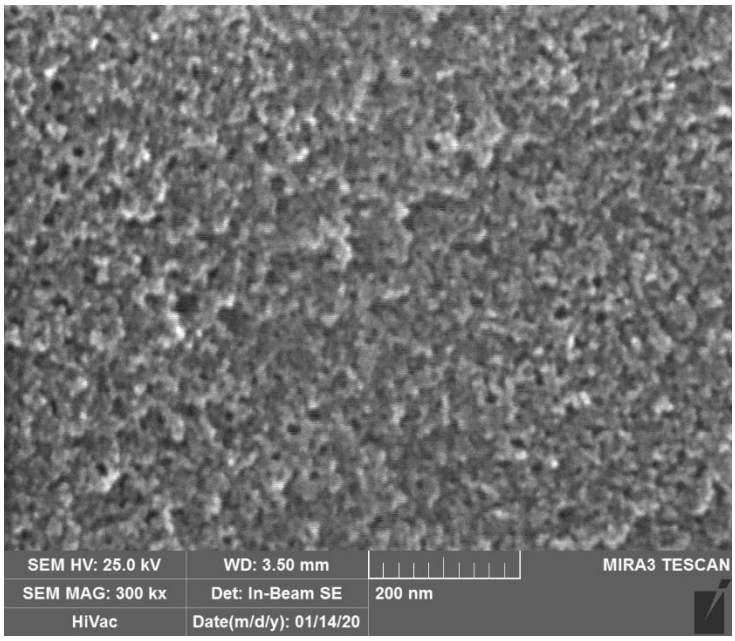

Figure 33 SEM image of TMOS/DMF silica gel doped with PEG@AgNPs at 300k magnification.

It was possible to create 4 times and 100 times concentrated monoliths by using concentrated AgNPs solutions. The resulting monoliths were dark orange, and it was not possible to register the UV-Vis spectrum because of the saturation of the absorbance signal.

AgNPs conc. (NP/L)	$1.15*10^{14}$	$3.33*10^{15}$	$6.68*10^{16}$
Ag tot. (mol/L)	$5.8*10^{-5}$	$4.66*10^{-4}$	$9.3*10^{-3}$

Figure 34 TMOS silica gel AgNPs monoliths at different concentration; Table of monoliths concentration expressed in Total Ag and NPs/L.

2.3.2.4 TMOS silica gel monoliths doped with AuNPs 20 nm

The preparation of silica gel monoliths doped with AuNPs 20 nm was carried out following the procedure described in paragraph 2.2.3.5. The obtained monoliths are red, transparent and almost crack free. The UV-Vis absorption spectrum displays the expected LSPR band of the AuNPs inside the material. It was also possible to create 10 times concentrate monoliths (spectrum not measurable, due to saturation).

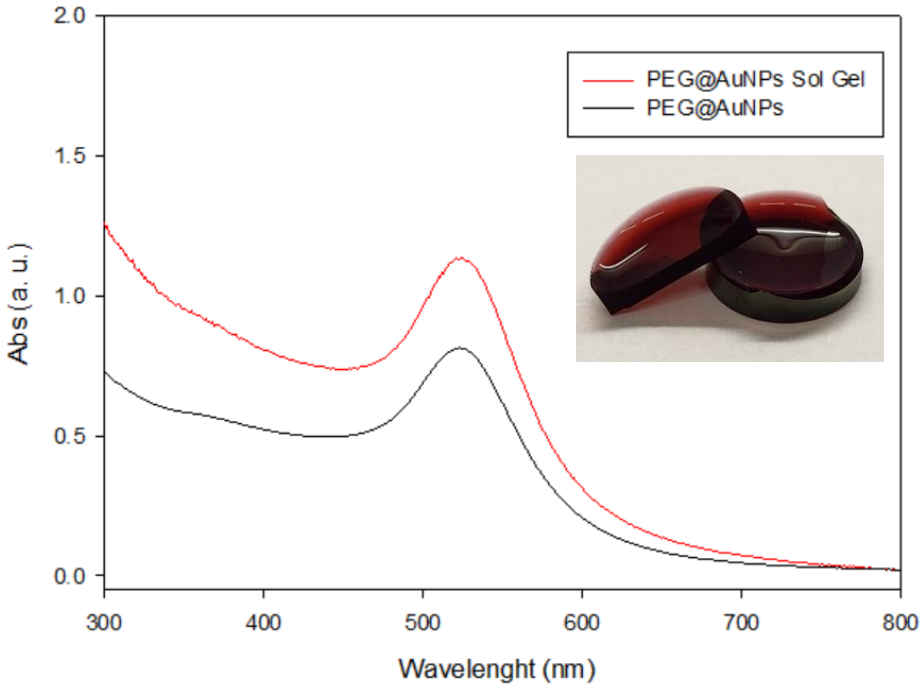

Figure 35 Silica gel doped with PEG@AuNPs monolith image and extinction spectrum.

Interestingly, the absorption spectrum on the monoliths does not show peak enlargement or new bands. This demonstrates that also in the solid the nanoparticles are kept well separated one from the other. This is an important feature, if we wish to use these materials for the selective reuptake of (spherical) nanoparticles, based on their dimensions: collapsed agglomerates of NP would in fact generate large cavities with no specific shape.

2.3.2.5 TMOS silica gel monoliths doped with AuNPs 100 nm

In order to better characterize the monoliths on the imaging point of view, and also to prepare monoliths with larger cavities, we worked to prepare silica gel monoliths with embedded AuNPs of ~100 nm diameter. The obtained monoliths are blue-purple and almost crack-free. The UV-Vis absorption spectrum shows the LSPR band of the AuNPs embedded inside the material, with no significant variation with respect to the same NP dispersed in solution. It was also possible to create monoliths with100 and 1000 times higher concentration, by using concentrated NPs solutions obtained as described by ultracentrifugation processes.

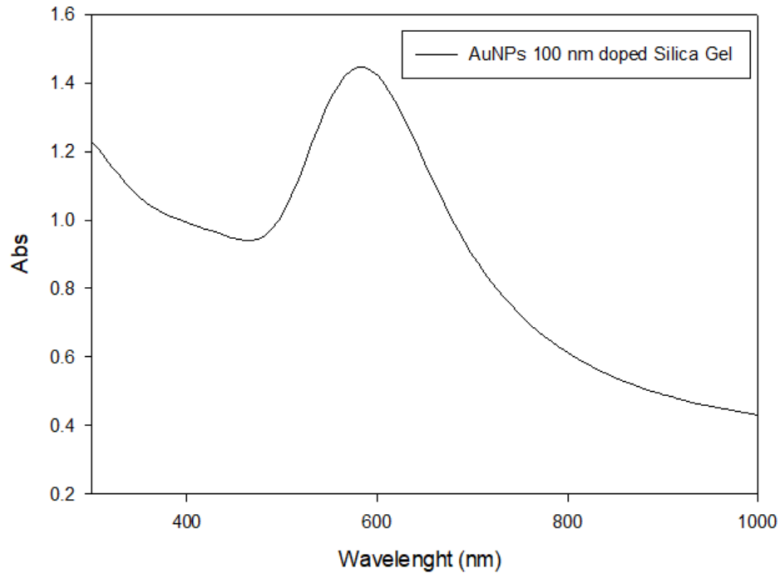

Figure 36 Silica gel doped with 100 nm PEG@AuNPs monolith extinction spectrum.

AuNPs conc. (NP/L)	$7.19*10^{10}$	$7.19*10^{12}$	$7.19*10^{13}$
Au tot. (mol/L)	$2.8*10^{-5}$	$2.8*10^{-3}$	$2.8*10^{-2}$

Figure 37 Silica gel AgNPs monoliths at different concentration; Table of monoliths concentration expressed in Total Ag and NPs/L.

2.3.2.6 TMOS silica gel monoliths doped with AgNPs 100 nm

We also created silica gel monoliths embedding AgNPs with ~ 100 nm diameter. The products are brown-green non-transparent monoliths, almost crack free. In this case, we used Ag $1.5*10^{-2}$ M concentration, and due to this and to the more intense scattering and absorption of these larger AgNP (see Figure 21C) it was not possible to register any UV-Vis spectrum, (it can also be noticed that the solid was not transparent, Figure 38).

Figure 38 silica gel monolith 100 nm AgNPs doped monolith.

2.3.3 Oxidation of template metal nanoparticles

Different strategies were used to remove by oxidation both silver and gold nanoparticles from the silica matrix, using reagent that do not damage the silica matrix.

2.3.3.1 Oxidation process of silver nanoparticles inside silica gel monoliths

In the absence of added agents, the oxidation of silver nanoparticles in water to silver ions is a slow, irreversible reaction that uses the oxygen dissolved in water as an oxidant. The reaction can be accelerated by addiction of reagents such as acids, ligands, or oxidant species.

Cysteamine Hydrochloride solution

From a previous work made in our laboratory it was found that Cysteamine Hydrochloride solution can be used to promote the AgNPs oxidation by O_2 thanks to the formation of complex the species $[Ag(Cys)_2]^+$.[48] The reaction can be summarized as

$$2Ag + ½O_2 + 4HS(CH_2)_2NH_3^+ \rightleftharpoons 2[Ag(S(CH_2)_2NH_3)_2]^+ + 2H^+ + H_2O$$

Thanks to the intrinsic porosity of the silica gel monoliths' structure, the reagents can reach the internal parts of the solid to react with AgNPs. The oxidative removal procedure is described in paragraph 2.2.4.1. The reaction kinetics of AgNPs dissolution in 3 mL of CysHCl 0.1 M was followed by spectrophotometric absorption. The complete oxidation requires about 1 hour ($t_{1/2}$=30 min). This reagent can oxidize both 7 and 100 nm AgNPs, and the monoliths after the treatment are completely transparent and colorless. The same kind of monoliths were also dipped in bidistilled water as a control, observing no change in their absorption spectrum.

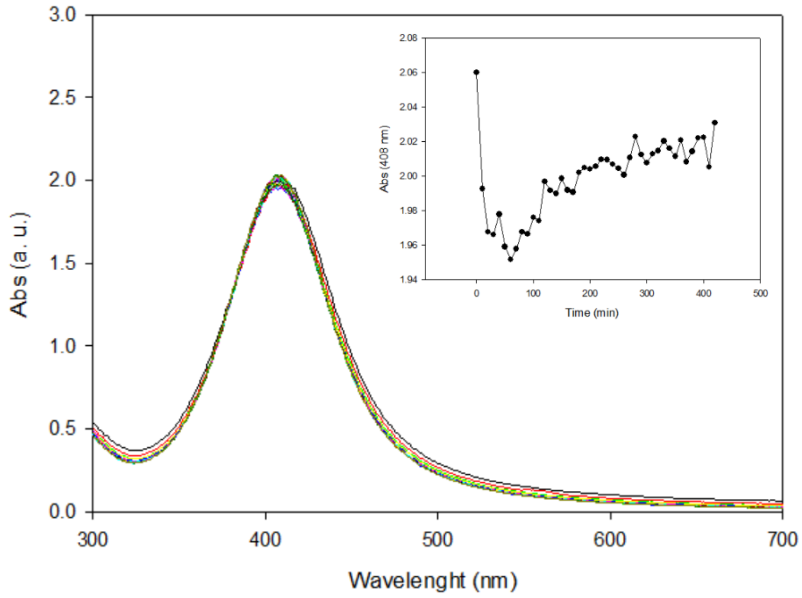

Figure 39 7 nm AgNPs doped silica gel monolith in bidistilled water.

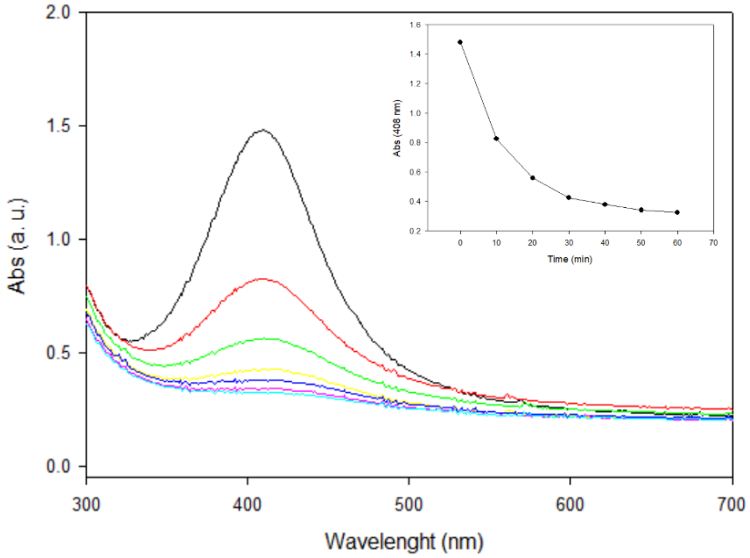

Figure 40 kinetic of 7 nm AgNPs doped silica gel monolith in cysteamine solution 0.5 M.

Iron(III)Nitrate solution

It's known that the ion Fe^{3+} can promote the etching of AgNPs by the redox reaction between Ag^0 and Fe^{3+} allowed by the nanometric size of nanoparticles.[49] The involved reaction is

$$Ag + Fe^{3+} \rightleftharpoons Ag^{+} + Fe^{2+}$$

The kinetic of reaction of AgNPs dissolution in 3 mL of $Fe(NO_3)_3$ 0.1 M was followed by spectrophotometric absorption. The oxidation reaction has $t_{1/2}$=1 hour for 7 nm

AgNPs. The complete oxidation of 100 nm AgNPs take place in about 24 hours. This reagent can remove both 7 and 100 nm AgNPs and the monoliths after treatment are completely transparent and colorless.

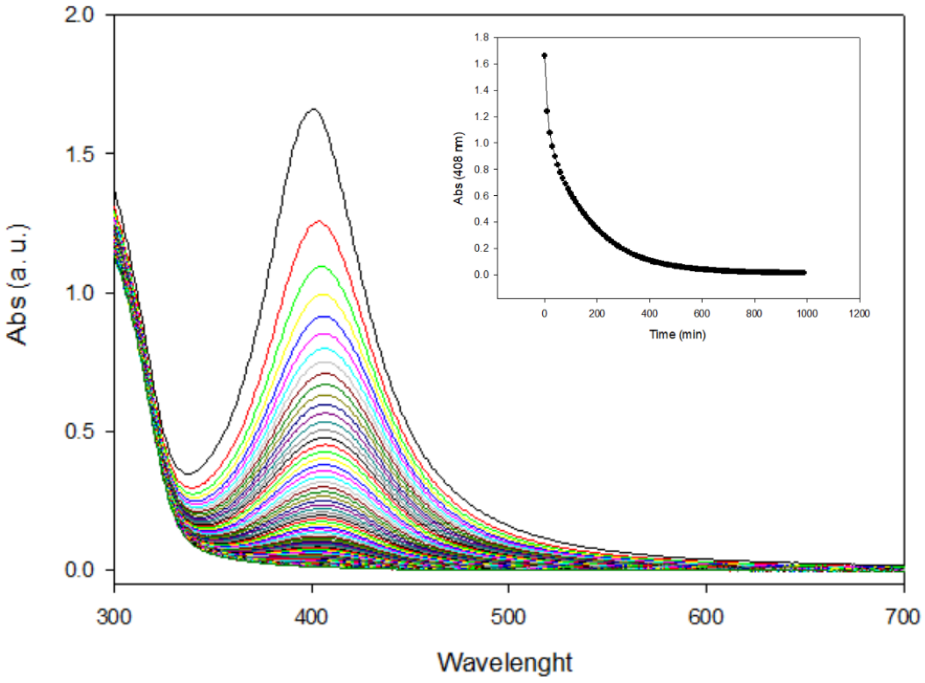

Figure 41 kinetic of oxidation of 7 nm AgNPs doped silica gel monolith in iron nitrate solution 0.5 M.

It should be noticed that the E° for the Ag^+/Ag couple is 0.800V. The E° value for the Fe^{3+}/Fe^{2+} couple (0.771 V) is slightly lower than that of Ag^+/Ag. However, both the E° decrease expected when the dimensions of solid Ag enter the nano range and the use of an excess Fe^{3+} makes the reaction to proceed quickly.

Nitric acid solution

To achieve reaction times in the order of seconds or few minutes it was used aqua regia. However, the presence of Cl^- species in the washing solution left AgCl insoluble residues inside the monolith, i.e. the obtained cavities were not void. It was therefore used nitric acid for the rapid and complete removal of AgNPs from silica gel. The process in this case is

$$3Ag + NO_3^- + 4H^+ \rightleftharpoons 3Ag^+ + NO + 2H_2O$$

The total silver removed from a monolith with concentration $4.66*10^{-4}$ M was analyzed by ICP-OES, allowinhg24 h of release time from the monolith to the nitric acid solution.

We analyzed the Ag^+ released both from an integer monolith and from monolith powder obtained by grinding with mortar and pestle. It was first calculated the total expected Ag inside one monolith from these data: $C_{Ag\ monolith}$=50.3 mg/L (obtained from ICP analysis of a solution of AgNPs which had the same concentrations and volume of a gelling solution used to prepare a monolith, i.e. 500 µL). The total Ag inside one monolith is thus 0.02515 mg.

Table 1 Silver release of full monoliths and ground monoliths.

Sample	Ag release (mg/L)	Mass Ag (mg)	Total Ag release%
Monolith 1	2.5	0.02503028	99.52398
Monolith 2	2.3	0.02298996	91.41137
Monolith 3	2.1	0.021459657	85.32667
Powder 1	2.4	0.023817509	94.70182
Powder 2	2.2	0.021985012	87.41556
Powder 3	2.2	0.022292657	88.6388

Total Ag released from solid monolith resulted 92%. Total Ag released from powder resulted 90%. Samples become colorless and transparent in about 2 minutes. We also further treated an oxidized powder for additional 24h hour with nitric acid, finding a further release of ~8% on the total silver of a monolith. This data agrees with the previous results. Both 7 and 100 nm were removed by nitric acid.

2.3.3.2 Oxidation process of gold nanoparticles inside silica gel monoliths

The oxidation of a gold nanoparticles solution by smooth reagents is a very difficult challenge. PEGylated AuNPs of spherical or different shape, embedded inside a silica matrix can be even harder. Oxidation was tried with O_2/Cysteamine Hydrochloride, Iron nitrate, sodium sulphite solutions.[50] None of these reagents was found to react with

AuNPs. Excluding the use of O_2/CN^- for safety reasons, the only reagent for a rapid and complete removal of AuNPs from silica monolith was aqua regia. Total Au release was analyzed by ICP-OES. The total Au included in a single monolith was first calculated from the data: $C_{Au\ monolith}$=343.08 mg/L, obtained from ICP analysis of a solution of AuNPs identical to those used in the gelation process, and the volume used to prepare a single monolith (500 µL). The total Au inside one monolith is thus 0.1715 mg.

Table 2 Gold release of full monoliths.

Sample	C Au release (mg/L)	Mass Au (mg)	%Au release
Monolith 1	13.0	0.13	76
Monolith 2	13.4	0.134	78
Monolith3	13.3	0.133	78

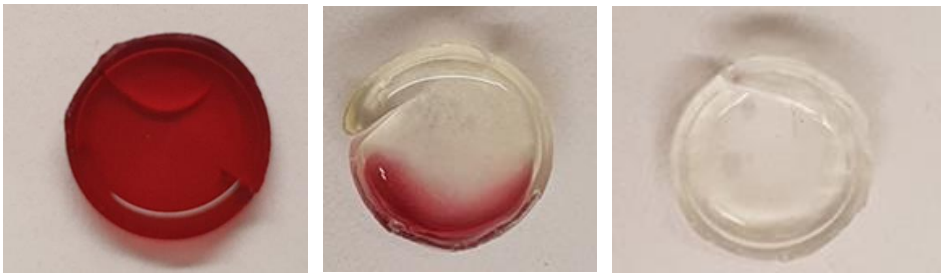

Figure 42 Oxidation steps of AuNPs doped silica gel monolith: From the left (before treatment) to the right (after treatment).

The total Au released from a solid monolith resulted 78-80% of the expected quantity. Monoliths turns colorless in few seconds of contact with aqua regia.

2.3.4 Characterization of emptied monoliths

A full morphological and compositional characterization of the doped and emptied monoliths was performed, in order to investigate the morphological properties of the materials after the removal of the templating nanoparticles and to characterize the obtained complementary cavities. For a better understanding of the morphology, monoliths doped with AgNPs and AuNPs at different size and concentration were used.

2.3.4.1 Internal structure

The internal structure of the monoliths was investigated by porosimetric analysis as described in paragraph 2.2.1.3. It was first performed measures on a set of three samples: monoliths doped with 7 nm AgNPs $1.15*10^{14}$ NP/L (A), monoliths doped with 7 nm AgNPs $1.15*10^{14}$ NP/L after the removal process made by cysteamine Hydrochloride 0.1 M (B) and blank monoliths(C).

A

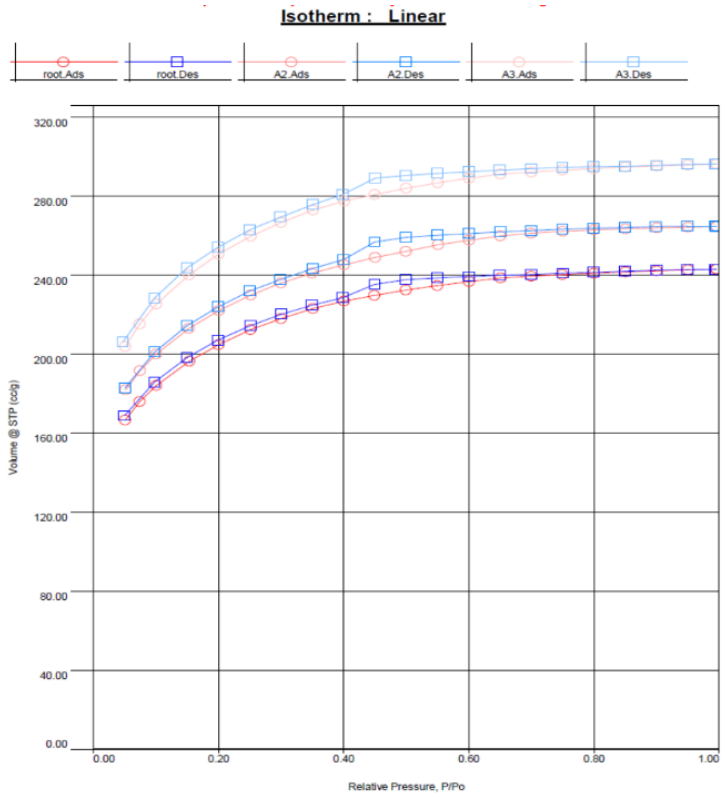

B

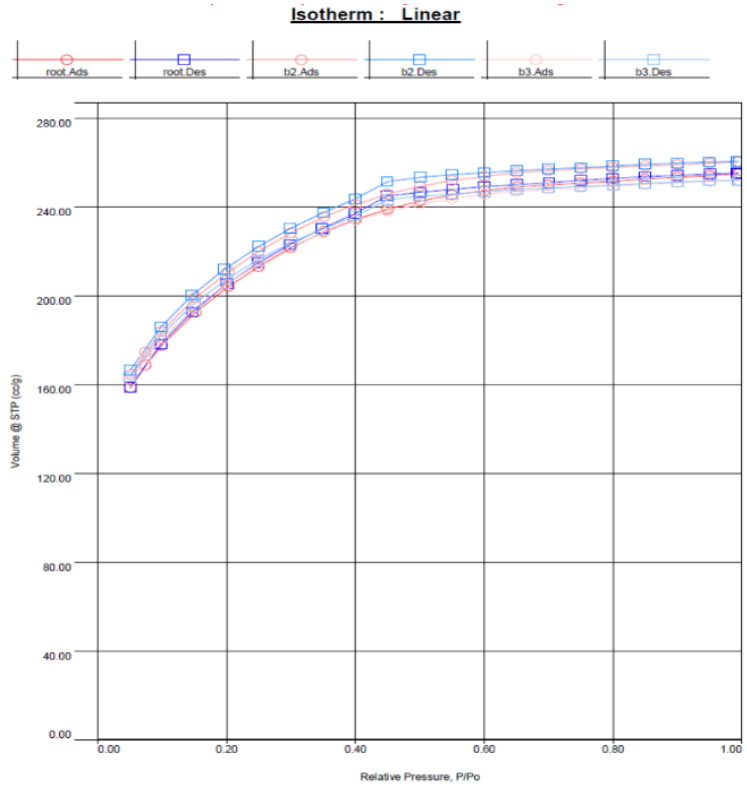

C

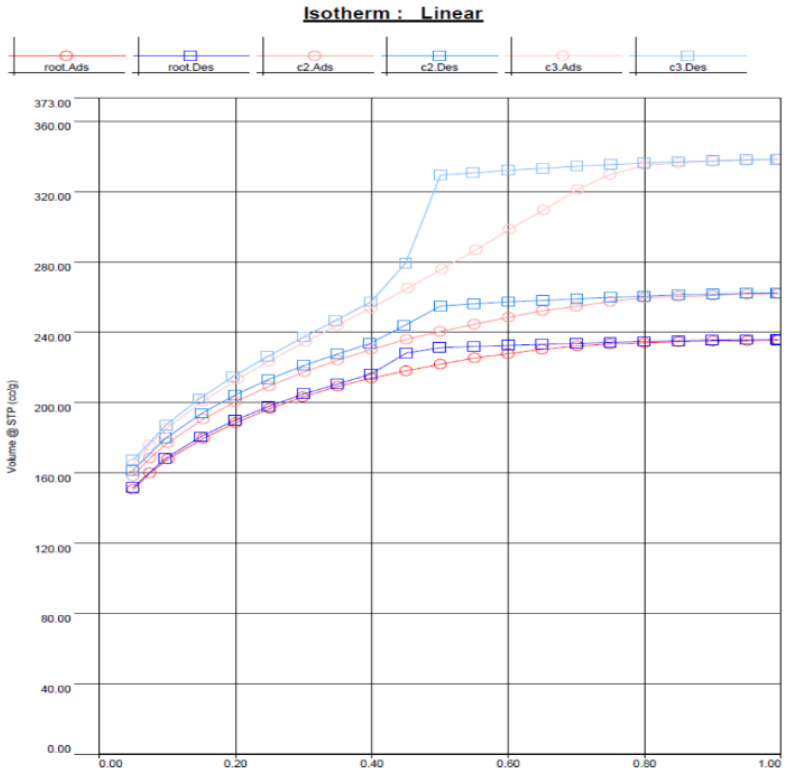

Figure 43 A) linear isotherm of samples A1, A2 and A3; B) linear isotherm of samples B1, B2 and B3; C) linear isotherm of samples C1, C2 and C3.

The experimental nitrogen sorption isotherms relative to samples A, B and C are given in Fig 43 According to the International Union of Pure and Applied Chemistry (IUPAC) isotherm classifications, the obtained isotherms are those of type IV, typical of mesoporous materials as shown in image 44. Moreover, the type of hysteresis found for all the analysed samples is of type H2(b), i.e., that typical of materials presenting pores with a narrow pore body size W and a large neck size Wc (W>Wc).[51]

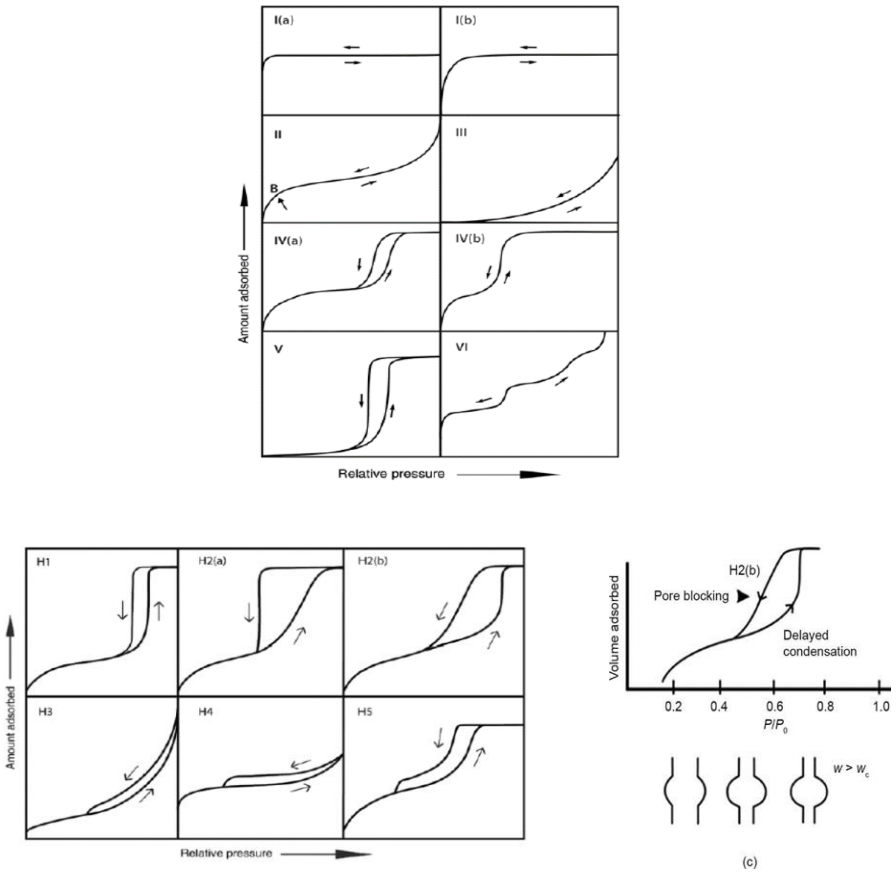

Figure 44 Classification of isotherms [51]

The isotherms were processed using different mathematical models to evaluate the specific surface area (SSA), the pores total volume, the size and type of pores inside the SiO_2 samples both in the presence and absence of nanoparticles. The obtained results are given in Tables 3 and 4 for the monolith samples obtained before and after the AgNPs removal. The SSA was calculated by applying the BET theory to the adsorption data in

the pressure range P/P0 between 0.05 and 0.2 by the MICROPORE ASSISTANT software. However, since the BET equation is usually applicable to non-porous, mesoporous, and macroporous materials, but is less applicable to microporous materials, the t-Plot method has been applied in the range P/P_0 between 0.25 and 0.45 in order to calculate SSA value. The micropore surface area has been calculated as subtraction of the SSA value calculated by BET theory and that calculated by t-plot method. The BJH method has been employed for the evaluation of pore size, even if it is well known in literature that this method underestimates mesopores of dimension lower than 100 Å.[52]

Table 3 SSA values calculated by BET theory and t-plot method, SSA contributed by micropores and average pore radius calculated at P/P0= 0,99 and BJH method for the SiO_2 samples before and after the AgNPs removal.

** values calculated on the adsorption isotherm*

SAMPLE	***P/P0 value linear BET Assistant***	***B.E.T. Specific Surface Area (m^2/g)***	***BET Costant C***	***External Surface Area by t-plot (m^2/g)***	***Micropore Area (m^2/g)***	***Surface area contributed by micropores (%)***	***Average Pore Radius calculated P/P0= 0,99 (Å)***	***Pore* Radius by BJH (Å)***
A1	0,05-0,15	739,02	282	224,221	514,80	69,65	11,85	15,29
A2	0,0518-0,1532	801,25	308	213,42	587,83	73,36	11,27	17,07
A3	0,0511-0,1532	904,32	281	240,41	663,91	73,41	11,16	15,30
B1	0,0514-0,1520	738,45	145	291,52	446,93	60,52	11,47	15,30
B2	0,0518-0,1519	762,49	159	290,92	471,56	61,84	11,37	15,29
B3	0,0514-0,1530	743,58	166	266,12	477,45	64,2	10,47	15,29
C1	0,0504-0,1536	680,48	216	241,75	438,71	64,47	10,71	15,27
C2	0,0501-0,1531	725,1	180	297,55	427,55	58,96	12,07	17,07
C3	0,0512-0,1522	769,44	147	469,91	299,52	38,92	13,60	17,09

Table 4 Total pore volume calculated at P/P0=0,99, micropore volume calculated by t-plot method, mesopore volume calculated as difference between total pore and micropore volumes, mesopore and micropore volumes expressed as percentage with respect to the total pore volume for the SiO_2 samples.

** For the calculation a P/P0 value from 0.2 to 0.45 applied to the adsorption isotherm was considered; ** Mesopore volume was calculated from the difference between total pore volume and micropore volume from the curve of the t plot.*

SAMPLE	***Total Pore Volume P/P0=0,99***	***Micropore* Volume by t-plot and α-plot***	***Micropore* Volume by α-plot***	***Mesopore** volume***	***% Micropore volume***	***% Mesopore volume***
	(cc/g)	***(cc/g)***	***(cc/g)***	***(cc/g)***	***(%)***	***(%)***
A1	0,3755	0,224	0,226	0,1495	60,19	39,81
A2	0,4094	0,257	0,257	0,1524	62,78	37,22
A3	0,4583	0,291	0,291	0,1673	63,50	36,50
B1	0,3946	0,195	0,196	0,1986	49,68	50,32
B2	0,4029	0,206	0,207	0,1969	51,13	48,87
B3	0,3896	0,209	0,209	0,1806	53,65	46,35
C1	0,3645	0,193	0,193	0,1715	52,95	47,05
C2	0,4055	0,186	0,187	0,2195	45,87	54,13
C3	0,5233	0,125	0,128	0,3983	23,89	76,11

It was calculated the average SSA for every set of samples:

SAMPLE	***Average B.E.T. Specific Surface Area (m^2/g)***
A	814.9
B	748.2
C	725.0

From this first set of data it was not possible to appreciate a significant change in the internal surface area after the removal process with cysteamine solution. It was therefore used a new set of samples with increased NPs concentration and bigger NP size:

The sample series A (A1-A2) are silica gel monoliths doped with 100 nm AgNPs. Samples A1 and A2 are produced in the same conditions to test the reproducibility of the experiment. The AL sample series (AL1-AL2) are the silica gel monoliths after the removal of 100 nm AgNPs through the chemical treatment with ferric nitrate. The B sample series (B1-B2) are silica gel monoliths doped with AgNPs of smaller dimension, approximately 7 nm in size with concentration $3.33*10^{15}$, while the BL sample series (BL1-BL2) are the silica gel monoliths after the removal of the AgNPs by the ferric nitrate treatment.

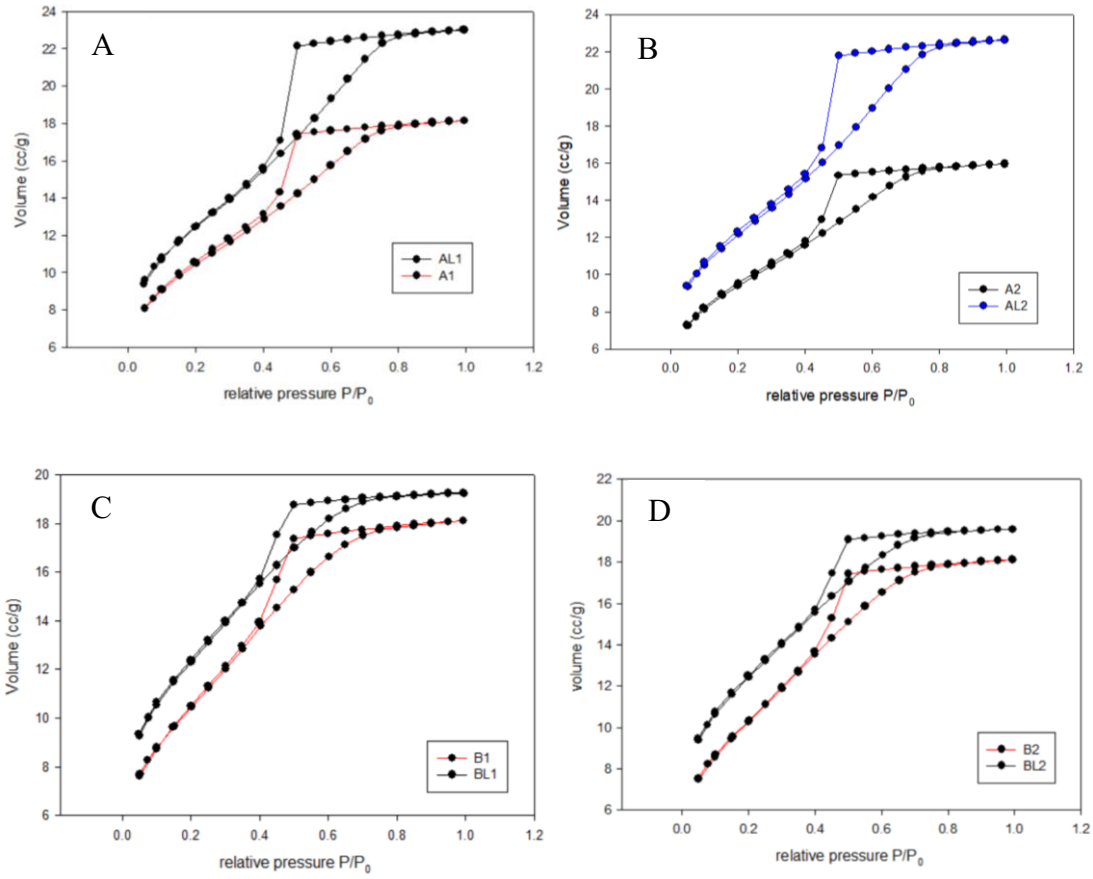

Figure 45 A) linear isotherms of samples A1 and AL1; B) linear isotherms of samples A2 and AL2; C) linear isotherms of samples B1 and BL1; D) linear isotherms of samples B2 and BL2.

The SSA was calculated by applying the BET theory to the adsorption data in the pressure range P/P0 between 0.05 and 0.2 by the MICROPORE ASSISTANT software. However, since the BET equation is usually applicable to non-porous, mesoporous, and macroporous materials, but is less applicable to microporous materials, the t-Plot method has been applied in the range P/P_0 between 0.25 and 0.45 in order to calculate SSA value. The micropore surface area has been calculated as subtraction of the SSA value calculated

by BET theory and that calculated by t-plot method. The BJH method has been employed for the evaluation of pore size, even if it is well known in literature that this method underestimates mesopores of dimension lower than 100 Å.

Table 5 SSA values calculated by BET theory and t-plot method, SSA contributed by micropores, and average pore radius calculated at P/P0= 0,99 and BJH method for the SiO_2 samples.

** values calculated on the adsorption isotherm*

SAMPLE	***B.E.T. Specific Surface Area (m^2/g)***	***BET Costant C***	***Specific Surface Area by t-plot (m^2/g)***	***Micropore Specific Surface Area (m^2/g)***	***Specific Surface Area contributed by micropores (%)***	***Average Pore Radius Calculated at P/P0= 0,99 (Å)***	***Pore Radius* by BJH (Å)***
A1	643,386	168	483,398	159,988	24,86	15,04	19,70
AL1	721,134	166	577,696	143,438	19,89	16,00	15,32
A2	671,912	153	508,031	163,881	24,39	14,67	15,31
AL2	704,212	158	582,794	121,418	17,24	16,13	15,32
B1	583,656	94	570,003	13,652	2,34	14,81	17,12
BL1	628,182	120	507,178	121,004	19,26	13,42	17,06
B2	636,113	92	624,548	11,565	1,81	15,00	17,03
BL2	686,335	127	542,973	143,362	20,88	13,58	15,28

Table 6 Total pore volume calculated at P/P0=0,99, micropore volume calculated by t-plot method, mesopore volume calculated as difference between total pore and micropore volumes, mesopore and micropore volumes expressed as percentage with respect to the total pore volume for the SiO_2 samples.

** For the calculation a P/P0 value from 0.2 to 0.45 applied to the adsorption isotherm was considered; ** Mesopore volume was calculated from the difference between total pore volume and micropore volume from the curve of the t plot.*

SAMPLE	***Total Pore Volume P/P0=0,99***	***Micropore Volume by t-plot***	***Mesopore volume***	***% Micropore volume***	***% Mesopore volume***
	(cc/g)	***(cc/g)***	***(cc/g)***	***(%)***	***(%)***
A1	0,4840	0,067	0,4160	14,05	85,95
AL1	0,5770	0,059	0,5180	10,22	89,75
A2	0,4930	0,069	0,4230	14,20	85,50
AL2	0,5681	0,048	0,5201	8,45	91,55
B1	0.4321	0.002	0.4301	0.46	99.5
BL1	0.4215	0.051	0.3705	12.09	87.91
B2	0.4771	0	0.4771	0	100
BL2	0.4659	0.061	0.4049	13.09	86.91

In the complete A series (A1-AL1 and A2-AL2), from the evaluation of the isotherms and the experimental data given in Tables 1 and 2, the removal of silver nanoparticles (AL1-AL2) leads to an increase in SSA with a decrease in the micropores area compared to the starting situation. Furthermore, since the amplitude (depth) of the hysteresis loop is normally linked to the size of the pores inside the material, in this series the size of the pore diameter is certainly greater than in the B series.

In the complete B series (B1-BL1 and B2-BL2), the removal of silver nanoparticles (BL1-BL2) leads to an increase in SSA, a decrease in the SSA calculated by t-plot and therefore to a noticeable increase in the area of the micropores compared to the starting situation.

Sol gel powder obtained by grinding in a mortar the silica gel doped with AgNPs with a diameter of about 7 nm has been labelled as P1, while P2 is the same powder after the

removal of the AgNPs. Analogously, P3 and P4 are the sol-gel powders before and after the chemical removal of 100 nm in size AgNPs, respectively.

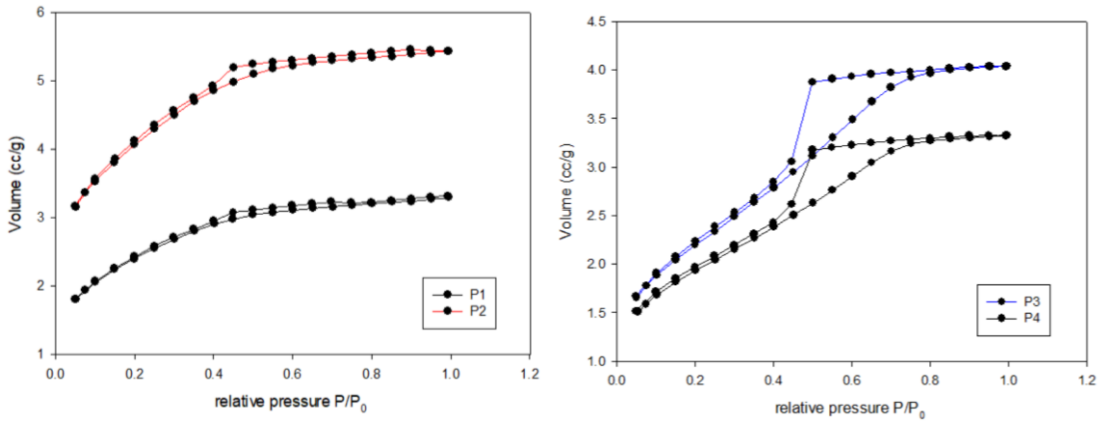

Figure 46 A) linear isotherms of samples P1 and P2; B) linear isotherms of samples P3 and P4.

Table 7 SSA values calculated by BET theory and t-plot method, SSA contributed by micropores, and average pore radius calculated at P/P0= 0,99 and BJH method for the SiO_2 samples.

** values calculated on the adsorption isotherm*

SAMPLE	***B.E.T. Specific Surface Area (m^2/g)***	***BET Costant C***	***Specific Surface Area by t-plot (m^2/g)***	***Micropore Specific Surface Area (m^2/g)***	***Specific Surface Area contributed by micropores (%)***	***Average Pore Radius Calculated at P/P0= 0,99 (Å)***	***Pore Radius by BJH (Å)***
P1	492,709	110	277,047	215,662	43.77	11.75	15,31
P2	669,386	169	360,657	308,730	46.12	11.57	15,27
P3	510,404	118	443,838	66,566	13.04	15.80	17,05
P4	821,765	164	621,480	200,285	24.37	14,91	15,30

Table 8 Total pore volume calculated at P/P0=0,99, micropore volume calculated by t-plot method, mesopore volume calculated as difference between total pore and micropore volumes, mesopore and micropore volumes expressed as percentage with respect to the total pore volume for the SiO_2 samples.

** For the calculation a P/P0 value from 0.2 to 0.45 applied to the adsorption isotherm was considered; ** Mesopore volume was calculated from the difference between total pore volume and micropore volume from the curve of the t plot.*

SAMPLE	***Total Pore Volume P/P0=0,99***	***Micropore Volume by t-plot***	***Mesopore volume***	***% Micropore volume***	***% Mesopore volume***
	(cc/g)	***(cc/g)***	***(cc/g)***	***(%)***	***(%)***
P1	0,2897	0.096	0.1937	33.14	66.86
P2	0.3874	0.139	0.2484	35.88	64.12
P3	0,4032	0.026	0,3772	6,45	93,55
P4	0,6125	0.085	0,5275	13,88	86,12

The comparison between the P1 and P2 isotherms shows that the removal of nanoparticles leads to an increase in SSA and an increase in the area of micropores. The comparison between the P3 and P4 isotherms shows that the removal leads to an increase in SSA and a substantial increase in the area of the micropores.

Powder of sol gel powder doped with 100 nm gold nanoparticles before and after the removal process with aqua regia (P5-P6) were analyzed:

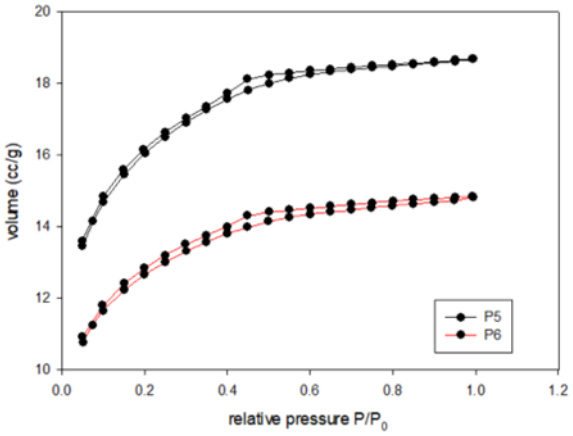

Figure 47 linear isotherms of samples P5 and P6.

Table 9 SSA values calculated by BET theory and t-plot method, SSA contributed by micropores, and average pore radius calculated at P/P0= 0,99 and BJH method for the SiO_2 samples.

** values calculated on the adsorption isotherm.*

SAMPLE	***B.E.T. Specific Surface Area*** ***(m^2/g)***	***External Surface Area by t-plot*** ***(m^2/g)***	***Micropore Area by t-plot*** ***(m^2/g)***	***Surface area contributed by micropores*** ***(%)***	***Average Pore Radius calculated P/P0= 0,99*** ***(Å)***	***Pore Radius by BJH*** ***(Å)***
P5	600,517	163,001	437,515	72,85	9,72	15,26
P6	663,427	172,272	491,155	74,03	9,82	15,28

Table 10 Total pore volume calculated at P/P0=0,99, micropore volume calculated by t-plot method, mesopore volume calculated as difference between total pore and micropore volumes, mesopore and micropore volumes expressed as percentage with respect to the total pore volume for the SiO_2 samples.

** For the calculation a P/P0 value from 0.2 to 0.45 applied to the adsorption isotherm was considered; ** Mesopore volume was calculated from the difference between total pore volume and micropore volume from the curve of the t plot.*

SAMPLE	***Total Pore Volume P/P0=0,99*** ***(cc/g)***	***Micropore Volume by t-plot*** ***(cc/g)***	***Mesopore volume*** ***(cc/g)***	***% Micropore volume*** ***(%)***	***% Mesopore volume*** ***(%)***
P5	0,2929	0,182	0,1109	62,14	37,86
P6	0,3257	0.205	0.1207	62,94	37,06

Concerning samples P5 and P6, from the evaluation of the isotherms and the experimental data, the removal of gold nanoparticles certainly leads to an increase in SSA, an increase in the external area and a significant increase in the area of the micropores compared to the initial situation.

2.3.4.2 Composition

FTIR Spectroscopy

A compositional analysis of silica monoliths doped with 7 nm AgNPs, before and after the removal process, was carried out by FTIR spectroscopy. FTIR spectra were taken on samples of silica gel powders. The first result was obtained on blank silica gel for the proper understanding of the structure of the silica matrix, see Figure 48.

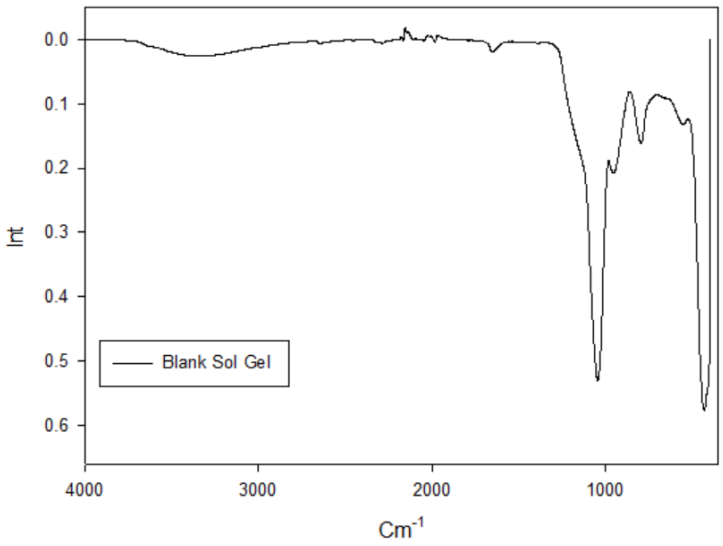

Figure 48 FTIR spectrum of blank silica gel monolith.

The IR spectrum from the blank silica gel exhibited a broad peak at 3342 cm^{-1} caused by the superimposed stretching modes of Si–OH groups and of the hydroxyl groups of physically adsorbed water, while peaks at 1657 cm^{-1}, 1395 cm^{-1}, were assigned to the bending vibrations of water and silanol, respectively. Peaks at 1052 cm^{-1} and 949 cm^{-1} reflected the Si– O–Si stretch vibration modes of the silica gel. The peak at 471 cm^{-1} was assigned to ΞSi–O–SiΞ stretching vibration.[53]

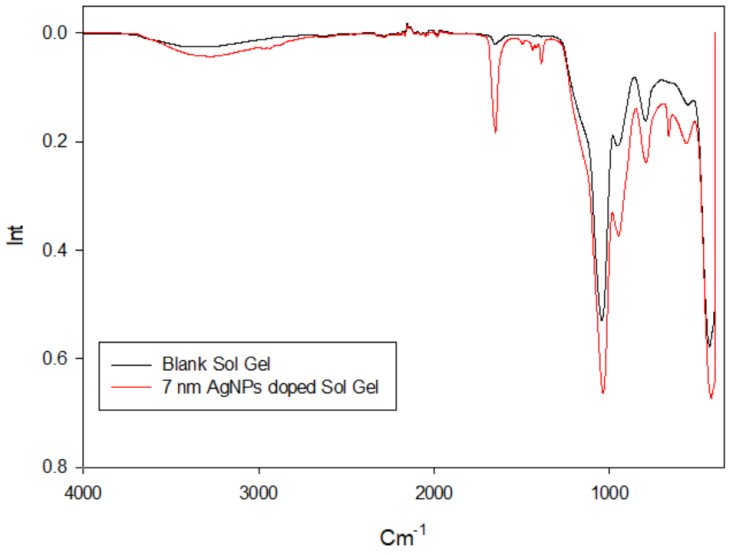

Figure 49 FTIR of blank silica gel monolith and 7 nm AgNPs doped silica gel monolith.

The IR spectrum of the AgNPs doped monolith (Figure 49) exhibited the peaks associated to the organic coating of the NPs: a broad peak at 2940 cm^{-1} associated to C-H stretching; a peak at 1653 cm^{-1} associated to the stretching of CO-NH group inside the PEG structure; finally peaks at 1495 cm^{-1}, 1443 cm^{-1}, 1390 cm^{-1}, associated to C-O stretching and C-H bending.[54]

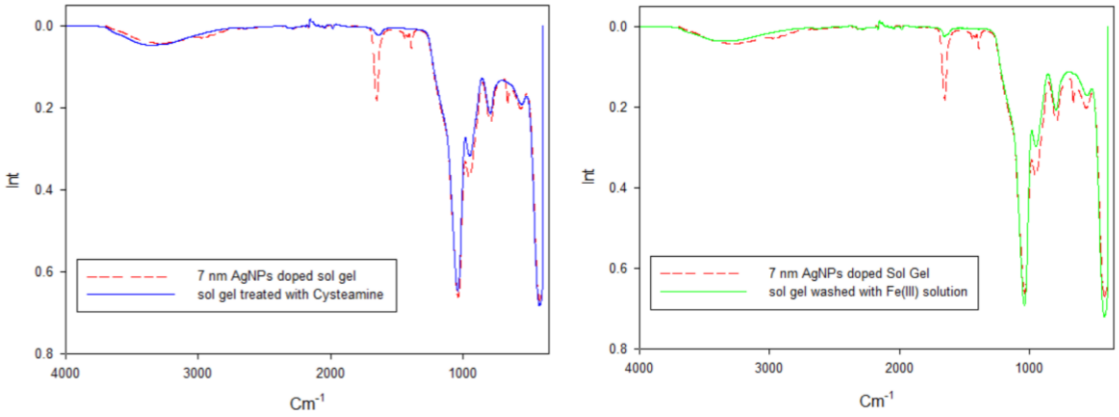

Figure 50 FTIR of 7 nm AgNPs doped silica gel monolith after the removal process with cysteamine Hydrochloride (left) and Iron nitrate (right) solutions.

Figure 50 compares the spectra of the silica powders with embedded 7nm pegylated AgNPs (red dashed lines) with those obtained on the powders after AgNPs removal with air/cysteamine (left) and Fe(III) (right), evidencing that the peaks associated with the

organic coating are removed. On the other hand, as no new peaks are detected, it can be assumed that the reagents are fully removed from the monolith.

Raman spectroscopy

Raman spectra were collected on blank monoliths, on monoliths with embedded AgNPs of 7 nm and on monoliths after AgNPs removal. Laser was focused on the upper surface of the sample by confocal microscope with magnification ×100 integrated in the instrument, as described in paragraph 2.2.1.3. 100% of laser power was used, because it was found that the samples were particularly resistant to photodegradation.

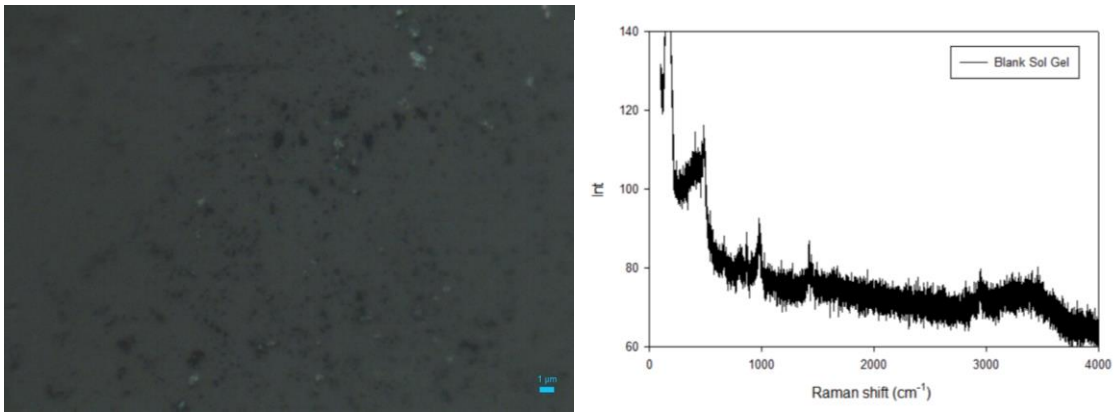

Figure 51 imagine of the blank silica gel monolith magnification 100x made with confocal microscope (left); Raman spectrum of the blank silica gel surface (right).

In agreement with the literature the Raman spectrum of amorphous blank monolith SiO_2 gel, displayed in Figure 51, is characterized by four main bands. There is a shoulder near 400 cm^{-1} that corresponds to the "bond-rocking" motion in which the atoms move roughly perpendicular to the Si-O-Si planes. An intense band at 486 cm^{-1} is induced by symmetric stretch oxygen vibration of three network oxygen atoms connected to a silicon atom that has become decoupled from the network via a terminating hydroxyl group. A band at 803 cm^{-1} is present in the Raman spectrum of SiO_2 gel and is also characteristic of fused SiO_2. It is due to bond-bending vibration parallel to the bisector of the Si-O-Si angle. A last, rather intense, band located around 982 cm^{-1} is due to symmetric stretch vibrations of silanols in SiO_2, Si-OH groups.[55]

The same parameters were used for the analysis on 7 nm AgNPs doped monolith before and after the treatment with cysteamine washing solution.

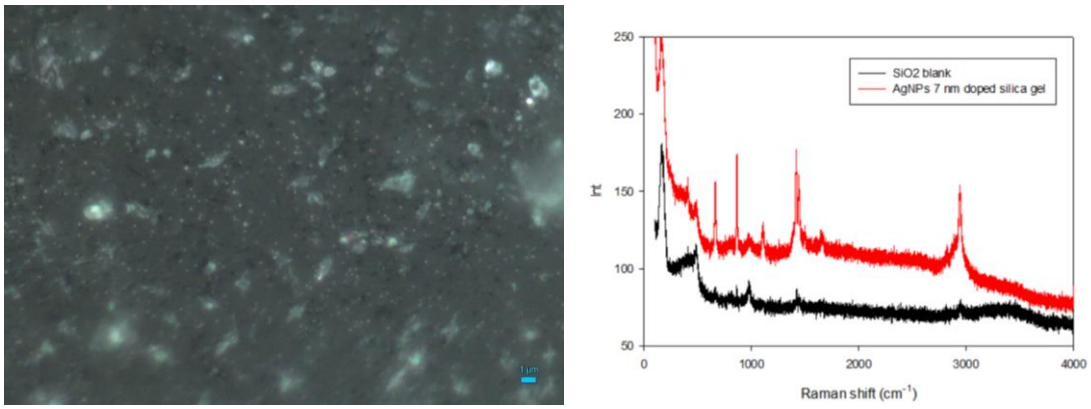

Figure 52 imagine of the 7 nm AgNPs doped silica gel monolith magnification 100x made with confocal microscope (left); Raman spectrum of the 7 nm AgNPs doped silica gel surface (right).

In Figure 52, left, it can be observed the presence of AgNPs as bright spots inside the matrix of the monolith due to backscattered light. The Raman spectrum shows peaks at 1417 cm^{-1}, 1659 cm^{-1}, 2957 cm^{-1}, that are associated to the PEG coating of the AgNPs.[56] Noticeably, both signals of PEG grafted to the NPs and the silica matrix signals appear to be amplificated by the SERS effect exerted by the AgNPs.

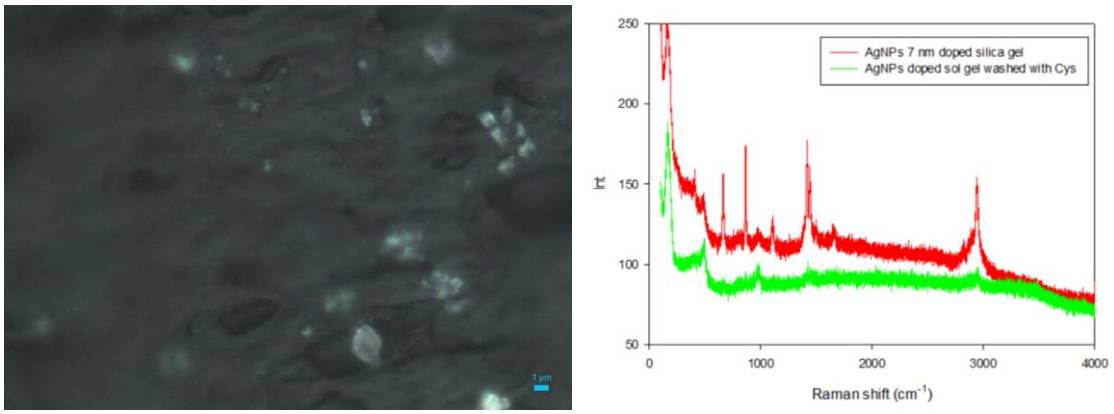

Figure 53 imagine of the 7 nm AgNPs doped silica gel monolith washed with cysteamine hydrochloride solution magnification 100x made with confocal microscope (left); Raman spectrum of the 7 nm AgNPs doped silica gel washed with cysteamine hydrochloride solution surface (right).

After the washing process with Cysteamine Hydrochloride solution the removal of AgNPs can be seen in the Raman spectrum and imaging. In theFigure 53, left, the silica matrix does not show anymre the bright spots associated to backscattering by AgNPs. Moreover, the Raman spectrum after the washing process (right) loses the amplification of signals and becomes like the blank one.

The same results are observed on 100 nm doped AuNPs monoliths before and after the removal process with aqua regia.

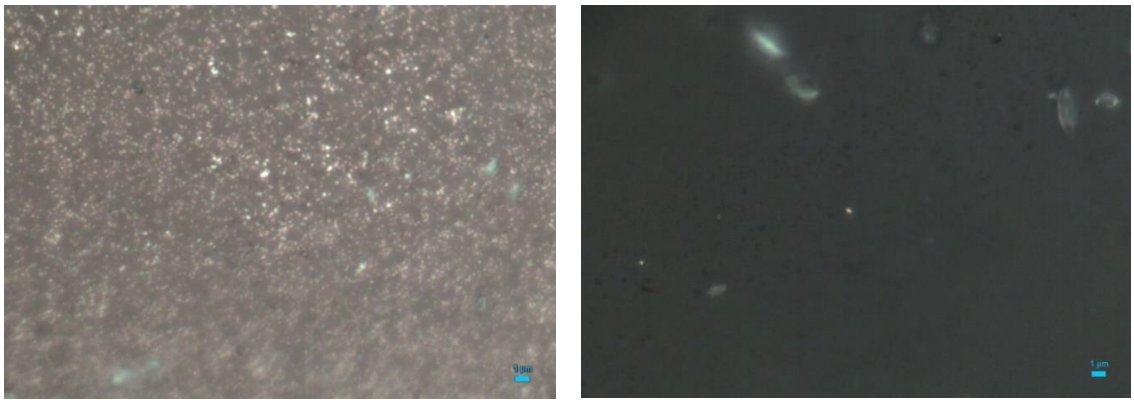

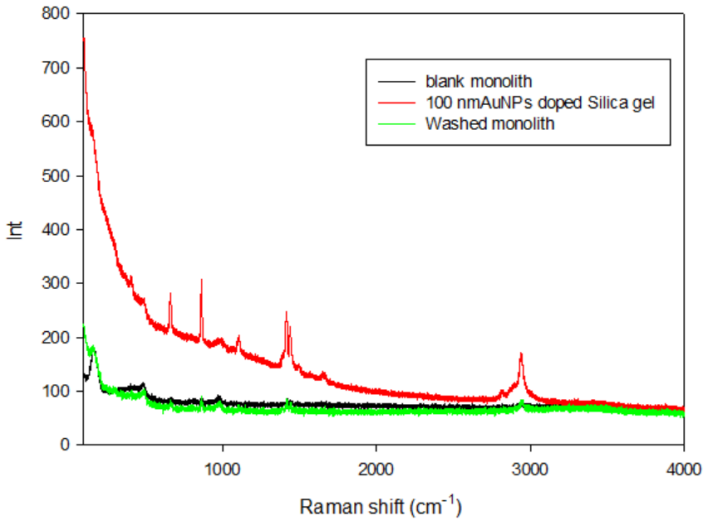

Figure 54 imagine of the 100 nm AuNPs doped silica gel monolith before and after the removal process with aqua regia magnification 100x made with confocal microscope; Raman spectrum of the 100 nm AuNPs doped silica gel monolith before and after the removal process with aqua regia solution surface.

XRD analysis

Silica gel powders were analyzed by XRD as described in paragraph 2.2.1.3. In the diffractogram of blank monolith only a large peak centered at 23° was found. This peak is associated to the amorphous silica domain as seen with spectroscopic techniques.[57]

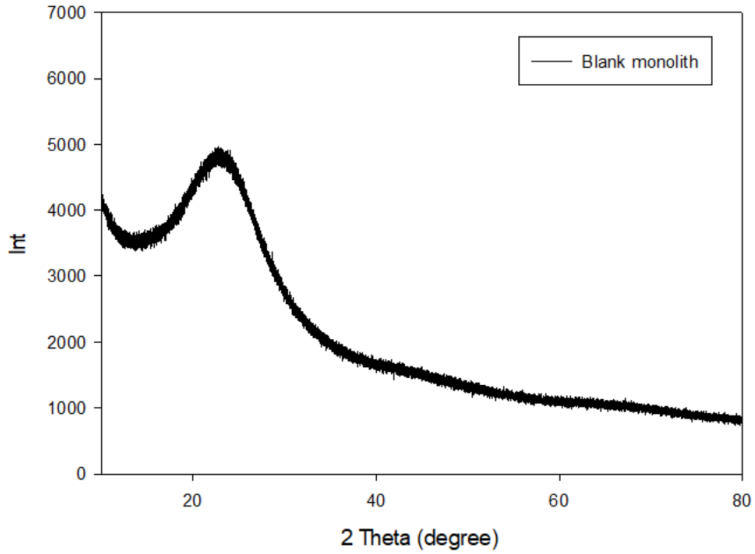

Figure 55 Diffractogram of blank silica gel monolith powder.

In the AgNPs 7 nm doped monolith powder (4x concentrated AgNPs $3.33*10^{15}$ NP/L)diffractogram a small peak appears at 38°. It can be attributed to the 111 crystalline structures of the face centered cubic (FCC) synthesized silver nanocrystal. The small

dimension and the low concentration of the AgNPs in the sample allow to observe only the most intense peak associated to the FCC lattice, the 111.

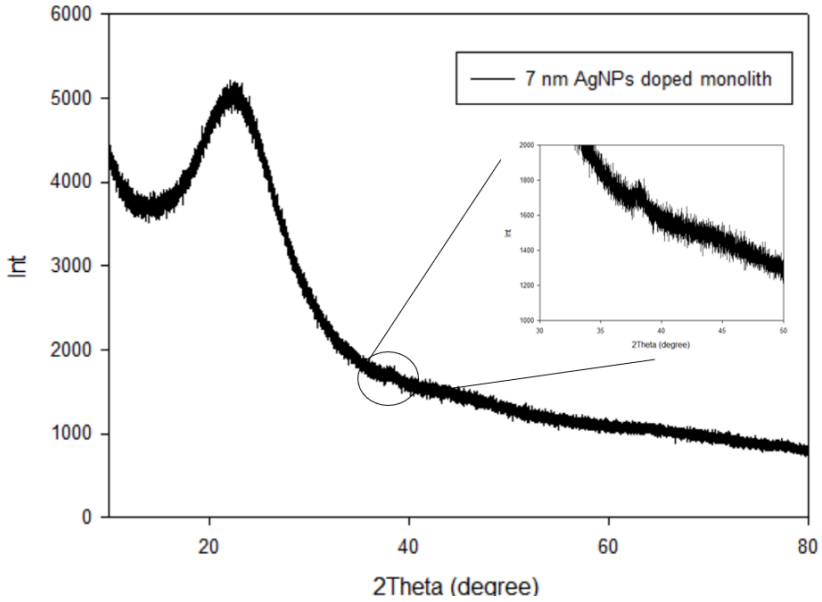

Figure 56 diffractogram of 7 nm AgNPs doped silica gel powder. Magnification of the peak at 38°.

Diffractograms were also recorded also on silica gel powders templated with 100 nm AgNPs (100x concentrated AgNPs $2.08*10^{11}$ NP/L) and AuNPs (100x concentrated AuNPs $7.19*10^{12}$ NP/L) before and after the removal process.

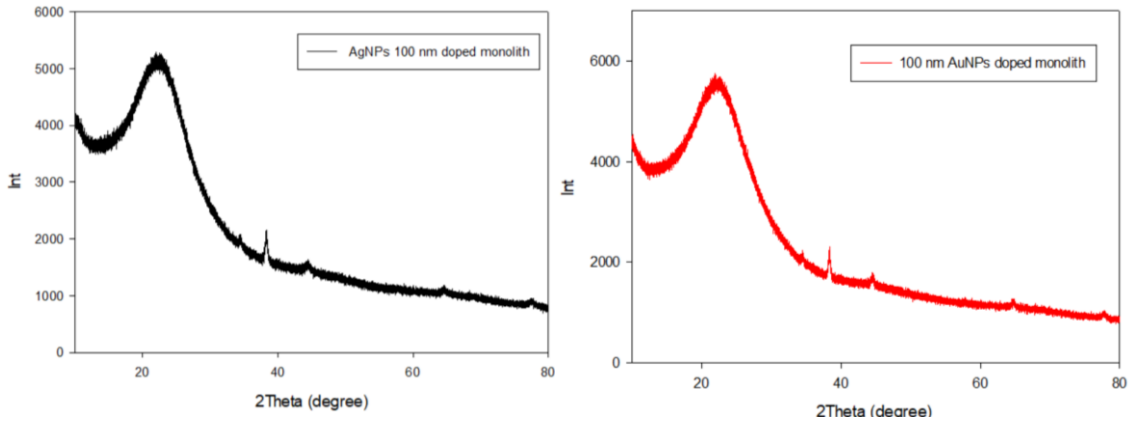

Figure 57 diffractogram of 100 nm AgNPs doped silica gel powder (left); diffractogram of 100 nm AuNPs doped silica gel powder (right).

The XRD diffractogram in the wide angle range of 2θ (10° < 2θ < 80°) ascertained the presence of sharper peaks at 38°, 44°, 64.4° and 77.2° that agree with the 111, 200, 220, and 311 crystalline structures of the face centered cubic (FCC) gold and silver nano-crystals.[54]

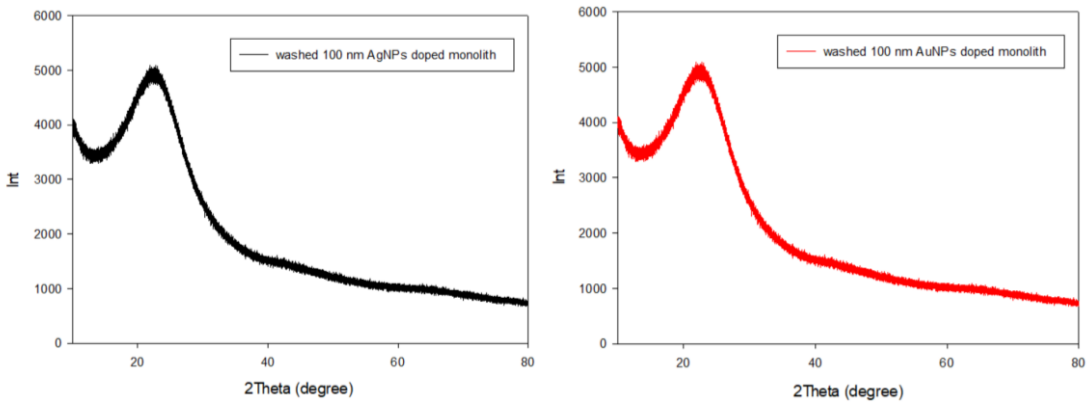

Figure 58 diffractogram of 100 nm AgNPs doped silica gel powder after removal process (left); diffractogram of 100 nm AuNPs doped silica gel powder after removal process (right).

After the removal process on both gold and silver 100 nm NPs, the signals associated to the FCC lattice disappear.

2.3.4.3 Morphology

SEM imaging on 7 nm AgNPs doped monolith

To obtain information about the morphology of the monoliths, SEM images were collected on different preparations. AgNPs 7 nm doped monoliths with concentration $3.33*10^{15}$ NP/L (4x concentrated monolith, $Ag_{tot}=4.66*10^{-4}$ M) were first investigated. The solid doped with metal nanoparticles resulted conductive and no sputtering was applied. The silica gel matrix resulted the same observed in section 2.3.2.3, but nanoparticles cannot be seen most probably due to their small number and small size, that makes the few NP on the surface indistinguishable with respect to the surface roughness.

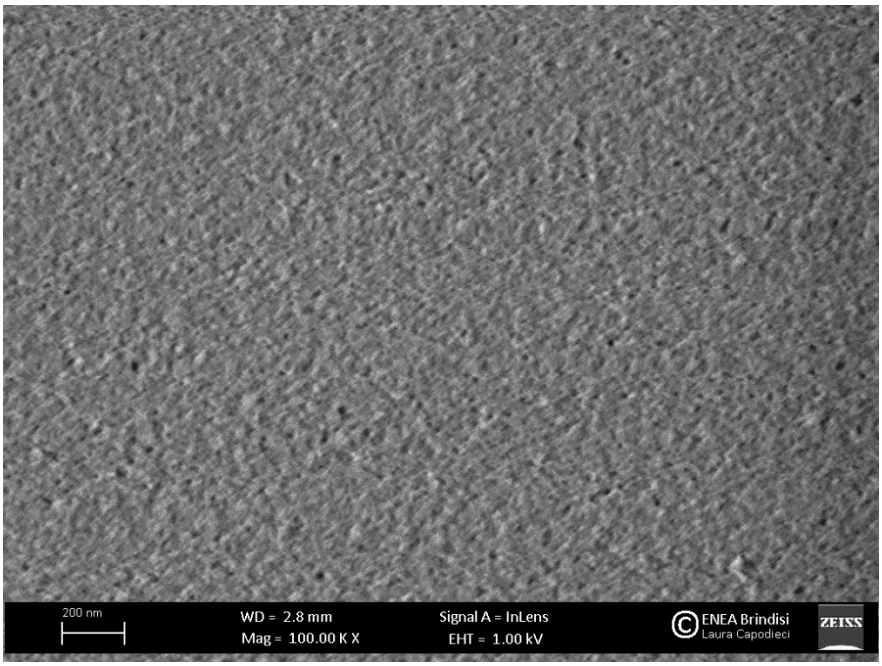

*Figure 59 SEM image of AgNPs 7 nm doped monolith with concentration 3.33*10^{15}, 100k magnification.*

SEM imaging on 100 nm AuNPs doped monolith

All SEM images were collected on 100x concentrated 100 nm AuNPs doped monolith (7.19*10^{12} NP/L, Au_{tot}=2.8*10^{-3} M) to check the NPs presence and behavior inside the silica matrix. It took about 5 hours to create the vacuum necessary for the analysis as the samples proved to be highly hygroscopic. It was possible collect SEM images in both faces of the monolith and in section. No sputtering was applied to perform analysis.

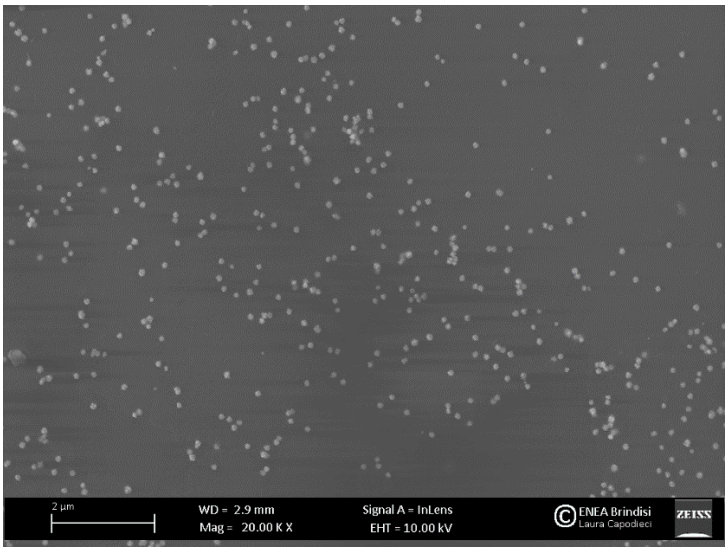

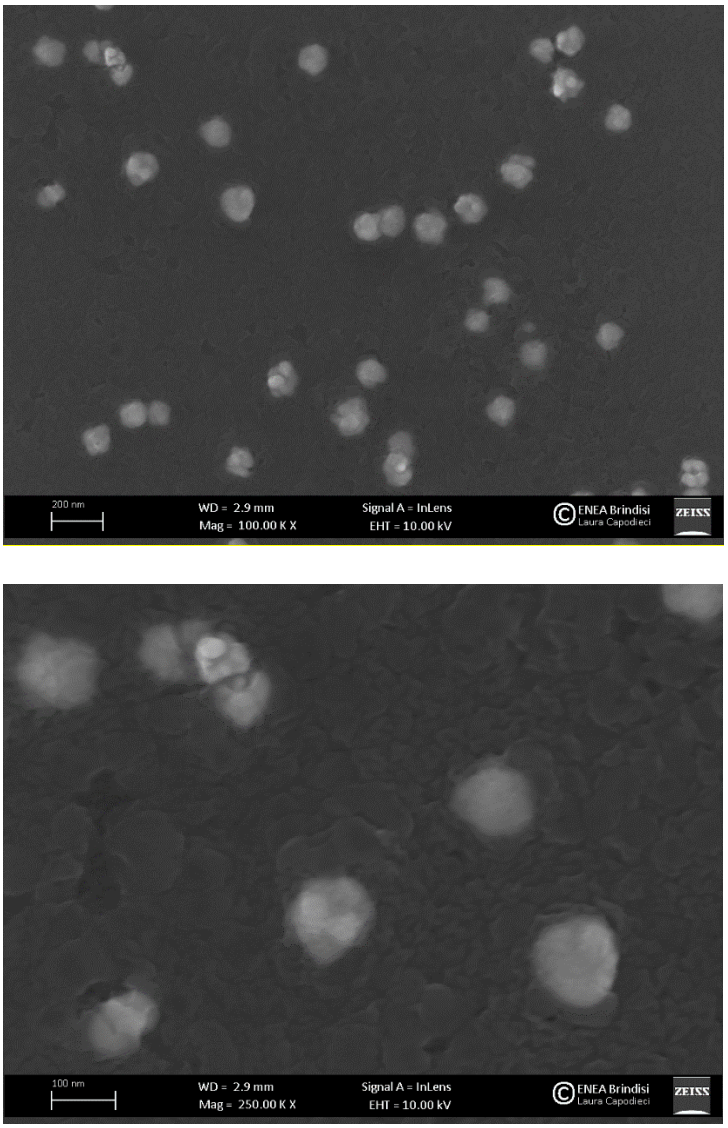

Figure 60 SEM images of the upper face of 100 nm doped AuNPs silica gel monolith at magnification x20k, x100k, x250k.

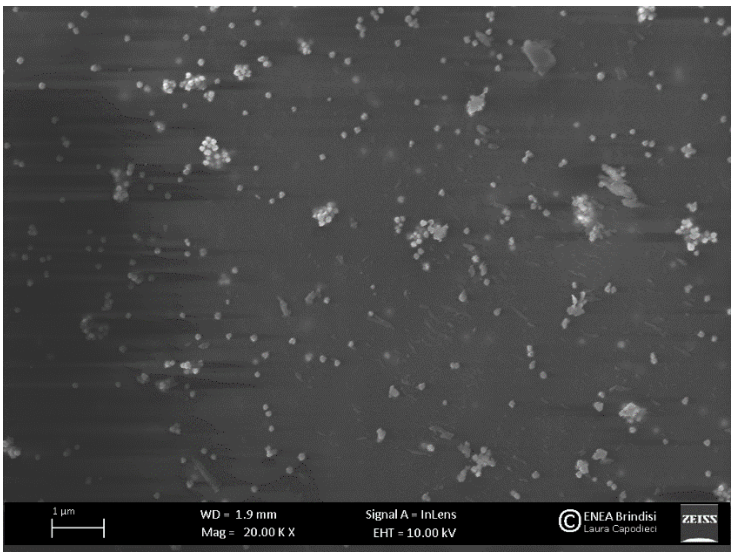

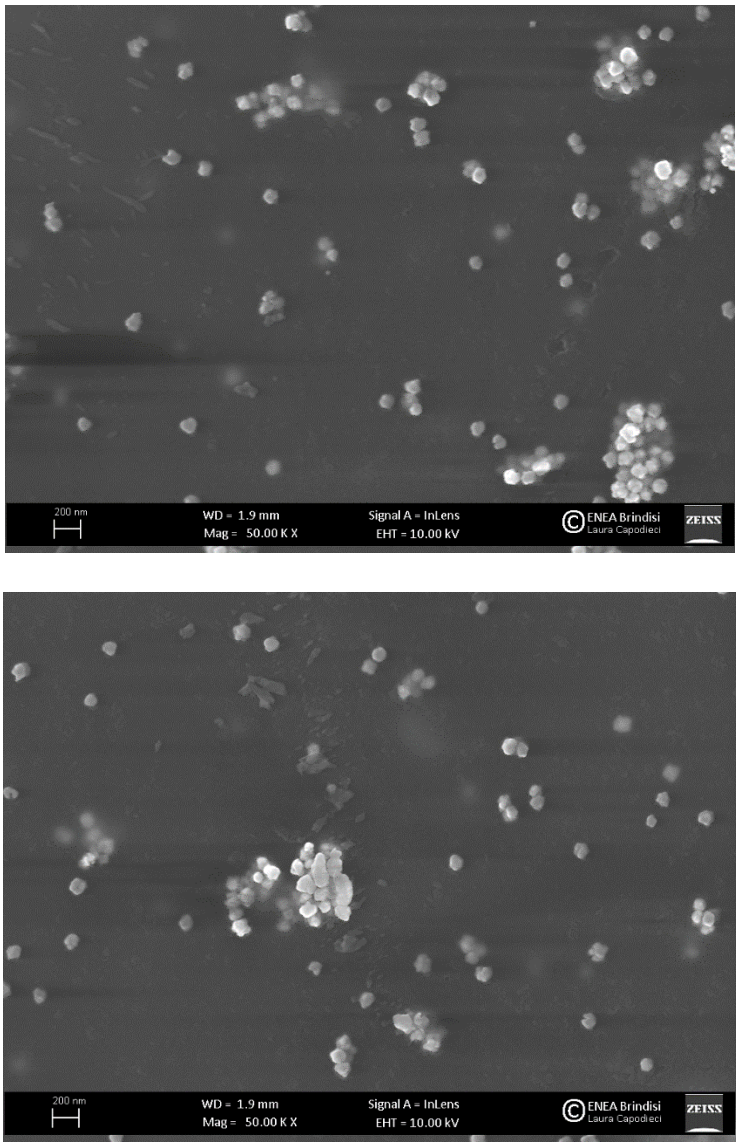

Figure 61 SEM images of the bottom face of 100 nm doped AuNPs silica gel monolith at magnification x20k and x50k.

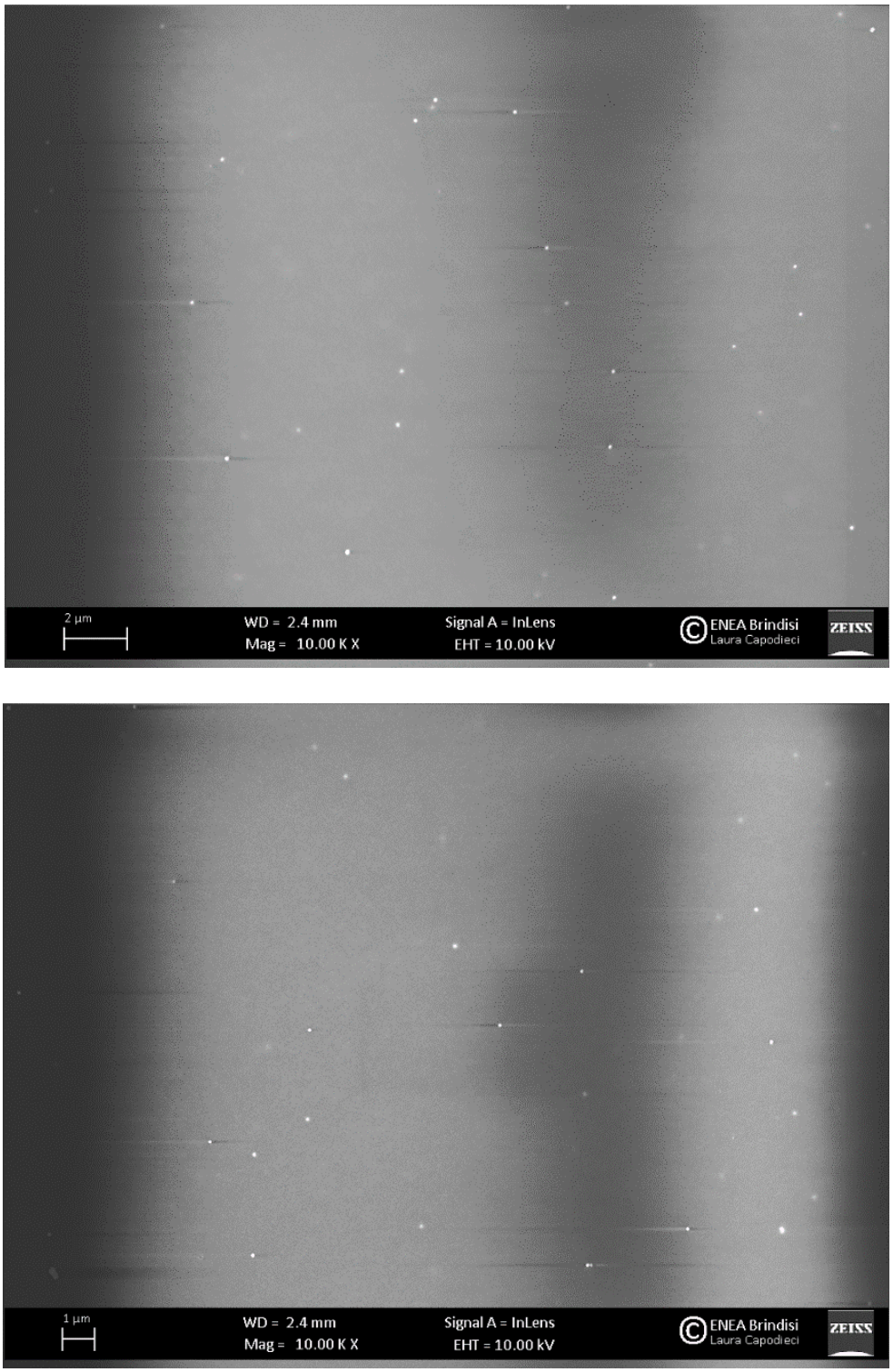

Figure 62 SEM images of the section of 100 nm doped AuNPs silica gel monolith at magnification x10k.

From these images can be observed the gold nanoparticles are present in the monolith. Upper face (Figure 60) presents AuNPs uniformly dispersed on/under the surface of the silica gel matrix. On the bottom face (Figure 61) some aggregates are present, most probably due to a selective precipitation of the heavier NPs during the long gelation process. In Figure 62, AuNPs are visible as bright spots in the section of the monolith in high concentration. The low quality of the section images is due to debris on the surface caused by the cutting of the monolith. Images 60, 61 and 62 were taken on fragments of the same Monolith.

The same samples were observed after the AuNPs removal process with aqua regia. Pretreatment at 80°C for 24 hours was performed to reduce humidity absorbed in the sample. The sample resulted sufficiently conductive, so that no sputtering was applied.

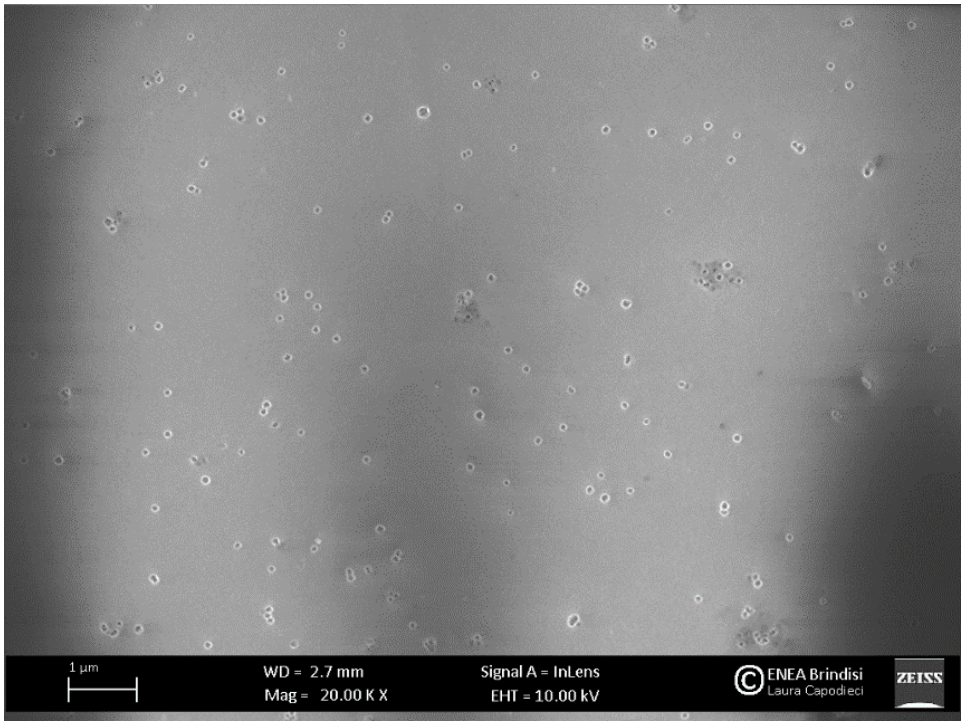

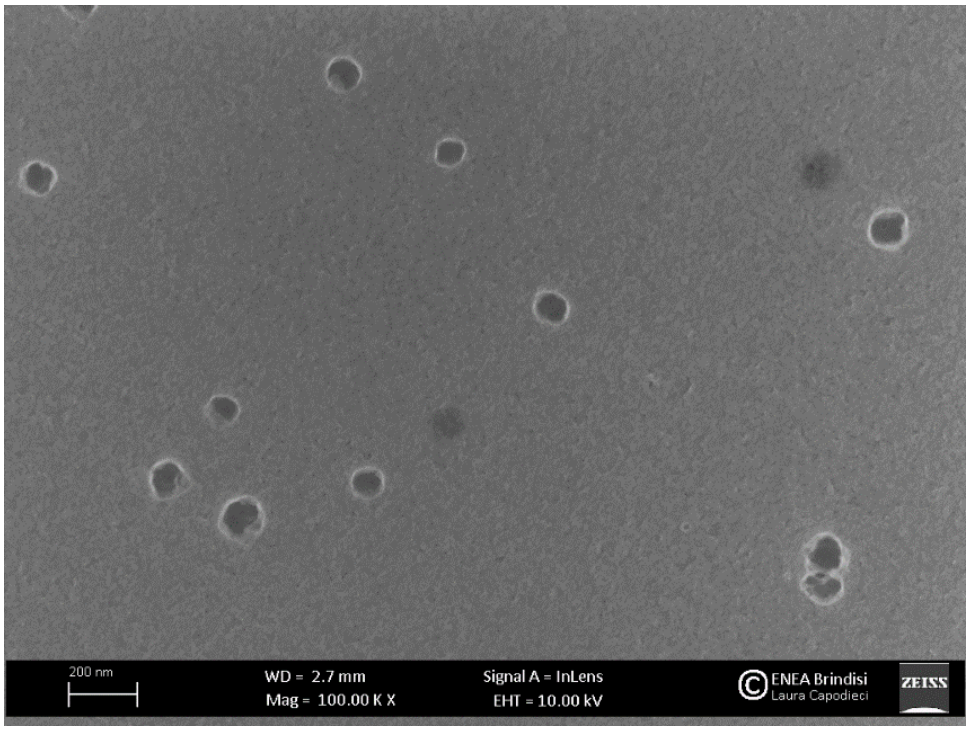

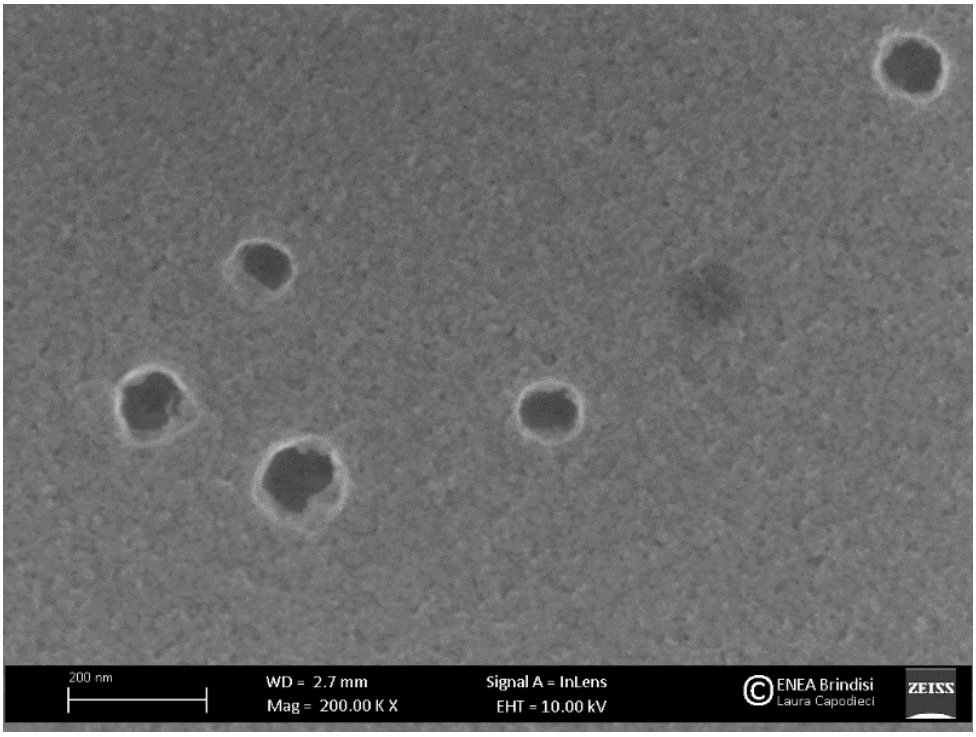

Figure 63 SEM images of 100 nm AuNPs doped monolith after the removal process with aqua regia, magnification x10k, x100k, x200k.

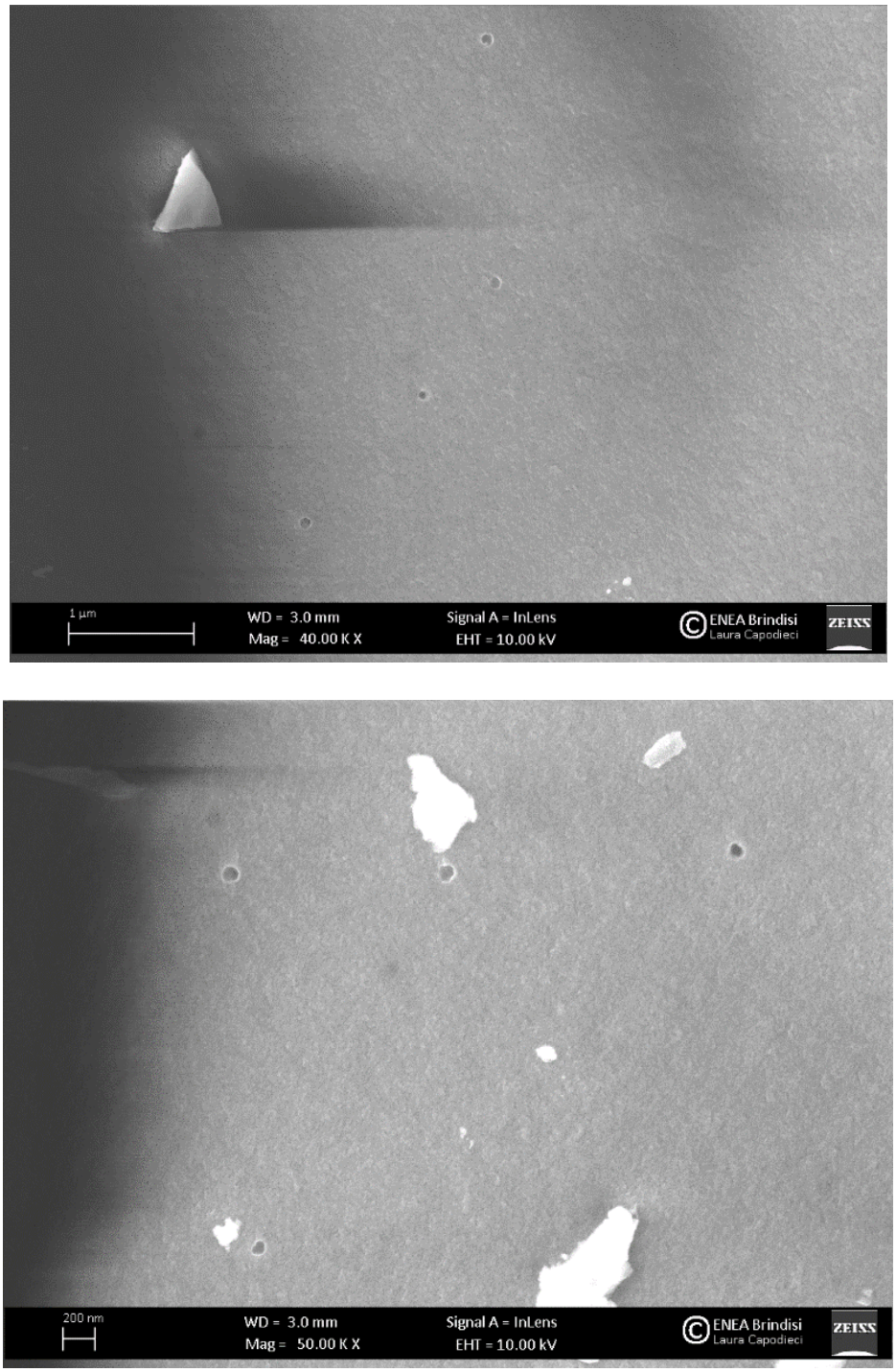

Figure 64 SEM images of section of 100 nm AuNPs doped monolith after the removal process with aqua regia, magnification x40k and x50k.

These cavities seem distributed with a comparable concentration with respect to the AuNPs before removal. Moreover, the dimensions of the cavities are coherent with the dimensions of the removed NPs, in both surfaces and section of the monolith. No alteration of the silica gel structure was observed after the treatment with aqua regia, indicating a fair inertness of the matrix in the removal treatments.

SEM imaging on 100 nm AgNPs doped monolith

SEM images were also collected on 100 nm AgNPs doped monoliths. From a first experiment carried out on 100x concentrated AgNPs monoliths ($2.08*10^{11}$ NP/L),, it was not possible to see the NP in the matrix, maybe due to low concentration. Imaging was thus repeated on a monolith (with the same AgNPs concentration) created with an "AgNPs concentrated" bottom face made by sedimentation of the NPs during the gelation process.

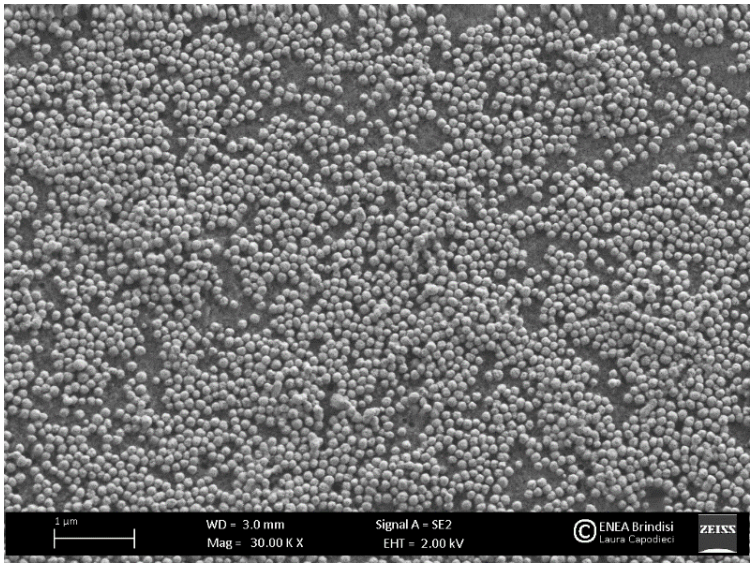

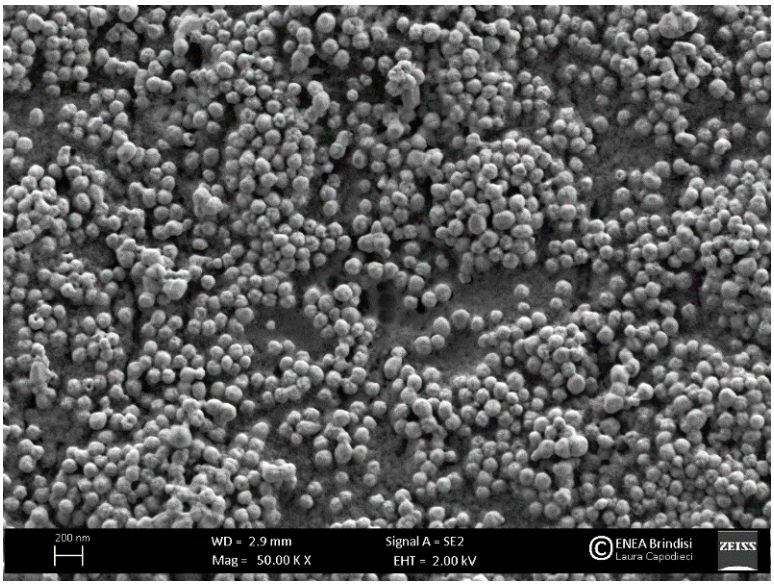

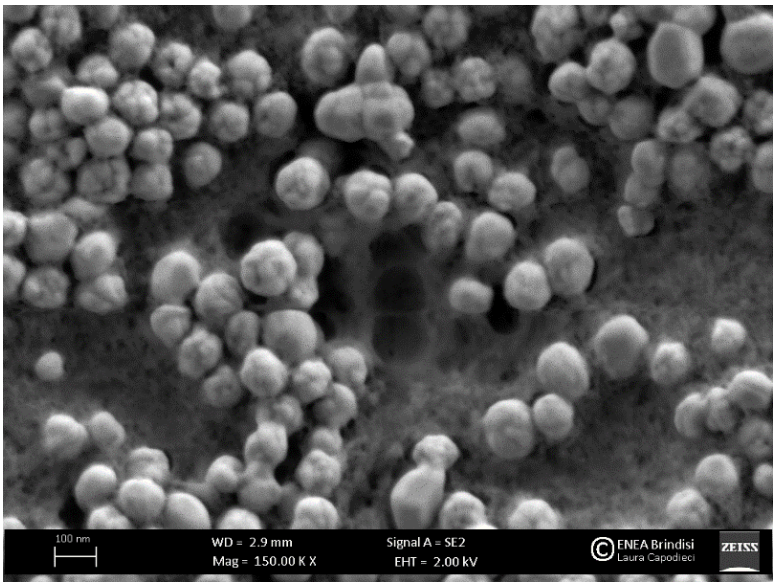

Figure 65 SEM images of the bottom face of 100 nm doped AgNPs silica gel monolith at magnification x30k, x50k, x150k.

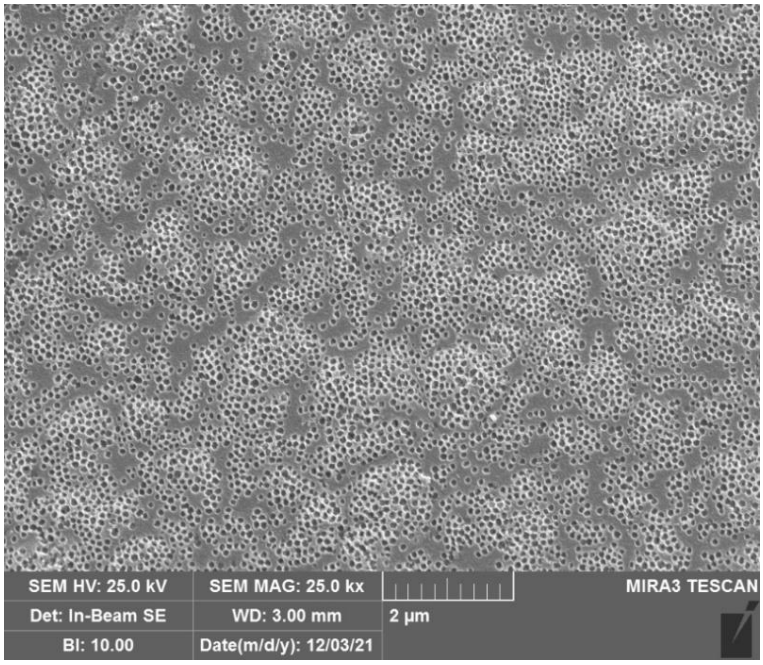

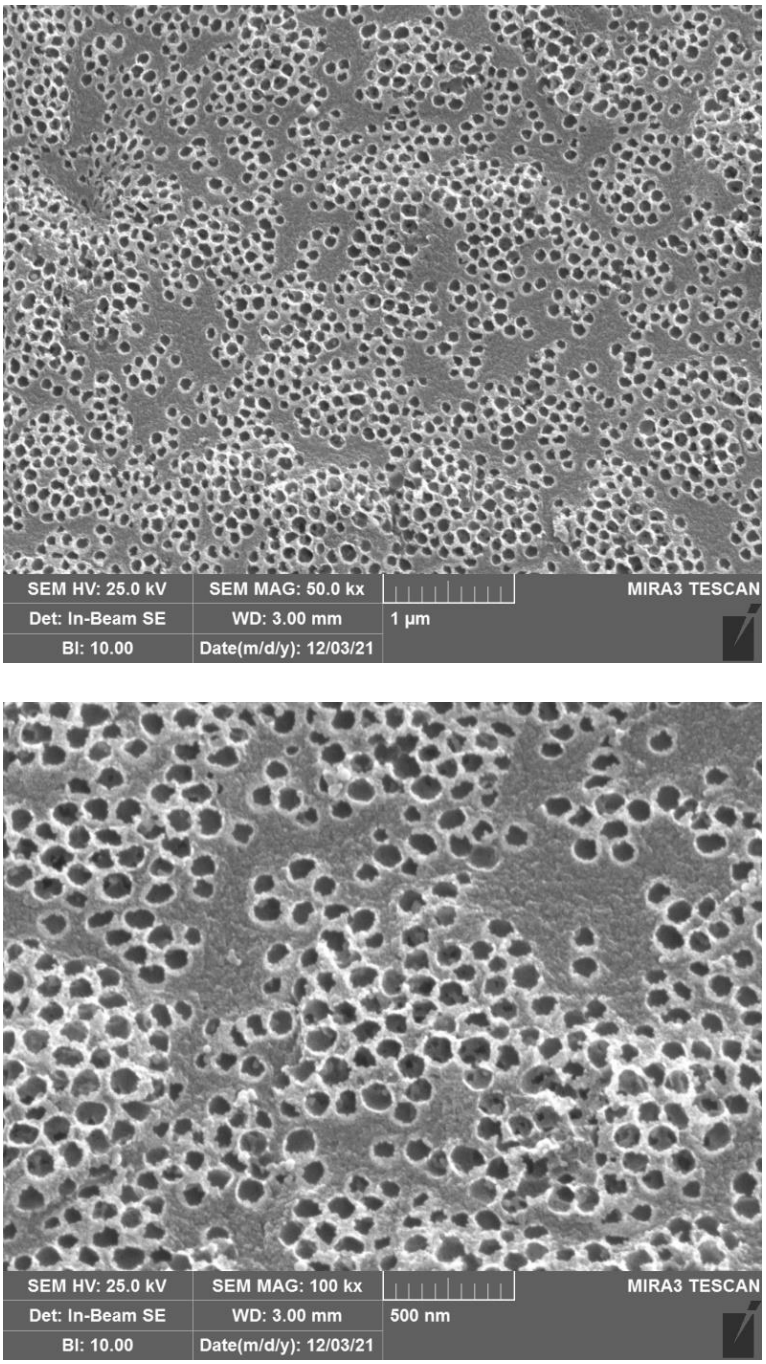

Figure 66 SEM images of the bottom face of 100 nm AgNPs doped silica gel monolith after removal process with cysteamine hydrochloride, magnification x25k, x50k, x100k.

After the treatment of the sample with concentrated nitric acid solution it was also possible to see the templated cavities in the bottom face of the monolith, that corresponds in dimensions to the diameter of the removed NPs.

XPS analysis

XPS analysis was performed on monoliths with embedded 7 and 100 nm AgNPs (Standard solutions, $1.15*10^{14}$ NP/L) for a better understanding of the separation by

gravity ("precipitation") during the gelation process, i.e. on the differences between bottom and upper faces. Ag XPS peaks were thus measured on upper face, bottom face and along the section every 200 μm.

Table 11 Concentration of silver in 7 nm and 100 nm AgNPs doped monoliths (Ag w/w%) on both monolith faces and in section. Each section is taken every 200 μm. Numbering of the sections starts with the one closer to the upper face

Measure site	AgNPs 100 nm doped monolith (Ag w/w%)	AgNPs 7 nm doped monolith (Ag w/w%)
Upper face	0	0.23
Section 1	1	0.37
Section 2	0.22	0.35
Section 3	0.41	0.29
Section 4	0.17	0.34
Section 5	0.27	0.39
Section 6	0.22	0.44
Section 7	0.41	0.31
Section 8	0.3	0.28
Section 9	3.4	0.35
Bottom face	22	0.32

From the table 11 it can be seen that monoliths with embedded AgNPs with larger dimensions (100 nm AgNPs) led to a gradient of concentration along the section, with the highest concentration of AgNPs on the bottom face. The 7 nm AgNPs doped monolith has almost a homogeneous concentration. These results confirm that during the gelation of the monolith a separation, or concentration process (similar to precipitation) takes place for bigger nanoparticles. On the contrary, small nanoparticles remain uniformly dispersed during the gelation of the monolith.

2.3.5 Silica Gel doped with anisotropic nanoparticles

Silica gel monoliths doped with anisotropic nanoparticles were synthesized with the purpose to check if the cavity left after the removal of the template maintain the shape of the starting nanoparticles.

2.3.5.1 Silica gel doped with Gold nanostars

The monolith was produced as described in the paragraph 2.2.3.6. It is turbid, black material, almost free of cracks. Monoliths were prepared using only 100x concentrated GNS solutions (Au_{tot}=5*10^{-2} M), it was therefore impossible to obtain UV-Vis absorption spectrum, due to saturation. The removal process of GNS was performed with aqua regia but the presence of silver as a constituent of the GNS (10-20%, used as "shape catalyst" during the preparation) led to the deposition of AgCl salt inside the structure. The monolith remained turbid after treatment. SEM images were collected on the external faces of the monolith before and after the washing process. A layer of gold was sputtered on the sample.

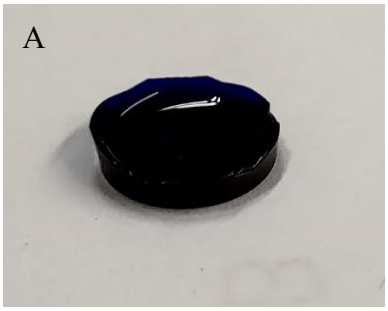

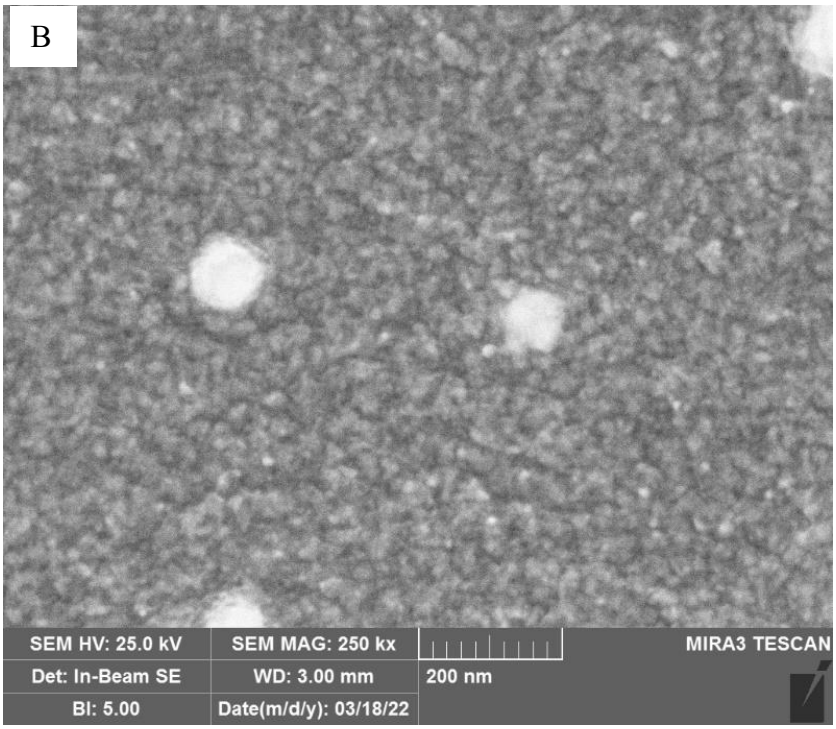
B
SEM HV: 25.0 kV
SEM MAG: 250 kx
MIRA3 TESCAN
Det: In-Beam SE
WD: 3.00 mm
200 nm
BI: 5.00
Date(m/d/y): 03/18/22

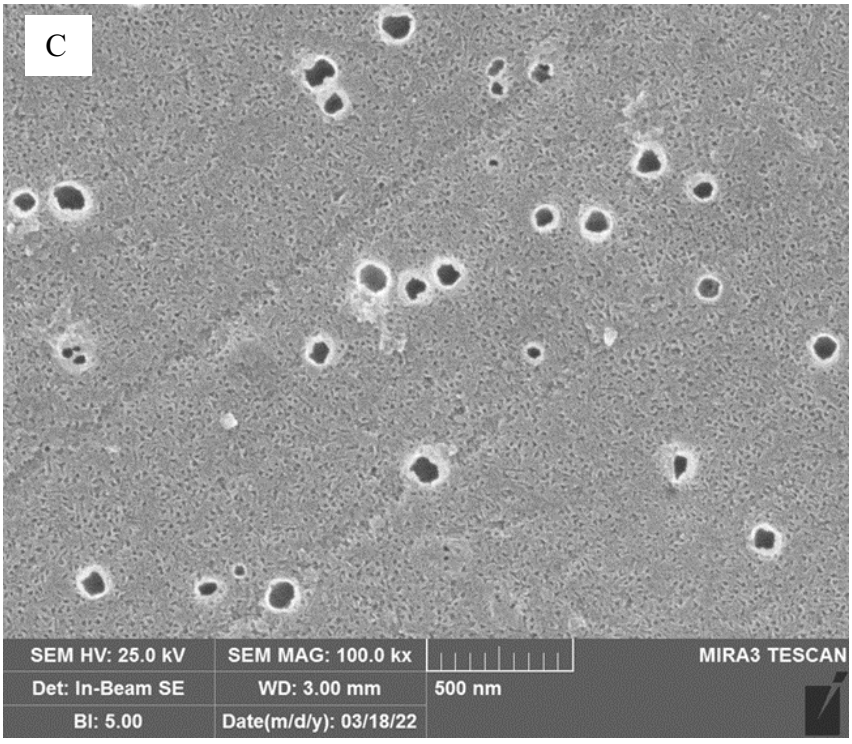
C
SEM HV: 25.0 kV
SEM MAG: 100.0 kx
MIRA3 TESCAN
Det: In-Beam SE
WD: 3.00 mm
500 nm
BI: 5.00
Date(m/d/y): 03/18/22

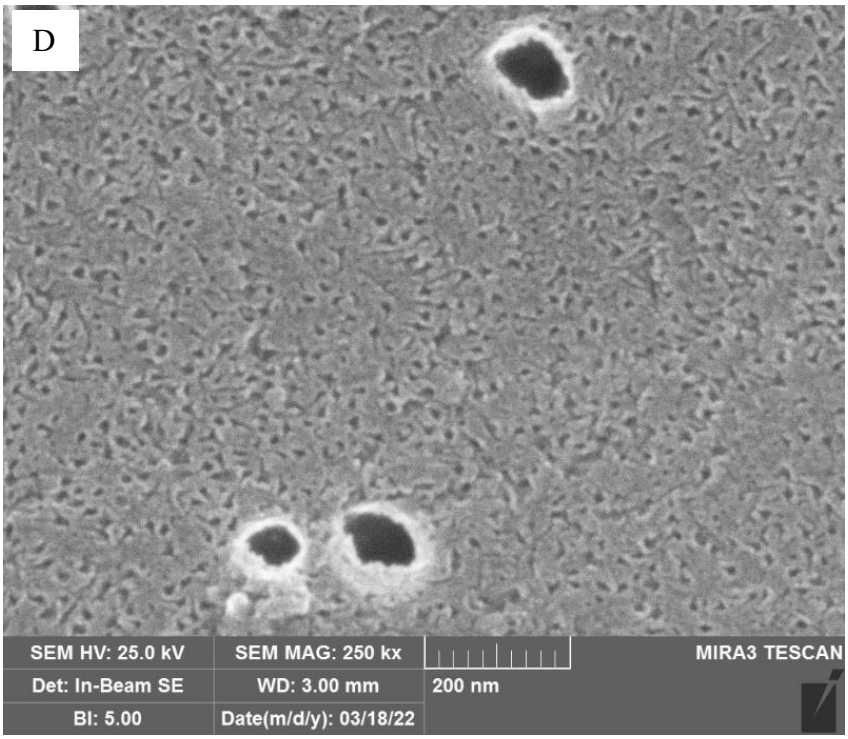

Figure 67 Image of GNS doped silica gel monolith(A); SEM image of GNS doped monolith (B) after removal process with aqua regia magnification 100kx(C); after removal process with aqua regia magnification 250kx(D).

From the collected images it was not possible to spot GNS on the surface of the monolith (probably due also to the use of a sputtered conductive layer), and only big bright spots were observed. However, in emptied monoliths it was observed a dense pattern with holes similar to the GNS shape. Large holes associated to aggregates were also present. Due to the large shape and dimensional distribution of the starting GNS colloidal solution (reflected in the shape of the imprinted voids after GNS removal) the study of this material was abandoned.

2.3.5.2 Silica gel doped with Prussian Blue nanoparticles

Monoliths were produced as described in paragraph 2.2.3.8. They are turbid dark blue almost crack free materials. Only monoliths made with more concentrated PBNPs were prepared, and therefore it was not possible to obtain a UV-Vis absorption spectrum, due to saturation. PBNPs can be easily degrade at basic pH, but at high pH values the degradation of silica gel structure could also take place (although with slower kinetics). At any rate, the removal process of PBNPs from the monolith was carried out with a Phosphate buffer 0.33 M, at the weakly basic pH of 7.4. It took 10 days to obtain full

decoloration of the monolith, that was also fully transparent. SEM images were collected on both doped and washed samples. A layer of gold was sputtered on the sample.

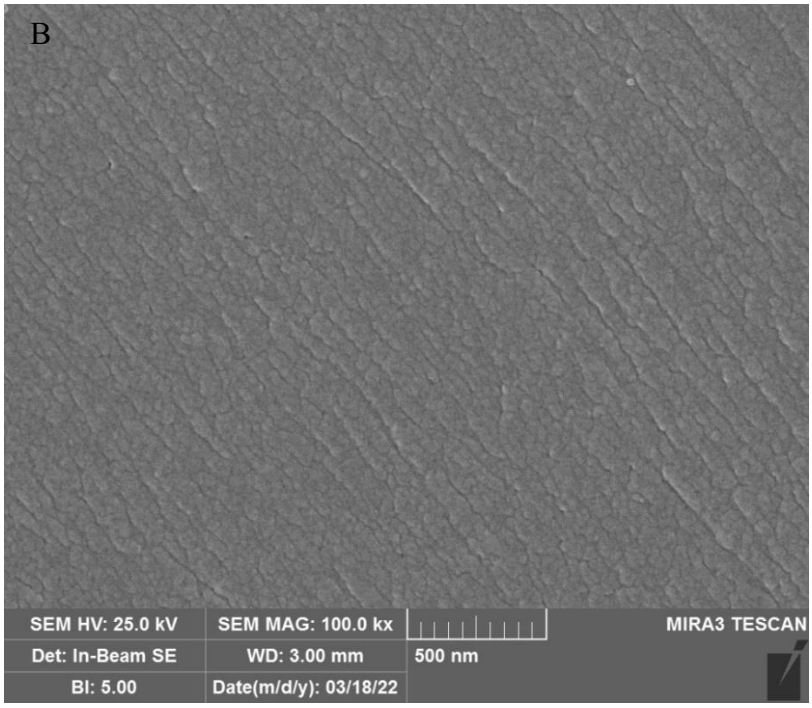

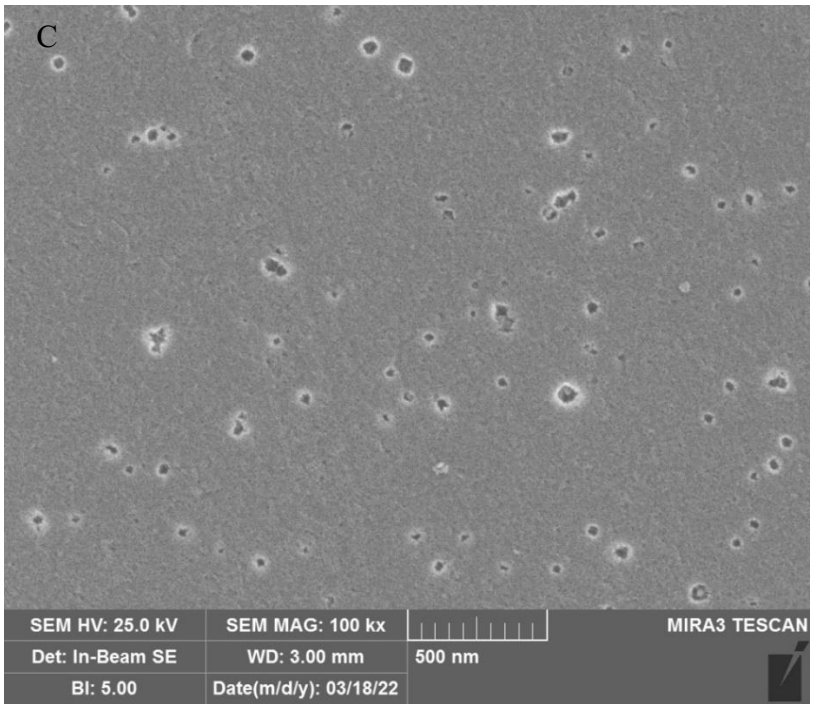

Figure 68 Image of PBNPs doped silica gel monolith(A); SEM image of PBNPs doped monolith before (B) and after removal process with pH 7.4 buffered solution(C).

PBNPs were not observed in the images (Figure 68 B) while after washing the monoliths, cubic cavities were detected with the proper size of the starting NPs reported (see paragraph 2.3.1.6 and Figre 28). The sputtered gold layer probably did not allow to observe PBNPs in Figure 68B, as they were not sufficiently protruding from the surface. On the other hand, the presence and the shape of PBNPs is confirmed by Figure 68C, where complementary cavities are clearly observed.

2.3.6 Reuptake process of 7 nm silver nanoparticles

2.3.6.1 Preparation of active templated Silica gel powder

From the SEM imaging of the upper face, lower face, and section (and also from the XPS analysis) it seems that most of the nanoparticles, and consequently of the voids, concentrate on the monoliths' surfaces. This could be due to an "exclusion" phenomenon, connected both to gravitation effects (lower face, precipitation) and also to a poor affinity of the coated particles with the forming silica matrix. However, a significant number ot nanoparticles, and consequently of cavities after NPs removal, are found inside the solid monolith. Due to the low dimensions of the intrinsic pores of the monoliths surfaces, these cavities are excluded from contact when reuptake processes are carried out. We thus decided to increase the number of available cavities by grinding monoliths. To obtain

small grains in the dimensional range of hundreds of microns, ball milling was first used, with different milling times: 10, 20, 30 and 60 minutes. The SEM imaging of the corresponding powders are displayed in Figure 69 A, B, C and D, respectively.

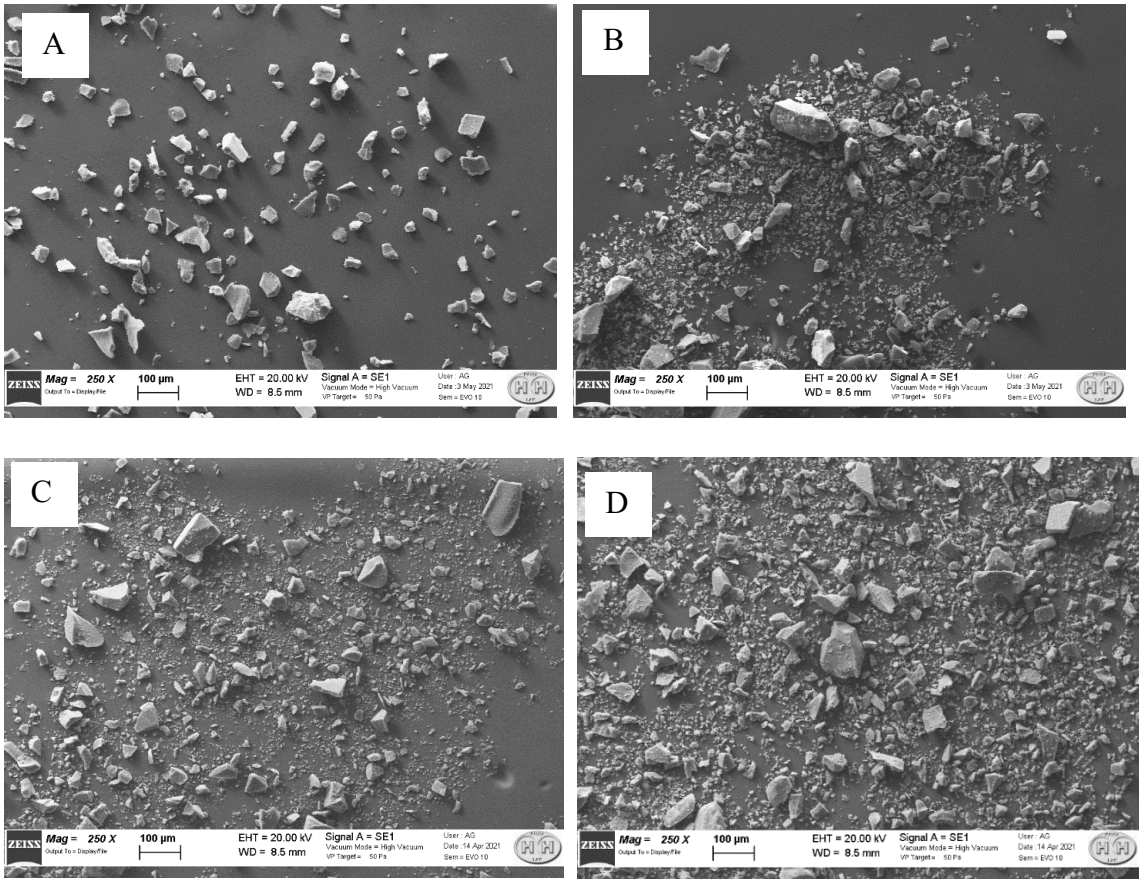

Figure 69 SEM images of silica gel powder at magnification x250 for 10 min(A), 20 min(B), 30 min(C), 60 min(D) ball milling time.

As it can be seen in Figure 69, different ball milling times led always heterogeneous size distribution, and after the grinding process big “non ground” residues remained. The best results wehwe obtained with 10 minutes grinding time, that gives an average size of the grains of about 50 µm. However, as it will be described in the next sections, the reuptake process of 7 nm AgNPs implied a centirfugation step, in which silica grains are made to precipitate (with the reuptaken AgNPs), while non-bound AgNPs remain in solution. Unfortunately, when using milling, a significant part of the milled materials remained in suspension under the used conditions, making the solution turbid and thus preventing to calculate by absorption spectroscopy the fraction of reuptaken AgNPs. We also carried out grinding of monoliths by mortar and pestle, a simple technique that allowed to bypass the just mentioned problem. SEM imaging shows that the size distribution is not too

distant from that observed with ball milling, with average size of 100 µm. This was assumed as the best grinding method and used in all the following studies.

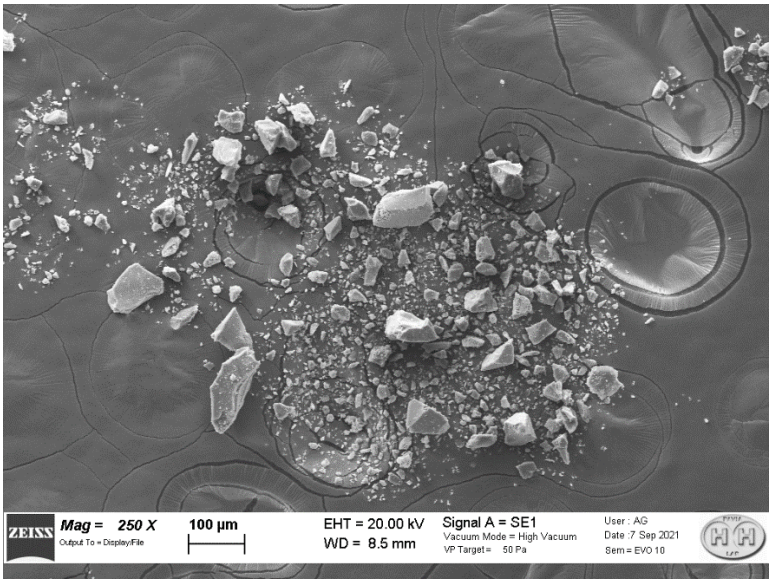

Figure 70 SEM image of mortar ground silica gel powder, magnification x250.

Doped silica gel powders were treated for the complete removal of NPs as described in paragraph 2.2.5.2 (nitric acid oxidation) It was also checked the pH of the dried powders by suspending it in bidistilled water. The pH of the supernatant remains about 7. The final product is a white powder.

Figure 71 7 nm doped Silica gel powder before (left) and after the removal process with nitric acid (right).

Washing process and purification was used as standard procedure for the removal of AgNPs 7 nm and AuNPs of 20 and 100 nm sizes. The final products were nominated: ESG7nm (Emptied Sol Gel 7 nm templated cavities); ESG20nm (Emptied Sol Gel 20 nm templated cavities); ESG100nm (Emptied Sol Gel 100 nm templated cavities). To have

homogeneous results, the Blank silica gel without nanoparticles was treated as these three samples and it was denominated SGB (blank silica gel).

2.3.6.2 Reuptake process of AgNPs 7 nm by monolith powder in suspension

The best experimental setup for the reuptake of 7 nm AgNPs solution is the direct suspension of the templated powder in a solution of 7nm AgNPs as described in paragraph 2.2.5.3. It should be mentioned again that this process is only possible with the small 7 nm AgNPs, because only these parti kind of NPs t can be separated by ultracentrifugation from the suspended silica powder (all larger AgNPs or AuNPs precipitate as well as the silica particles under the used conditions)

2.3.6.3 Reuptake process of AgNPs 7 nm by different monolith powders

Reuptake process was first performed with reaction time of 1 hour. AgNPs were used with a 10 times dilution ([Ag] = $5.8*10^{-5}$ M) to decrease the absorbance of the solution and allow to use a cuvette with an optical path 1 cm to determine the AgNPs concentration in the starting solution and after removal by emptied silica powders. The silica gel powder that we used was that doped with AgNPs 7 nm at a NP concentration of $6.68*10^{16}$ NP/L. As a control, also a silica gel for columns (230-400 mesh) purchased from Sigma Aldrich was used for reuptake. Moreover, Blank silica gel powder, AgNPs 7 nm doped silica gel powder and the corresponding empty silica gel powder with cavities of 7 nm were used for reuptake. A control solution of AgNPs $5.8*10^{-5}$ M was treated as the samples but without the addition of silica powder, to normalize the observed data for the possible loss of absorbance of the process.

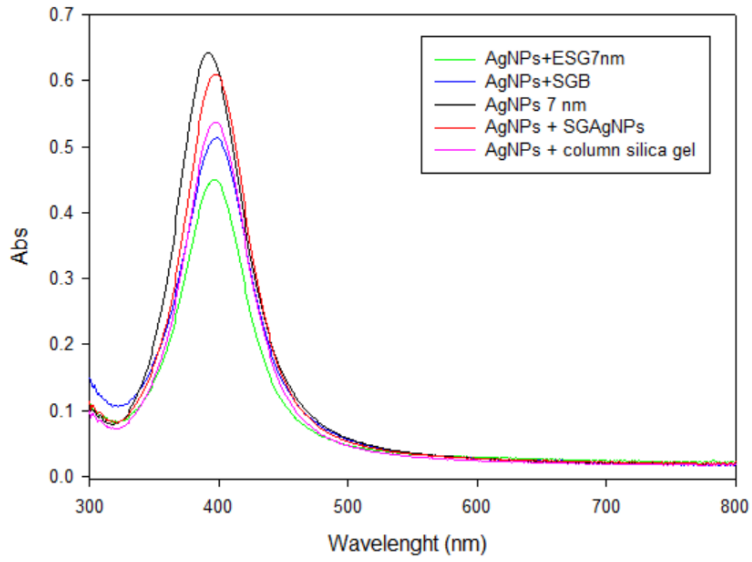

Figure 72 Extinction spectra of the AgNPs solution after reuptake process with different silica gel powders: Emptied sol gel with 7 nm cavities (green line); Blank sol gel without cavities (blue line); Sol gel templated with 7nm AgNPs (orange line); Column silica gel 230-400 mesh (pink line); control AgNPs solution (black line)

Table 12 Loss of absorbance during the reuptake process of 1 hour with different kind of silica gel powders

Powder of ground Sol Gel	**ΔAbs% (1 hour)**
Column Silica Gel	18
Sol Gel doped with AgNPs 7nm	5.6
Blank Sol Gel	20.2
Emptied Sol Gel	30.4

From the series of spectra displayed in Figure 72 it can be seen that after 1 hour of reaction a small decrease of absorbance took place in every sample. This can be attributed to the intrinsic ability of silica to establish Van Der Waals aspecific interactions with AgNPs. Significantly, the Δabs found with the column silica and the blank gel powders are very similar. The powder of the silica with still embedded AgNPs is instead the less efficient in the adhesion process (maybe due to the reduced SiO2 surface available for silica-

AgNPs interaction). To our aims, the most interesting result is that the higher value of ΔAbs is associated to the silica gel powder with empty cavities, with a reuptake value of 30.4%..

2.3.6.4 Reuptake process of AgNPs 7 nm with longer contact times (reuptake kinetics)

The reuptake process using ESG7nm was repeated with different contact times in a solution of 7nm AgNPs. The process was carried out in the same conditions of the previous experiment. Six samples were prepared and kept under stirring. After the chosen time (as reported in Table 13) a sample was ultracentrifugated and the UV-Vis spectrum was acquired.

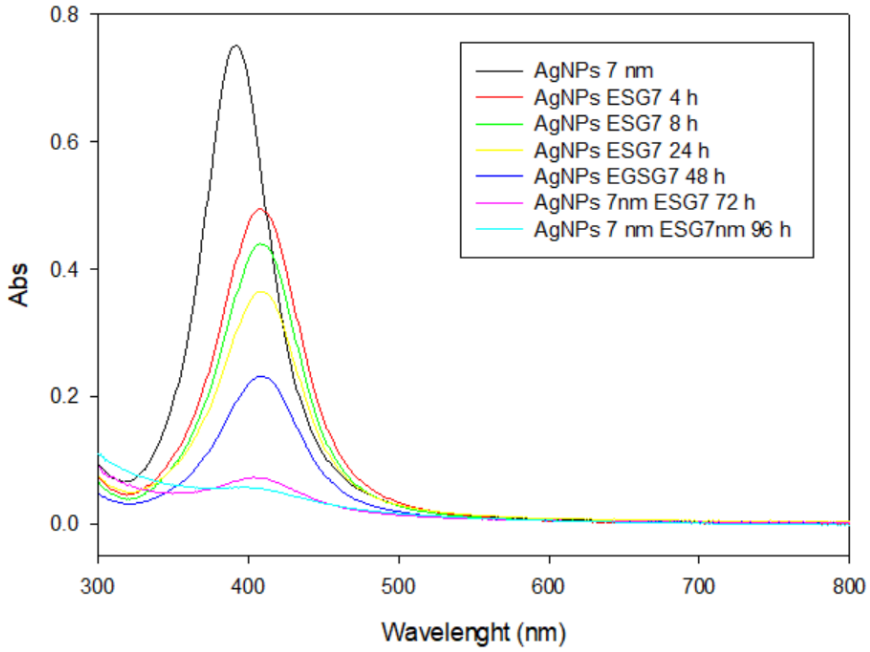

Figure 73 Extinction spectra of the AgNPs solution during reuptake process at different times.

Table 13 Loss of absorbance during the reuptake process at different times.

Time (hour)	Δabs%
4	34.45
8	42.23
24	51.84
48	69.82
72	90.75
96	92.57

From the reported results it seems clear that the reuptake process is time dependent, with slow kinetics. An approximate $t_{1/2}$=24 h could be calculated, while the reuptake process is almost complete after three days. After the reaction and separation by ultracentrifugation the supernatant solutions were pale yellow or almost colorless, depending on contact time. In turn, the white powder ESG7 powder turned increasingly yellow with increasing contact time.

2.3.6.5 Reuptake process of AgNPs 7 nm at different concentrations

A reuptake process was carried out with 72 h contact time, using 7nm AgNPs solutions with different concentrations. A starting AgNPs solution of $5.8*10^{-4}$ M (concentration as per standard synthesis) was diluted 2, 5 and 10 times. A cuvette with an optical path of 1 mm was used to avoid the saturation of the absorbance signal of the concentrated solutions.

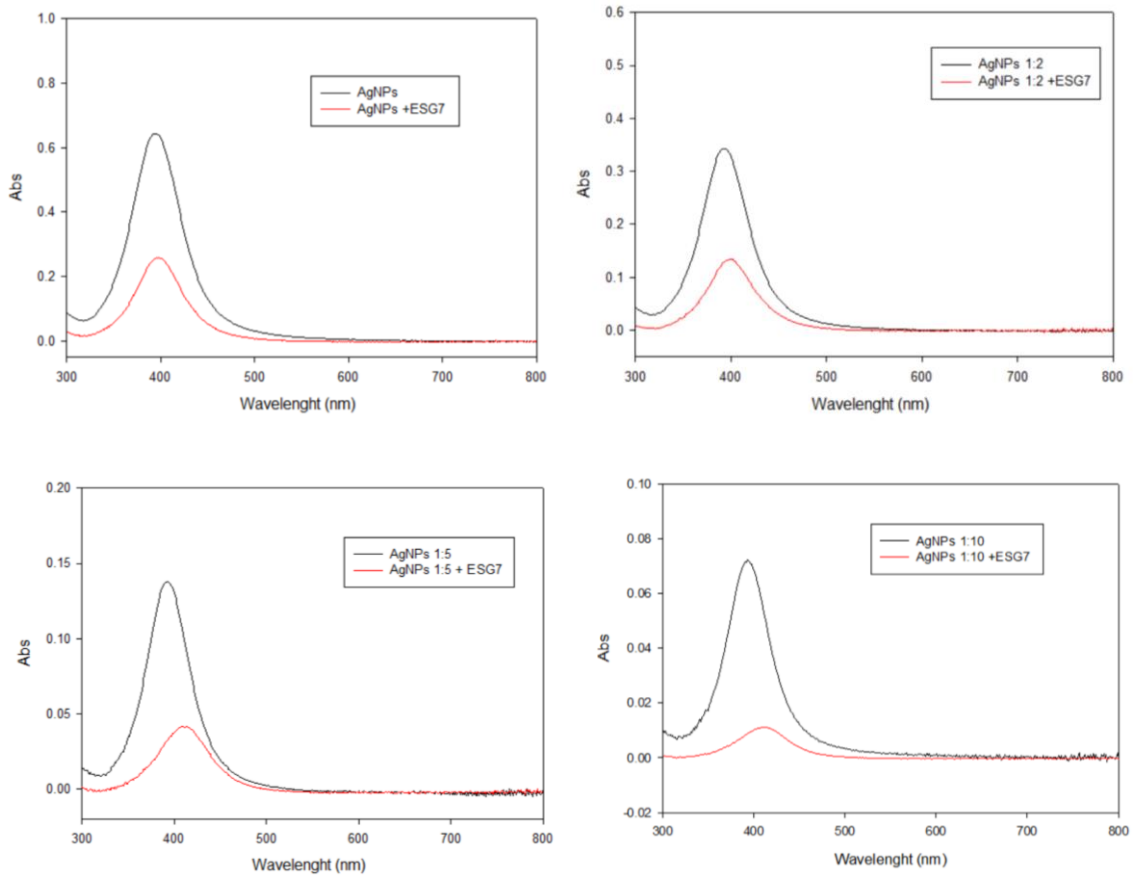

*Figure 74 Extinction spectra of AgNPs at different concentrations after 3 days of reuptake process. A) Starting solution of AgNPs 5.8*10^{-4} M; B) 1:2 diluted solution; C) 1:5 diluted solution; D) 1:10 diluted solution. Please note that the Abs scale is different in each panel*

The ΔAbs% calculated are: AgNPs solution 60%; 1:2 AgNPs solution 65%; 1:5 AgNPs solution 73%; 1:2 AgNPs solution 86%. As expected, the ΔAbs decreases with increasing the AgNPs concentration, most probably because of the saturation of the available cavities inside the silica structure.

2.3.6.6 Reuptake process of AgNPs 7 nm with powders featuring cavities with different dimensions (size selectivity)

Reuptake process on 10 times diluted AgNPs solution (with respect to standard synthetic concentration) were carried out also using powders templated with different size NP, i.e. featuring cavities of 7, ~ 20 and ~ 100 nm. First, silica gel powders were used with comparable concentration of templated cavities: ESG7nm (1.15*10^{14} NP/L), ESG20nm (1.40*10^{14} NP/L), ESG100nm (7.20*10^{13} NP/L). The reaction was made on three sets of samples per cavity size to calculate a reliable standard deviation.

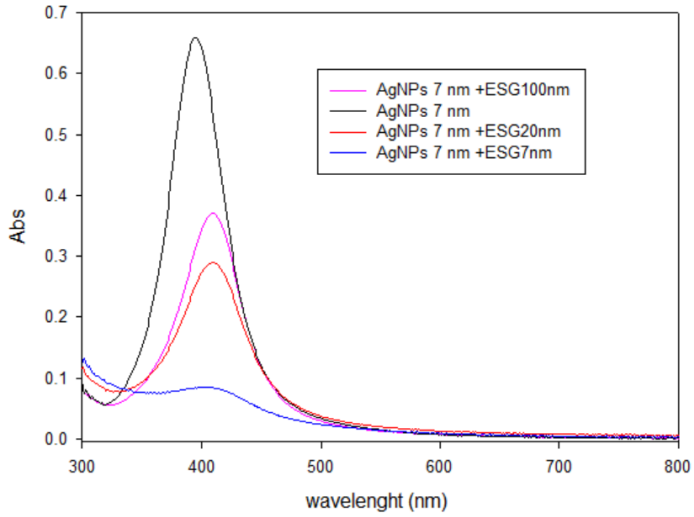

Figure 75 Extinction spectra of AgNPs solution after 72 h of reuptake process with powders featuring different size cavities at the same concentration

Table 14 summarizes the results expressed as ΔAbs% after 72h contact time.

Table 14 Loss of absorbance during the reuptake process at with powders with different size cavities at the same concentration.

cavity size (nm)	ΔAbs%	Std.dev.	cavity conc (n/L)
7	87.1	1.4	$1.15*10^{14}$
20	68.1	8.1	$1.40*10^{14}$
100	44.3	7.7	$7.20*10^{13}$

As it can be seen from the Table 14, an also as it is visualized by Figure 75, the ΔAbs value increases as the NPs diameter becomes similar to the cavity size. This result suggests that the templated material has a selectivity for the NPs of the proper size of the cavities. The experiment was repeated using silica gel powders with different cavities concentration: ESG7nm ($6.68*10^{16}$ NP/L), ESG100nm ($7.19*10^{12}$ NP/L), ESG20nm ($1.14*10^{14}$ NP/L).

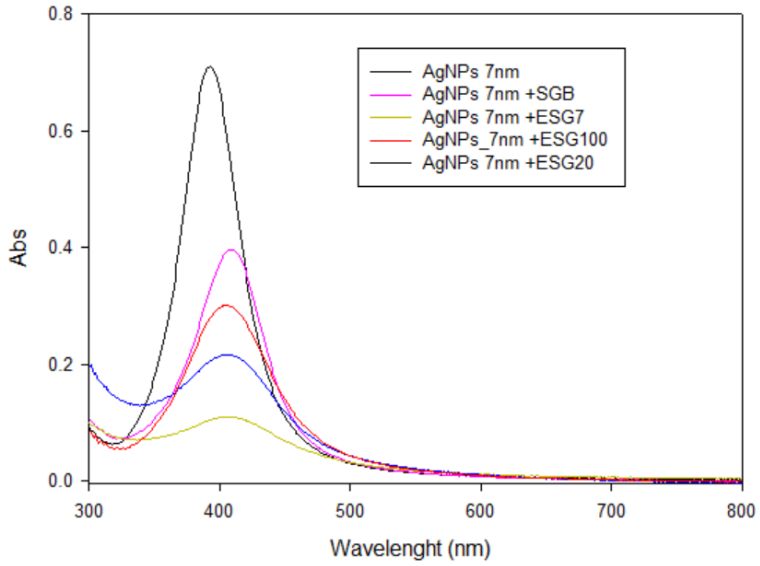

Figure 76 Extinction spectra of AgNPs solution after 3 days of reuptake process with powders with different size cavities at different concentrations.

Table 15 Loss of absorbance during the reuptake process at with powders with different size cavities at different concentration.

cavity size (nm)	ΔAbs%	Std.dev.	cavity conc (n/L)
7	87.3	3.0	$3.3*10^{15}$
20	68.1	8.1	$1.40*10^{14}$
100	53.20	4.5	$7.20*10^{12}$
Blank	39.88	4.7	0

Data show that different concentrations of cavities give similar results to what obtained when similar cavities concentration were used, maintaining the observed cavity fit selectivity.

2.3.7 Geometrical modelling of size selective cavity-nanoparticle interaction

Nanoparticle-size interaction geometrical model have been created on the basis of the previous results. The low point of zero charge of silica (reportedly between pH 2 and 3), and the neutral, slightly acidic pH of the AgNPs solutions to be reuptaken (always > 4-5), points towards a negative charge of the surface of the silica particles. 7nm AgNPs have a citrate coating that imparts them a negative charge too. As a matter of fact, no attractive electrostatic interaction is possible between silica particles and the used 7nm AgNPs. Thus, we built a model hypothesizing that Van Der Waals interactions (London attractive forces) are the only responsible of the adhesion of AgNPs to the silica particles.

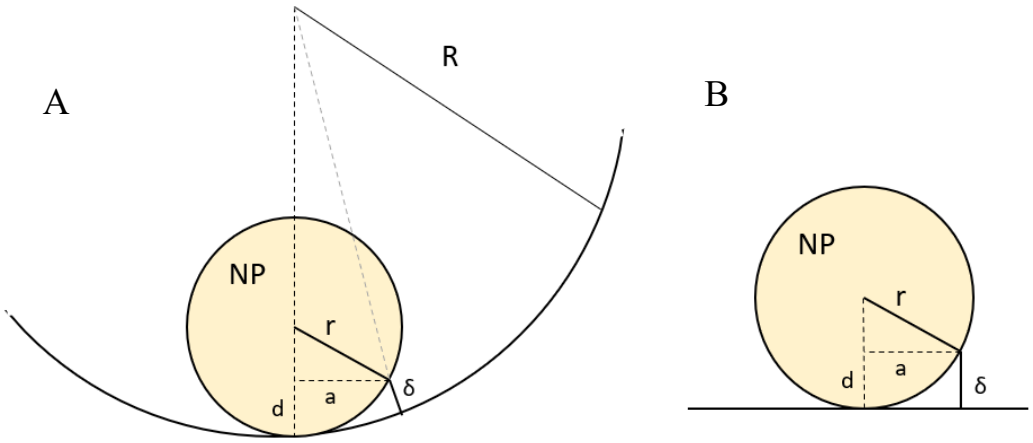

Figure 77 Geometrical models for the interaction of a NP-curved cavity (A) and a NP-flat surface (B). R: cavity radius; r: NP radius; δ: distance of interaction cut off (in flat surface d= δ)

VdW interactions decay very fast with the distance "d" between the particle and the surface of a solid material. We can therefore define a cut off distance (δ), considering that only the fraction of the particle surface that is close enough to the solid surface (e.g. d< δ) will contribute to the Van der Waal attraction forces. Under this assumption, when a spherical particle interacts with a flat surface, only a small fraction of the sphere will contribute to the attractive forces, for instance, considering a cut off distance δ =1nm and a spherical NP of r=4nm, we can estimate that only 12% of the particle surface can interact with a flat solid surface, reducing therefore the effective strength of the attraction forces.

Similarly, when the NP interacts with a curved surface, such as the inner surface of a cavity, it is possible to calculate the fraction of the particle surface interacting with the curved cavity. In this case, the fraction of interacting NP surface will depend on the ratio between the particle size (r) and the radius of curvature of the cavity (R), leading to a

relative increase of the particle-cavity interactions as this ratio increases (see Figure 78). In fact, within a curved cavity, we can expect a larger fraction of the NP surface to be close enough to the solid material, compared to a flat surface of the same material. This effect can be modelled using simple geometrical considerations (see figure 77), leading to the conclusion that the interactions will be stronger when the particle size and the radius of curvature of the cavity are similar.

Triangle 1: $(R-\delta)^2 = a^2 + (R-d)^2$

Triangle 2: $r^2 = a^2 + (r-d)^2$

$(R-\delta)^2 - r^2 = (R-d)^2 - (r-d)^2$

$(R-\delta)^2 - r^2 = (R+r-2d)(R-r)$ With R≠r

$$d = -\frac{(R-\delta)^2 - r^2}{2(R-r)} + \frac{1}{2}(R+r)$$

$$d = \frac{1}{2}[(R+r) - \frac{(R-\delta)^2 - r^2}{(R-r)}$$ Curved surface

This simple geometrical model can explain the selectivity of the silica materials decorated with cavities, in the reuptake process of AgNPs.

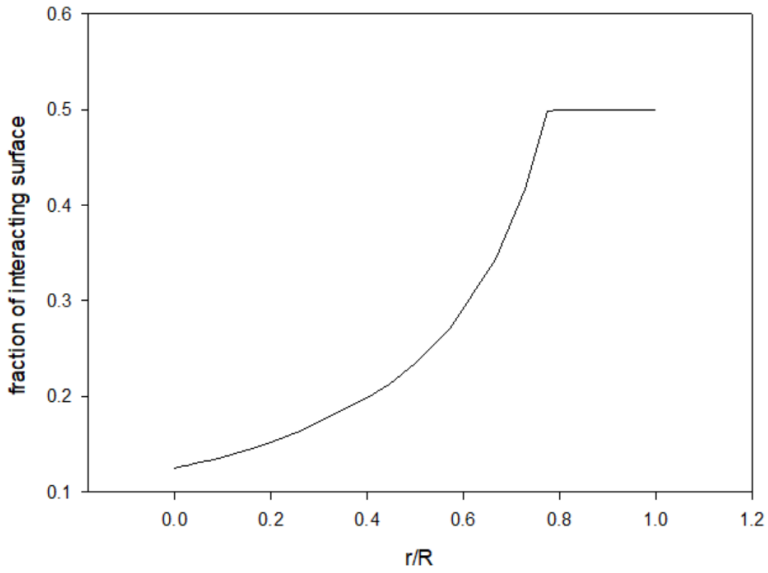

Figure 78 Increasing of interacting surface as the reaching of the R value.

It is important to note that within this model we have assumed that cavities are half-hemispheres, to allow for the NP to enter (i.e. when the size of the NP is close to the cavity radius, the NP can only enter the cavities that have been cut through at least by half). For this reason, the limiting value of the NP surface fraction is 0.,5 when NP and cavity sizes become equal. This assumption is not limiting the overall interpretation of the results and become irrelevant for cavities much larger than the NP size.

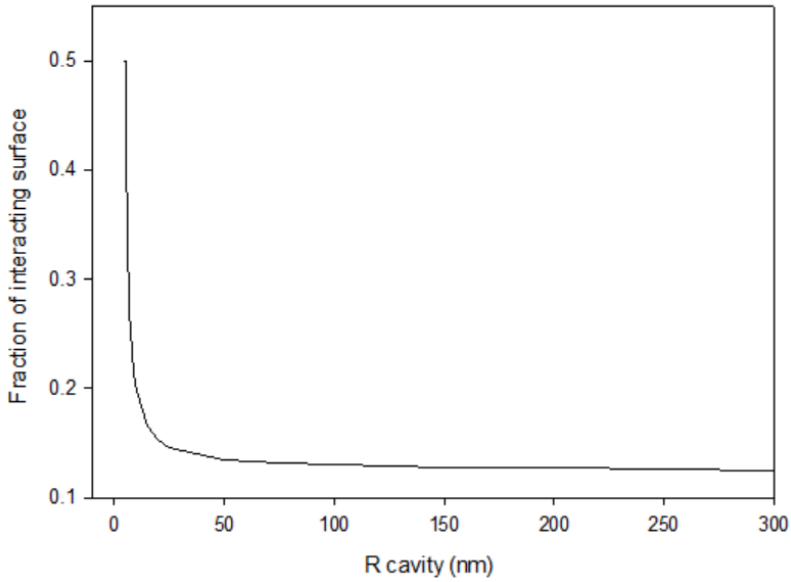

Figure 79 Fraction of interacting surface VS the cavity size.

2.3.8 Preparation of functionalized Quartz crystal microbalances sensing system

In order to exploit the found selectivity of the templated void silica materials, we first imagined their possible use as sensors. As it was described in the introduction, AgNPs are extensively used for many commercial applications, and their leakage in the environment (air, water) may be an issue, especially considering that oxidation by air may take several days/weeks to be complete. Accordingly, an attempt was made to functionalize the surface of quartz crystals for microbalances with the silica materials used in this research. The approach that was chosen consisted of spin-coating the active crystals with PDMS, to be used as an adhesive layer to "glue" a further thin layer of imprinted silica powders, during the spinning process.

To optimize the functionalization parameters of QCM, it was first studied the maximum of deposited load weight. However, the excess of load on QCM led to the loss of resonance frequency. The experiment consisted of the functionalization of silver electrodes QCM with resonance frequency 10 MHz with solutions of PDMS with rising concentration in THF from 1% to 10%. The PDMS film was applied as described in paragraph 2.2.6.

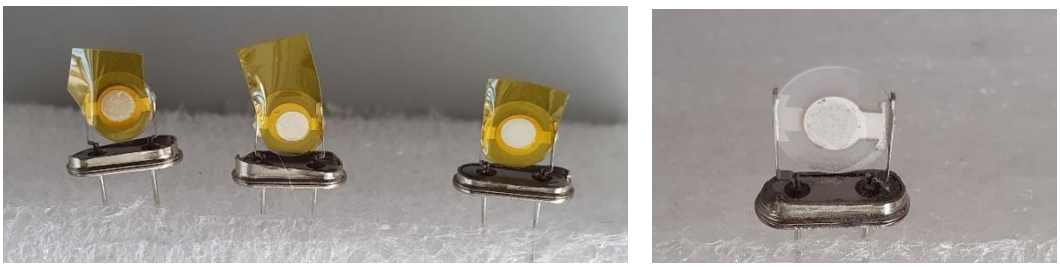

Figure 80 Silver electrodes QCMs masked with Kapton (left); silver electrodes QCM functionalized with silica gel powder (right).

Table 16 Variation of mass and resonance frequency with % of PDMS in the deposited solution.

%PDMS in THF	Δm (mg)	ΔFreqency (MHz)
1	0	0.0042
2	0	0.0067
3	0	0.0060
4	0	0.0062
5	0.1	0.0099
6	0.3	Off scale
7	0.3	Off scale
8	0.4	Off scale
9	0.4	Off scale
10	0.5	Off scale

It was found that the supported load weigh must be ≤0.1 mg. This value resulted too low for a complete functionalization of the QCM. The same load limit was also found on the QCM with frequency of 20 MHz. The functionalization of gold electrodes QCM with frequency of 10 MHz was also tried. This kind of QCM is very expensive therefore the method of functionalization was developed and perfected on test slides. The method allowed the controlled deposition of 0.3 ± 0.1 mg. It was tried the functionalization of all the electrode surface (1 mg deposited) and the functionalization of a small part of the electrode (0.2 mg deposited).

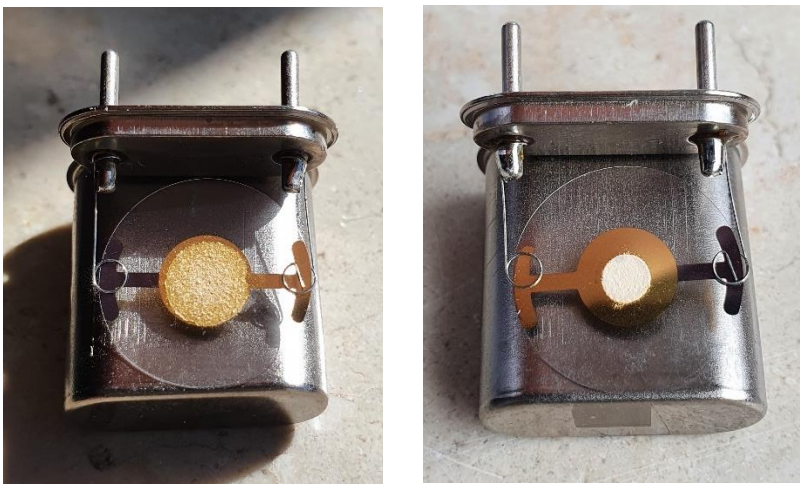

Figure 81 Silica gel powder functionalized gold electrodes QCMs, on the left full electrode functionalization (1 mg deposited), on the right partial functionalization of the electrode (0.3 mg deposited).

Despite the bigger stability and dimensions of the gold electrodes QCMs, after the functionalization of the electrode, the resonance frequency shifted to an upper harmonic of value of 35 MHz. This frequency of oscillation is unstable and cannot be used for sensing purpose. From these results it is clear that the massive functionalization of the electrodes with silica gel powder unfortunately doesn't fit with the sensing method. Data suggest that only molecular monolayer can be used for this application.

2.3.9 Further applicative attempts

In this research work, it was demonstrated that the void, imprinted silica gel materials are able to efficiently and selectively capture silver nanoparticles from aqueous solutions. However, this observation regarded the lab bench level. Some attempts were made to use our materials in applications that may lead to technological transfer to industrial or daily life use. First, massive portions (2-3 cm height) of grinded powders were layered in a small diameter (1 cm) chromatography columns, in the attempt of filtering off AgNPs from an aqueous colloidal solution. However, the system gets clogged immediately, i.e. water was not able to flow through the column solid phase driven just by gravity. Even if we did not exert any pressure during the packing process, it was evident that the silica particles were too small, and the stationary phase too dense, to allow water flowing through it. Experiments carried out with non-imprinted silica powders prepared by the same procedure (grinding monoliths) drove to the same results.

We also imagined to use a flow system, in which the active, imprinted silica particles are fixed on the walls of a macroscopic fluidic pattern. We tried to glue (with superglue) the monoliths powder on the internal wall of a Pasteur pipette, but we obtained only unsatisfactory and irreproducible modified surfaces.

The preparation of more controlled macro/micro surfaces for fluidic systems (e.g. using spin coating) or the preparation of imprinted silica microparticles of more controlled dimensions and shape to be used as stationary phase in a filtering system, or even the use of pressure to promote the flow of aqueous solutions through a pellet of silica powders could be possible ideas for the practical use of our results.

2.4 CONCLUSIONS

Sol gel methods have been successfully used to produce silica gel monoliths containing embedded nanoparticles of different materials, shapes, dimensions. It has to be stressed that the synthetic method has been developed to obtain monoliths without cracks and a relatively uniform and controlled concentration of nanoparticles (although a concentration gradient between top and bottom surfaces was unavoidable, due to the effect of gravity). An important part of the thesis was also to study easy and possibly green methods to obtain the transformation of nanoparticles into metal ions. The general aim of the thesis was in fact sensing, capture and disposal of (noble metal) nanoparticles. Particularly in the case of AgNPs, we found that O_2 oxidation in the presence of cysteamine and Fe^{3+} lead to smooth, efficient oxidation to Ag^+ species at room temperature and pH close to neutrality. On the other hand, it was also found that a faster AgNPs dissolution can be obtained by using HNO_3. This was the reagent of choice, when removal of the template nanoparticles was to be carried out on the NPs embedded in the silica matrix. In the case of AuNPs, the reagent of choice was instead aqua regia.

The as-prepared templated monoliths have been fully characterized and compared with the ones doped with Ag or AuNPs for a better understanding of their structure. Very importantly for our aims, the results show that the removal of template nanoparticles under the chosen acidic conditions leaves complementary empty cavities inside the material, without degradation of the matrix and almost residue free.

The reuptake ability of the void silica materials bearing imprinted cavities have been tested on 7 nm silver nanoparticles solution. To increase the contact surface and expose the cavities created inside the matrix, powders from ground monoliths were used. It has been observed that even non imprinted silica gel samples give significant interactions with 7 nm AgNPs and partly remove them an aqueous colloidal solution. However, there is solid evidence that the removal ability increases with the presence of templated cavities. It was not unexpected to observe that the reuptake process depends by the starting concentration of the NPs and the reaction time. Quite surprisingly, it was also observed that these materials also show a hole-dimension-driven selectivity for 7 nm AgNPs. The result is not obvious, as the silica surface is expected to be negatively charged at the working pH, while also the 7 nm AgNPs are negatively charged. Van der Waals attractive forces are thus responsible of the silica-AgNPs interactions, and a simple geometrical

model has been proposed to explain the hole size-diameter selectivity found in our experiments.

The selective uptake ability of these materials makes them excellent candidates for the use in real-life or industrial environment, to remove nanoparticles from water or from air (as aerosols), or to use them in the construction of sensing devices. Although it was not possible to investigate this aspect during the 3 years of this PhD thesis, it can be hypothesized that the unspecific nature of the silica matrix-nanoparticles interaction could be exploited also for materials different from Ag or Au. This could lead to imprinted materials useful for the indiscriminate removal of "nanomaterials" from water or air, a precious tool in the fight against the emerging problem of nanopollution.

Acknowledgments

A special thanks to:

- Regione Lombardia for Grant the project “Sensing, capture and disposal of nanoparticulate”;
- ENEA for the collaboration, in particular ENEA Staff: Penza Michele, Burresi Emiliano, Capodieci Laura, Carbone Daniela, Palazzo Barbara, Palmisano Martino, Schioppa Monica, Pesce Emanuela;
- ENEA tutor Dr. Maria Lucia Protopapa for the organization and support during the period at the ENEA labs in Brindisi;
- Dr. Dario Della Sala for the supervision and organization of the PhD project.

BIBLIOGRAPHY

1. Curtis, J., Greenberg, M., Kester, J., Phillips, S., & Krieger, G. (2006). Nanotechnology and Nanotoxicology a Primer for Clinicians. In *Toxicol Rev* (Vol. 25, Issue 4).

2. Rambaran, T., & Schirhagl, R. (2022). Nanotechnology from lab to industry - a look at current trends. In *Nanoscale Advances* (Vol. 4, Issue 18, pp. 3664–3675). Royal Society of Chemistry. https://doi.org/10.1039/d2na00439a

3. Inshakova, E., Inshakova, A., & Goncharov, A. (2020). Engineered nanomaterials for energy sector: Market trends, modern applications and future prospects. *IOP Conference Series: Materials Science and Engineering*, *971*(3). https://doi.org/10.1088/1757-899X/971/3/032031

4. Krug, H. F., & Wick, P. (2011). Nanotoxicology: An interdisciplinary challenge. *Angewandte Chemie - International Edition*, *50*(6), 1260–1278. https://doi.org/10.1002/anie.201001037

5. Gehr, P., Bachofen, M., & Weibel, E. R. (1978). The normal human lung: ultrastructure and morphometric estimation of diffusion capacity'. In *Respiration Physiology* (Vol. 32).

6. Ryman-Rasmussen, J. P., Riviere, J. E., & Monteiro-Riviere, N. A. (2006). Penetration of intact skin by quantum dots with diverse physicochemical properties. *Toxicological Sciences*, *91*(1), 159–165. https://doi.org/10.1093/toxsci/kfj122

7. Crosera, M., Bovenzi, M., Maina, G., Adami, G., Zanette, C., Florio, C., & Filon Larese, F. (2009). Nanoparticle dermal absorption and toxicity: A review of the literature. In *International Archives of Occupational and Environmental Health* (Vol. 82, Issue 9, pp. 1043–1055). https://doi.org/10.1007/s00420-009-0458-x

8. Volkheimer, G. (1974). Passage of Particles through the Wall of of the Gastrointestinal Tract. In *Environmental Health Perspectives* (Vol. 9). https://about.jstor.org/terms

9. Wick, P., Malek, A., Manser, P., Meili, D., Maeder-Althaus, X., Diener, L., Diener, P. A., Zisch, A., Krug, H. F., & von Mandach, U. (2010). Barrier capacity of human placenta for nanosized materials. *Environmental Health Perspectives*, *118*(3), 432–436. https://doi.org/10.1289/ehp.0901200

10. Oberdörster, G., Oberdörster, E., & Oberdörster, J. (2005). Nanotoxicology: An emerging discipline evolving from studies of ultrafine particles. In *Environmental Health Perspectives* (Vol. 113, Issue 7, pp. 823–839). https://doi.org/10.1289/ehp.7339

11. Krug, H. F. (2014). Nanosafety research-are we on the right track? In *Angewandte Chemie - International Edition* (Vol. 53, Issue 46, pp. 12304–12319). Wiley-VCH Verlag. https://doi.org/10.1002/anie.201403367

12. Xia, T., Kovochich, M., Brant, J., Hotze, M., Sempf, J., Oberley, T., Sioutas, C., Yeh, J. I., Wiesner, M. R., & Nel, A. E. (2006). Comparison of the abilities of ambient and manufactured nanoparticles to induce cellular toxicity according to an oxidative stress paradigm. In *Nano Letters* (Vol. 6, Issue 8, pp. 1794–1807). https://doi.org/10.1021/nl061025k

13. Sengul, A. B., & Asmatulu, E. (2020). Toxicity of metal and metal oxide nanoparticles: a review. In *Environmental Chemistry Letters* (Vol. 18, Issue 5, pp. 1659–1683). Springer. https://doi.org/10.1007/s10311-020-01033-6

14. Buzea, C., Pacheco Blandino, I. I., & Robbie, K. (2007). Nanomaterials and nanoparticles: Sources and toxicity. In *Biointerphases* (Vol. 2).

15. Khan, M., Khan, M. S. A., Borah, K. K., Goswami, Y., Hakeem, K. R., & Chakrabartty, I. (2021). The potential exposure and hazards of metal-based nanoparticles on plants and environment, with special emphasis on ZnO NPs, TiO2 NPs, and AgNPs: A review. In *Environmental Advances* (Vol. 6). Elsevier Ltd. https://doi.org/10.1016/j.envadv.2021.100128

16. Sajid, M., Ilyas, M., Basheer, C., Tariq, M., Daud, M., Baig, N., & Shehzad, F. (2015). Impact of nanoparticles on human and environment: review of toxicity factors, exposures, control strategies, and future prospects. *Environmental Science and Pollution Research*, *22*(6), 4122–4143. https://doi.org/10.1007/s11356-014-3994-1

17. Pulit-Prociak, J., & Banach, M. (2016). Silver nanoparticles - A material of the future...? *Open Chemistry*, *14*(1), 76–91. https://doi.org/10.1515/chem-2016-0005

18. Roe, D., Karandikar, B., Bonn-Savage, N., Gibbins, B., & Roullet, J. baptiste. (2008). Antimicrobial surface functionalization of plastic catheters by silver nanoparticles. *Journal of Antimicrobial Chemotherapy*, *61*(4), 869–876. https://doi.org/10.1093/jac/dkn034

19. Li, Y., Li, L., Li, J., Yao, L., Mak, A. F. T., Ko, F., & Qin, L. (2009). Antibacterial properties of nanosilver PLLA fibrous membranes. *Journal of Nanomaterials*, *2009*. https://doi.org/10.1155/2009/168041

20. Nadworny, P. L., Wang, J. F., Tredget, E. E., & Burrell, R. E. (2008). Anti-inflammatory activity of nanocrystalline silver in a porcine contact dermatitis model. *Nanomedicine: Nanotechnology, Biology, and Medicine*, *4*(3), 241–251. https://doi.org/10.1016/j.nano.2008.04.006

21. Zhao Z., Z. B. , L. K. (2013). *Nano-silver antibacterial liquid soap and preparation method thereof*, CN102860923 B.

22. Holladay R.J. (2013). *Toothpaste or tooth gel containing silver nano particles coated with silver oxide,* US 20130017236 A1.

23. Horner C.J., K. A. , N. K. R. (2006). *Nanosilver as a biocide in building materials*, US 0272542 A1.

24. Kwon H., Y. H. , K. I. , G. S. (2005). *Antibacterial paint containing nano silver particles and coating method using the same*, US 0287112 A1.

25. Schiffman, S. S. (1997). The Biology of Livestock Odor" at the ASAS/ADSA Midwestern Mtg. In *J. Anim. Sci* (Vol. 76).

26. Nia J.R. (2009). *Nanosilver for preservation and treatment of diseases in agriculture field*, US 0075818 A1.

27. Yu, S. J., Yin, Y. G., & Liu, J. F. (2013). Silver nanoparticles in the environment. In *Environmental Sciences: Processes and Impacts* (Vol. 15, Issue 1, pp. 78–92). https://doi.org/10.1039/c2em30595j

28. Liu, J., & Hurt, R. H. (2010). Ion release kinetics and particle persistence in aqueous nano-silver colloids. *Environmental Science and Technology*, *44*(6), 2169–2175. https://doi.org/10.1021/es9035557

29. Navarro, E., Piccapietra, F., Wagner, B., Marconi, F., Kaegi, R., Odzak, N., Sigg, L., & Behra, R. (2008). Toxicity of silver nanoparticles to Chlamydomonas reinhardtii. *Environmental Science and Technology*, *42*(23), 8959–8964. https://doi.org/10.1021/es801785m

30. Xiu, Z. M., Zhang, Q. B., Puppala, H. L., Colvin, V. L., & Alvarez, P. J. J. (2012). Negligible particle-specific antibacterial activity of silver nanoparticles. *Nano Letters*, *12*(8), 4271–4275. https://doi.org/10.1021/nl301934w

31. Silva, B. F. da, Pérez, S., Gardinalli, P., Singhal, R. K., Mozeto, A. A., & Barceló, D. (2011). Analytical chemistry of metallic nanoparticles in natural environments. In *TrAC - Trends in Analytical Chemistry* (Vol. 30, Issue 3, pp. 528–540). https://doi.org/10.1016/j.trac.2011.01.008

32. Faccini, M., Borja, G., Boerrigter, M., Morillo Martín, D., Martìnez Crespiera, S., Vázquez-Campos, S., Aubouy, L., & Amantia, D. (2015). Electrospun Carbon Nanofiber Membranes for Filtration of Nanoparticles from Water. *Journal of Nanomaterials*, *2015*. https://doi.org/10.1155/2015/247471

33. Syafiuddin, A., Salmiati, S., Hadibarata, T., Kueh, A. B. H., Salim, M. R., & Zaini, M. A. A. (2018). Silver Nanoparticles in the Water Environment in Malaysia: Inspection, characterization, removal, modeling, and future perspective. *Scientific Reports*, *8*(1). https://doi.org/10.1038/s41598-018-19375-1

34. Turner, N. W., Jeans, C. W., Brain, K. R., Allender, C. J., Hlady, V., & Britt, D. W. (2006). From 3D to 2D: A review of the molecular imprinting of proteins. In Biotechnology Progress (Vol. 22, Issue 6, pp. 1474–1489). https://doi.org/10.1021/bp060122g

35. Wang, R., Wang, L., Yan, J., Luan, D., Tao sun, Wu, J., & Bian, X. (2021). Rapid, sensitive and label-free detection of pathogenic bacteria using a bacteria-imprinted conducting polymer film-based electrochemical sensor. Talanta, 226. https://doi.org/10.1016/j.talanta.2021.122135

36. Bruchiel-Spanier, N., Dery, L., Tal, N., Dery, S., Gross, E., & Mandler, D. (2019). Effect of matrix-nanoparticle interactions on recognition of aryldiazonium nanoparticle-imprinted matrices. *Nano Research*, *12*(2), 265–271. https://doi.org/10.1007/s12274-018-2129-2

37. Kato, M., Sakai-Kato, K., & Toyo'oka, T. (2005). Silica sol-gel monolithic materials and their use in a variety of applications. In *Journal of Separation Science* (Vol. 28, Issue 15, pp. 1893–1908). https://doi.org/10.1002/jssc.200500225

38. Deva Krupa, A. N., & Vimala, R. (2018). AgNPs doped TEOS sol–gel coatings to prevent the adhesion of marine fouling organisms. *IET Nanobiotechnology*, *12*(2), 99–105. https://doi.org/10.1049/iet-nbt.2017.0047

39. Lkhagvajav, N., Yaşa, I., Çelik, E., Koizhaiganova, M., & Sari, Ö. Antimicrobial activity of colloidal silver nanoparticles prepared by sol-gel method. In *Digest Journal of Nanomaterials and Biostructures* (Vol. 6, Issue 1).

40. Taglietti, A., Arciola, C. R., D'Agostino, A., Dacarro, G., Montanaro, L., Campoccia, D., Cucca, L., Vercellino, M., Poggi, A., Pallavicini, P., & Visai, L. (2014). Antibiofilm activity of a monolayer of silver nanoparticles anchored to an amino-silanized glass surface. *Biomaterials*, *35*(6), 1779–1788. https://doi.org/10.1016/j.biomaterials.2013.11.047

41. Xing, L., Xiahou, Y., Zhang, P., Du, W., & Xia, H. (2019). Size Control Synthesis of Monodisperse, Quasi-Spherical Silver Nanoparticles to Realize Surface-Enhanced Raman Scattering Uniformity and Reproducibility. *ACS Applied Materials and Interfaces*, *11*(19), 17637–17646. https://doi.org/10.1021/acsami.9b02052

42. Li, J., Wu, J., Zhang, X., Liu, Y., Zhou, D., Sun, H., Zhang, H., & Yang, B. (2011). Controllable synthesis of stable urchin-like gold nanoparticles using hydroquinone to tune the reactivity of gold chloride. *Journal of Physical Chemistry C*, *115*(9), 3630–3637. https://doi.org/10.1021/jp1119074

43. Pallavicini, P., Donà, A., Casu, A., Chirico, G., Collini, M., Dacarro, G., Falqui, A., Milanese, C., Sironi, L., & Taglietti, A. (2013). Triton X-100 for three-plasmon gold nanostars with two photothermally active NIR (near IR) and SWIR (short-wavelength IR) channels. *Chemical Communications*, *49*(56), 6265–6267. https://doi.org/10.1039/c3cc42999g

44. Krupa, A. N. D., & Vimala, R. (2016). Evaluation of tetraethoxysilane (TEOS) sol-gel coatings, modified with green synthesized zinc oxide nanoparticles for combating microfouling. *Materials Science and Engineering C*, *61*, 728–735. https://doi.org/10.1016/j.msec.2016.01.013

45. Seneviratne, J., & Cox, J. A. (2000). Sol-gel materials for the solid phase extraction of metals from aqueous solution. In *Talanta* (Vol. 52). www.elsevier.com/locate/talanta

46. Rottman, C., Grader, G., de Hazan, Y., Melchior, S., & Avnir, D. (1999). Surfactant-induced modification of dopants reactivity in sol-gel matrixes. *Journal of the American Chemical Society*, *121*(37), 8533–8543. https://doi.org/10.1021/ja991269p

47. Adachi, T., & Sakka, S. (1988). The role of N,N-dimethyformamide, a DCCA, in the formation of sol gel silica monoliths by sol gel method. In *Journal of Non-Crystalline Solids* (Vol. 99).

48. Pallavicini, P., Preti, L., Vita, L. de, Dacarro, G., Diaz Fernandez, Y. A., Merli, D., Rossi, S., Taglietti, A., & Vigani, B. (2020). Fast dissolution of silver nanoparticles at physiological pH. *Journal of Colloid and Interface Science*, *563*, 177–188. https://doi.org/10.1016/j.jcis.2019.12.081

49. Gao, X., Lu, Y., He, S., Li, X., & Chen, W. (2015). Colorimetric detection of iron ions (III) based on the highly sensitive plasmonic response of the N-acetyl-l-cysteine-stabilized silver nanoparticles. *Analytica Chimica Acta*, *879*, 118–125. https://doi.org/10.1016/j.aca.2015.04.002

50. Abolghasemi-Fakhri, Z., & Amjadi, M. (2021). Gold nanostar@graphene quantum dot as a new colorimetric sensing platform for detection of cysteine. Spectrochimica Acta - Part A: Molecular and Biomolecular Spectroscopy, 261. https://doi.org/10.1016/j.saa.2021.120010

51. Thommes, M., Kaneko, K., Neimark, A. v., Olivier, J. P., Rodriguez-Reinoso, F., Rouquerol, J., & Sing, K. S. W. (2015). Physisorption of gases, with special reference to the evaluation of surface area and pore size distribution (IUPAC Technical Report). *Pure and Applied Chemistry*, *87*(9–10), 1051–1069. https://doi.org/10.1515/pac-2014-1117

52. Cychosz, K. A., & Thommes, M. (2018). Progress in the Physisorption Characterization of Nanoporous Gas Storage Materials. In *Engineering* (Vol. 4, Issue 4, pp. 559–566). Elsevier Ltd. https://doi.org/10.1016/j.eng.2018.06.001

53. Degioanni, S., Jurdyc, A. M., Cheap, A., Champagnon, B., Bessueille, F., Coulm, J., Bois, L., & Vouagner, D. (2015). Surface-enhanced Raman scattering of amorphous silica gel adsorbed on gold substrates for optical fiber sensors. *Journal of Applied Physics*, *118*(15). https://doi.org/10.1063/1.4933280

54. Darmakkolla, S. R., Tran, H., Gupta, A., & Rananavare, S. B. (2016). A method to derivatize surface silanol groups to Si-alkyl groups in carbon-doped silicon oxides. *RSC Advances*, *6*(95), 93219–93230. https://doi.org/10.1039/c6ra20355h

55. Shameli, K., Ahmad, M. bin, Jazayeri, S. D., Sedaghat, S., Shabanzadeh, P., Jahangirian, H., Mahdavi, M., & Abdollahi, Y. (2012). Synthesis and characterization of polyethylene glycol mediated silver nanoparticles by the green method. *International Journal of Molecular Sciences*, *13*(6), 6639–6650. https://doi.org/10.3390/ijms13066639

56. Lin, C. H., Wang, P. H., Wang, T. H., Yang, L. J., & Wen, T. C. (2020). The surface-enhanced Raman scattering detection of N -nitrosodimethylamine and N -nitrosodiethylamine via gold nanorod arrays with a chemical linkage of zwitterionic copolymer. *Nanoscale*, *12*(2), 1075–1082. https://doi.org/10.1039/c9nr09404k

57. Elghniji, K., Virlan, C., Elaloui, E., & Pui, A. (2018). Synthesis, characterization of SiO2 supported-industrial phosphoric acid catalyst for hydrolysis of NaBH4 solution. *Phosphorus, Sulfur and Silicon and the Related Elements*, *193*(12), 806–821. https://doi.org/10.1080/10426507.2018.1515946